Interaction of the miR-106a~363 microRNA cluster and the $p27^{Kip1}$ CDK inhibitor in T cell development and lymphomagenesis

Daniel Kuppers

A dissertation

submitted in partial fulfillment of the

requirements for the degree of

Doctor of Philosophy

University of Washington

2011

Peter Nelson, Chair

Matthew Fero

Amy Weinmann

Program Authorized to Offer Degree:

Molecular and Cellular Biology

University of Washington

Abstract

Interaction of the miR-106a~363 microRNA cluster and the $p27^{Kip1}$ CDK inhibitor in T cell development and lymphomagenesis

Daniel A Kuppers

Chair of the Supervisory Committee:

Professor Peter S. Nelson

Molecular and Cellular Biology Program

MicroRNAs are 21-22 nucleotide RNAs that regulate gene expression by binding mRNA 3' UTRs and inhibiting translation or targeting them for degradation. The Xpcl1 locus, encoding the miR-106a~363 miRNA cluster, was first identified as a common integration site in a Moloney murine leukemia virus (M-MuLV) screen for oncogenes cooperating with $p27^{Kip1}$ loss. The miR-106a~363 cluster is one of three paralogous clusters that have been implicated in oncogenesis and regulate development. In this dissertation I have examined the gene expression profiles associated with the M-MuLV tumors and validated that the viral integrations at *Xpcl1* induced expression of the miR-106a~363 miRNAs. The gene expression profile associated with *Xpcl1* tumors involved functional classes similar to $p27^{-/-}$ tumors, but with an opposite pattern of expression. This suggests that $p27^{Kip1}$ loss may overcome an anti-oncogenic effect of the miRNAs. I

also determined that miR-106a~363 is primarily expressed in T cells and is differentially expressed during T cell development.

To validate miR-106a~363 as an oncogene, I generated transgenic mice overexpressing miR-106a~363 in T cells using the Lck promoter (Lx^+). These mice developed a T cell developmental phenotype characterized by increased DP thymocytes and a deficiency in SP thymocytes, but have normal numbers of mature T cells. I determined that the miR-106a~363 cluster inhibits expression of CD69, a negative regulator of lymphocyte egress from lymphoid organs. This suggests that the developmental phenotype is caused by an altered rate of thymocyte egress due to inhibition of CD69.

The Lx^+ mice also spontaneously develop T cell lymphomas with a 46% penetrance by one year. There is a synergistic effect of $p27^{Kip1}$ loss and miR-106a~363 overexpression, and double mutant mice develop lymphomas with a 94% penetrance by 28 weeks. The data suggests that the synergy is due to $p27^{Kip1}$ loss overcoming a miRNA induced anti-oncogenic increase in $p27^{Kip1}$ expression. The increase in $p27^{Kip1}$ occurs at the transcriptional level through the FoxO3a and FoxO4 transcription factors. The work in this dissertation validates miR-106a~363 as an oncogene, identifies its potential involvement in regulating T cell development, and determines the mechanism of cooperation between the miRNAs and $p27^{Kip1}$ loss in lymphomagenesis.

Table of Contents

List of Figures

List of Tables

Abbreviations and Acronyms

Ago2	Argonaute 2
CDK	Cyclin-dependent kinase
cDNA	Complementary DNA
CKI	Cyclin-dependent kinase inhibitor
Cx^+	Chicken β-actin-Xpcl1 transgene
DN	Double negative ($CD4^-/CD8^-$) thymocyte
DP	Double positive ($CD4^+/CD8^+$) thymocyte
dsRNA	Double-stranded RNA
FDR	False-positive discovery rate
GEO	Gene Expression Omnibus
HITS/CLIP	High-throughput sequencing of RNA from crosslinked IP
IP	Immunoprecipitation
Kip1	CDK inhibitory protein 1 (p27, Cdkn1b)
Kis2	Kaplan integration site 2
LTR	Long terminal repeat
Lx^+	Lck-Xpcl1 transgene
miRNA	microRNA
M-MuLV	Moloney murine leukemia virus
ncRNA	Non-coding RNA
p27	27 kDa Cdk inhibitor protein (Kip1, Cdkn1b)
PAM	Prediction analysis for microarrays
pri-miRNA	Primary microRNA transcript
RISC	RNA-induced silencing complex
RLV	Radiation Leukemia Virus
RT-qPCR	Reverse transcription, quantitative polymerase chain reaction
S1P	Sphingosine 1-phosphate
S1P1	Sphingosine 1-phosphate receptor
SP	Single positive ($CD4^+$ or $CD8^+$) thymocyte
TCR	T cell receptor
UTR	Untranslated region
Xpcl1	X-linked $p27^{Kip1}$ cooperating locus 1 (Kis2, miR-106a~363)

Acknowledgements

I first want to thank my advisor, Matthew Fero, who by taking me on as his first graduate student was willing to go through the adventure of graduate school with me. He has put up with my unique organizational style and being trusting enough to give me a lot of independence in my research. I have gained from him a wealth of knowledge about how to successfully approach science experimentally as well as an appreciation for attention to detail. Matthew provided countless simulating conversations about both science and non-science.

A special acknowledgement goes to Muneesh Tewari and the entire Tewari lab. I want to thank them for allowing me to present at their lab meetings and the useful advice and suggestions they have provided throughout graduate school. Even more so I want to thank them for adopting me as an honorary member of the lab saving me from a solitary life in the lab.

I want to thank my committee members, Drs. Peter Nelson, Robert Eisenman, Stephen Tapscott, and Amy Weinmann, for their time, helpful advice and support throughout graduate school. I particular I want to thank Peter Nelson and Amy Weinmann for taking the time to read my thesis.

I want to thank my family and friends who have supported me throughout graduate school. I particularly want to thank Tracey Au, our walks home always gave me something to look forward to at the end of the day good or bad. Also, I want to thank Drew MacKellar, with whom our numerous outdoor adventures provided a much-needed break from the stresses of research. Lastly, I want to acknowledge my parents. My mother, who has always been and continues to be my number one supporter and my father, who inspired me to enter science, was always up for discussion of my work and on the lookout for research articles that might be of interest.

Chapter 1. Introduction

The Biology of MicroRNAs

Discovery of microRNAs

The role of RNAs in regulating gene expression was first described in 1993 with the discovery of lin-4 in *C. elegans*. Lin-4 encodes a pair of 22-nucleotide RNAs that regulate development by inhibiting translation of a second C elegans gene, lin-14[1]. It was hypothesized that the regulation by lin-4 was mediated through repeats in the 3' UTR of lin-14 complementary in sequence to lin-4. In 2000 a second short RNA, let-7, was identified in C elegans[2]. This RNA was also expressed during development and sequences complementary to it were identified in the 3' UTR of a number of genes, supporting the hypothesis that regulation was mediated through 3' UTR RNA/RNA interactions.

In 1998 a method of RNA mediated gene silencing, RNA interference (RNAi), was reported in *C. elegans,* wherein exogenous double-stranded RNA (dsRNA) could inhibit expression of a gene to which it is homologous[3]. Prior to these discoveries, 21-25-nt long dsRNAs had been observed in Arabidopsis undergoing viral- or transgene-induced post-transcriptional gene silencing[4]. These short dsRNAs were complementary to the silenced genes and were processed from longer precursor RNAs. The processing of longer RNAs into the short dsRNAs and their involvement in silencing was recapitulated in Drosophila extracts[5-8]. Sequencing the product RNAs demonstrated that they were all 21-23-nt in length with small (2 nucleotide) overhangs at the 3' ends[9]. The size similarity of the RNAs used in RNAi and those observed in Drosophila, implicated a

universal mechanism of target gene silencing, an idea which spurred efforts to identify short RNAs in additional species.

This new class of short RNAs, termed microRNAs (miRNAs), has expanded rapidly to include more than 10,000 miRNAs from a diverse range of organisms, including viruses and vertebrates. Within mammals, there is strong evolutionary conservation of miRNAs, with more than 1000 miRNAs currently identified in humans, and nearly 700 miRNAs in mice[10]. About half of known mammalian miRNAs are encoded within the introns of protein coding genes or other non-coding RNAs (ncRNA). The other half are intergenic miRNAs, encoded in unique transcripts with their own promoters. Several intergenic miRNA genes were first identified as non-protein-coding RNAs activated by retroviruses in viral mutagenesis screens. The first of these is *Bic*, which was initially discovered as a common integration site for the avian leukosis virus, only later to be shown to encode miR-155[11-14].

MicroRNA biogenesis and function

MicroRNA primary transcripts (pri-miRNAs) are transcribed by RNA polymerase II and they are polyadenylated and capped (Fig. 1.1)[15,16]. They include miRNA sequences within hairpin structures due to adjacent regions of reverse complementarity. The mature miRNAs are generated through a multistep process beginning with cleavage of the pri-miRNA by a protein complex (Microprocessor complex) with the key components of the nuclear RNAse III enzyme, Drosha, and the dsRNA binding protein DGCR8 (Fig. 1.1)[17-19]. This results in a hairpin shaped pre-miRNA of ~70 nucleotides, which includes a 5' phosphate and a two- or three-nucleotide overhang at the 3' end. A Exportin-5 then transports pre-miRNA to the cytoplasm (Fig. 1.1)[20,21]. In the cytoplasm,

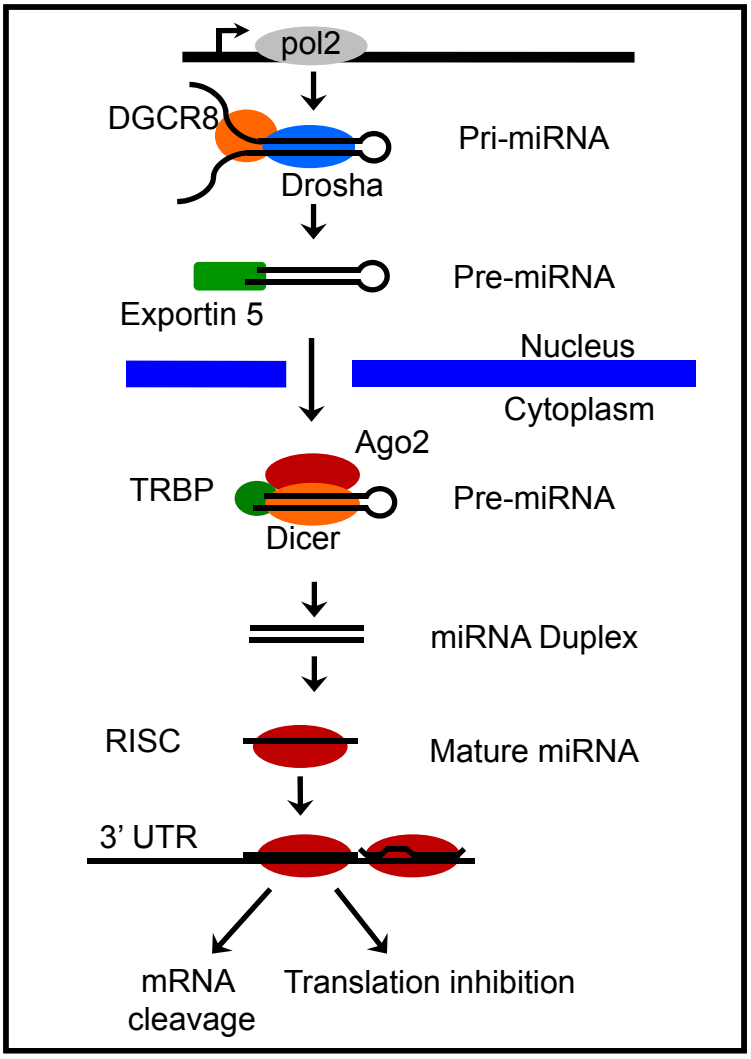

Figure 1.1 miRNA biogenesis. MicroRNA primary transcripts (pri-miRNAs) are transcribed by RNA polymerase II with the miRNA sequences within hairpin structures due to adjacent regions of reverse complementarity. The pri-miRNA is then processed by the Microprocessor complex, containing Drosha and DGCR8, to generate short pre-miRNA hairpins. Exportin-5 then transports the pre-miRNA to the cytoplasm where they are processed into an RNA duplex of ~21 nucleotides by Dicer and TRBP. The mature miRNA co-assembles into the RNA-induced silencing complex (RISC), whose essential elements are the Ago2 and GW182 proteins.

the pre-miRNA is processed to an RNA duplex of ~21 nucleotides by Dicer, an RNAse III enzyme, together with TRBP, a dsRNA binding protein (Fig. 1.1)[6,22-27]. The mature miRNA is defined as the strand of the duplex that was the 5' end of the pre-miRNA while the reverse strand is referred to as the star form (miRNA*). Either one of these strands may serve to target mRNAs by co-assembling in the RNA-induced silencing complex (RISC), whose essential elements are the Ago2 and GW182 proteins (Fig. 1.1)[28-30].

The miRNA component of the RISC complex functions as a template to guide the protein effector components to target transcripts. Predicting targets of specific miRNAs has been difficult since they do not exhibit perfect sequence complementarity. An important predictor is the near-perfect complementarity of the target to nucleotides 2-8 at the 5'-end of the miRNA, termed the "seed region"[31]. An overrepresentation of conserved adenosines in the target UTR, flanking the region of seed sequence complementarity, is also a factor[31]. Complementarity within the 3' region of the miRNAs, while less important, is able to compensate for imperfect 5' seed-sequence matches as well as complementarity with the middle 11-12 nucleotides of the miRNA[32,33]. Examples have also been found of miRNAs binding sites located outside of the 3' UTR, with the majority falling within coding sequences[34].

Ago associates with a large group of proteins in the RISC complex, and the translational inhibition function of miRNA is dependent on these protein components. The mechanism of translational inhibition by RISC is still not fully understood. The evidence suggests that RISC recruits eIF6, which in turn prevents productive assembly of the 80S ribosome[35]. RISC mediated mRNA degradation is better understood.

MicroRNAs that are nearly complementary to their target region cause endonucleolytic cleavage of the mRNA at the binding site by Ago2[29,36]. Ago2 localizes the complex to P-bodies where they integrate mRNA degrading enzymes CCR4-Not deadenylase, which leads to removal of the poly(A) tail, and the DCP:DCP2 decapping complex[37,38].

Identification of miRNA target genes

Currently, there are five main target prediction algorithms: TargetScan, PicTar, miRanda, PITA and RNA22. The various algorithms give different weight to four main characteristics: seed sequence complementarity, evolutionary conservation of the target site, characteristics of the mRNA in the area of the target site, and the free energy of miRNA/mRNA binding[39-44]. Rigorous comparisons of the predictive power of the different algorithms have not been done. A few early studies addressing this question found that algorithms with stringent seed sequence base-pairing requirements had higher sensitivity and specificity[45-47]. However, recent high-throughput analysis of Ago-bound miRNA-mRNA complexes have found 27% of miRNA target sites lack perfect seed sequence complementarity and 25% fall outside the 3' UTR, suggesting that these algorithms are missing a significant number of target sites[39]. Considering only conserved 3' UTR target sites, approximately 60% of human protein-encoding genes are predicted targets. However, when non-conserved target sites and non-3'UTR target sites are taken into account, target predictions identify the vast majority of genes[39].

A variety of experimental methods have also been utilized to identify miRNA targets. Overexpression or knockdown of a miRNA of interest followed by microarray analysis has been successfully used to identify putative targets[48]. A weakness of this approach is that it does not distinguish between direct and indirect effects of the miRNA,

and thus requires additional validation. This shortcoming has been partially addressed by immunoprecipitating Ago2 to isolate miRNA-bound mRNAs followed by microarray analysis, which limits the detection of genes altered by indirect effects[49]. One method of validating a candidate miRNA target is to demonstrate a negative correlation between expression levels of the miRNA and expression levels of the target genes mRNA and protein. Similarly, forced expression of a miRNA typically results in reduced expression of a target gene. Yet even forced expression may be complicated by secondary effects whereby miRNA targeting of other regulatory genes can indirectly lead to an increase or decrease in expression of the gene of interest. Thus, correlative studies, and forced expression cannot definitively rule in, nor exclude, a direct effect of a miRNA on a putative target. For this reason evidence of direct targeting is often sought by co-expressing a miRNA with reporter construct that contains the 3' UTR of the putative target. Luciferase is typically chosen as the reporter gene due to its short half-life and the broad range of sensitivity of a luciferase assay. To further demonstrate target site specificity, the precise miRNA target sites may be mutagenized to remove complementarity with the seed sequence. Possible shortcomings of the use of 3'UTR reporters is that they ignore the possibility of non-canonical sites, sites outside the 3'UTR, or may be overly sensitive due to artificially high levels of miRNA expression.

A recent advance has been made with the development of Ago2 HITS/CLIP, enabling the high-throughput identification of miRNA target sites[50]. The technique involves first crosslinking miRNA/mRNA heteroduplexes, and RNase digestion of the regions of mRNA not bound within the RISC complex. Immunoprecipitation of the Ago2 bound complexes and purification of the RNA miRNA:target RNA duplexes is then

followed by high throughput sequencing. The sequenced target fragments are then mapped to the transcriptome, whereby narrow clusters of sequence reads identifies the miRNA binding sites. The advantage of this method is the ability to simultaneously identify all genes being targeted by miRNAs in a sample, from both canonical and non-canonical target sites. While target validation may still be warranted, e.g. if the cluster amplitude is relatively small, the specificity of this approach is much higher than general gene expression studies.

Regulation of miRNAs and their role in disease

MicroRNA expression is regulated by a variety of mechanisms targeting all stages of miRNA biogenesis. Recent evidence indicates that post-transcriptional modifications of mature miRNAs also alters their stability[51]. The majority of pri-miRNAs are transcribed by RNA Pol II and have poly-A tails and 7-methyl-guanylate caps. Analysis of the promoters of 175 human miRNAs found that they are similar in structure to those from coding genes, and include a similar frequency of CpG islands, TATA boxes and other regulatory elements[52,53]. MicroRNA are also regulated epigenetically, by DNA methylation and histone modifications, similarly to protein coding genes[54,55].

Post-transcriptional regulation of pre-miRNA processing occurs through accessory proteins binding to the RNA helicases in the Drosha complex. Examples of this include binding of TGF-β regulated Smads and p53, which increase processing[56,57]. Estrogen signaling, through E2-ERα binding, decreases processing of specific pre-miRNAs[58]. MicroRNA processing is also regulated by proteins that selectively bind to particular pri-mRNA. In the case of the miR-17~92 cluster, hnRNP-A1 must be bound for pre-miR-18a processing[59]. In the case of the let-7 family, Lin-28 binds to a

conserved region in the hairpin to block processing[60]. In contrast to Drosha, whose expression levels are relatively invariant, Dicer expression is regulated by binding to TRBP and PACT which increase its stability[61,62]. Changes in Dicer activity on particular pre-miRNAs has also been observed, but the mechanism is unknown[63].

miRNAs have since been found to regulate a diverse range of biological processes including cellular proliferation, differentiation and apoptosis, all of which are deregulated in cancer. More than 40 miRNAs have been reported to possess tumor suppressive or oncogenic functions, and altered expression of miRNA has been reported a wide range of tumor types[64]. Not surprisingly, the altered expression of miRNAs in tumors has been found to occur through a variety of genetic events targeting miRNAs including: the deletion of miRNA, point mutations in miRNA sequences, genomic amplifications or translocations, and epigenetic silencing of miRNA loci[64]. Disruption of miRNA biogenesis has also been observed in cancer; including altered pre-miRNA nuclear export, mutation of Dicer binding partners and reduced miRNA processing in p53 mutant cells[57,61,65]. The first miRNAs described as having tumor suppressor activity were miR-15a and miR-16a, with the discovery that they are located in a region commonly deleted in B cell chronic lymphocytic leukemia[66]. These miRNAs have since been shown to target Bcl2 and thereby promote apoptosis[67]. The earliest reports of a non-coding RNA gene that had oncogenic activity was the discovery of *Bic,* which was activated by retroviral insertional mutations in mice[11]. Only later was it shown to encode miR-155 and be activate in human lymphoma[14]. MicroRNAs have been implicated in a wide range of other diseases, with 270 disease associations reported[68].

Xpcl1 and its paralogs

miR-106a~363 and paralogous miRNA clusters

The *Xpcl1* gene was originally identified as an insertion site in a retroviral insertional mutagenesis screen. The site, and its associated non-coding ESTs, was named *Xpcl1* (X-linked $p27^{Kip1}$ cooperating locus) because it was frequently targeted in mice lacking the $p27^{Kip1}$ Cdk inhibitor gene[69]. The gene was subsequently shown to encode miR-106a~363, an X-chromosomal miRNA cluster containing 6 miRNAs (miR-106a, miR-18b, miR-20b, miR-19b, miR-92 and miR-363). It is the member of a family of highly conserved miRNA clusters including two paralogs, the miR-17~92 and miR-106b~25 clusters (Fig. 1.2). Subsequent viral mutagenesis screens, using related retroviruses, also identified the locus in mice with intact $p27^{Kip1}$, and referred to the gene as Kis2 [70]. In contrast to miR-106a~363 and miR-17~92, which are both intergenic miRNA clusters, the miR-106b~25 cluster is located in the 13th intron of Mcm7 and encodes three miRNAs (miR-106b, miR-93 and miR-25). The miR-17~92 cluster is located on chromosome 14 in mice and chromosome 13 in humans and contains six miRNAs (miR-17, miR 18a, miR-19a, mir-20a, miR-19b and miR-92). The mature sequences of miR-19b and miR-92 are identical between miR-17~92 and miR-106a~363, however they differ in their pre-miRNA sequence (Fig. 1.2).

The evolutionary history of the three paralogous clusters has been reconstructed back through invertebrates with the clusters originating from three miRNAs and arriving at their current organization through a series of duplication and deletion events. The organization of the miRNAs into three clusters and the miRNA composition of each cluster is conserved in mammals, with the miR-106a~363 paralogs originating from

three miRNAs in bony fishes. The cluster expanded through a series of mutations and duplication events, resulting in the 3 paralogous clusters currently found in mice and humans[71]. Both the evolutionary analysis and the seed-sequence based grouping of miRNAs, found in miRBase, group the miRNAs into 3 families: the miR-17 family (miR-17,-18a,-18b,-20a,-20b,-93,-106a and -106b), miR-19 family (miR-19a and -19b) and miR-25 family (miR-25,-92a and -92b) (Fig. 1.2)[72].

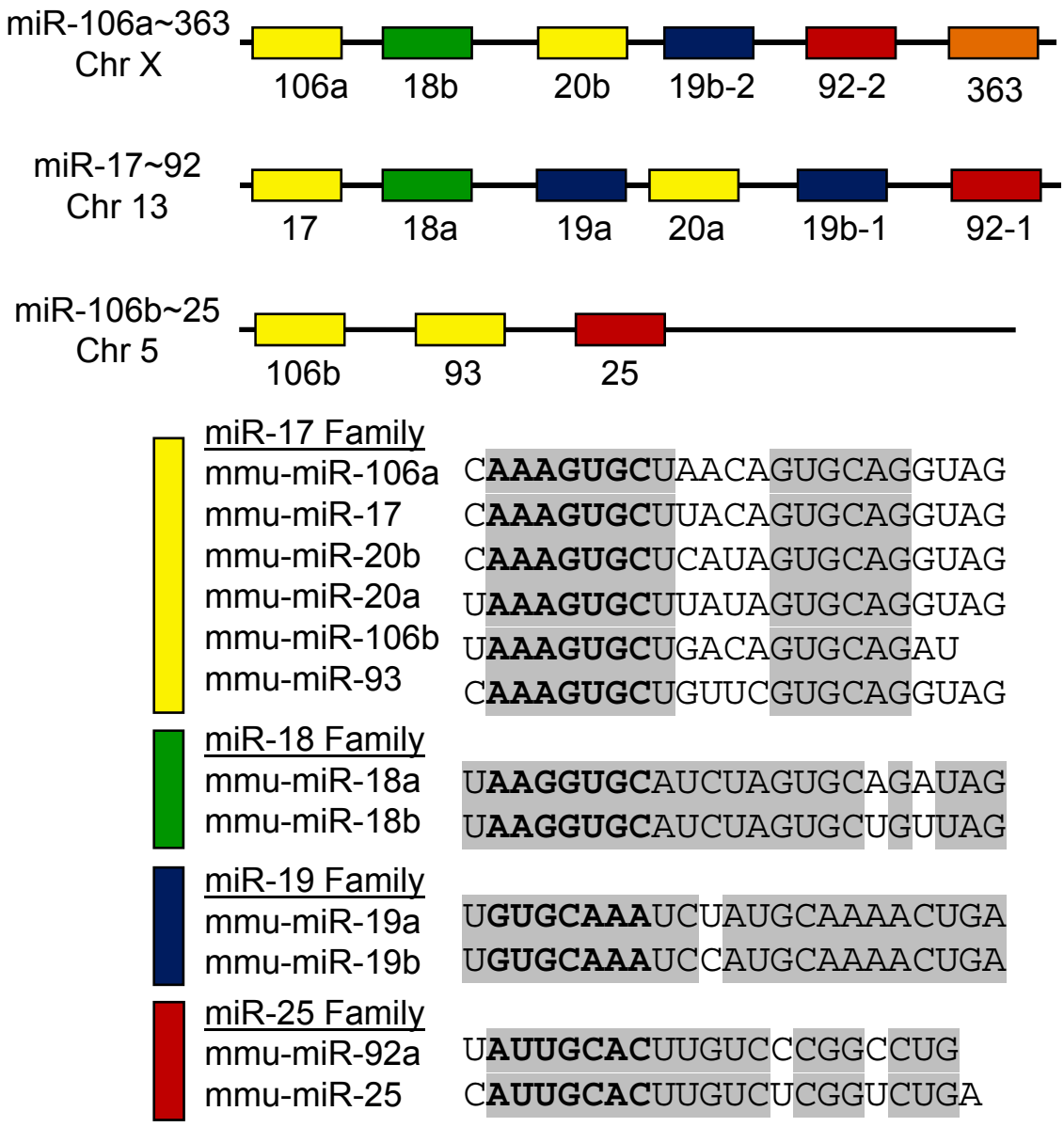

Figure 1.2 The miR-106a~363 cluster and paralogs. The miR-106a~363 cluster is one of three paralogous miRNA clusters. The miRNAs within the clusters can be clustered into 4 main families based on seed sequence similarity and are color coded by family. The seed sequence consists of the 2-8 nucleotides of the mature miRNA as is indicated in bold for each family. The miRNAs within each family also have high sequence homology outside of the seed sequence, indicated by grey shading.

Biological function of miR-106a~363 and paralogs

Since the miRNAs in the three clusters are highly similar in sequence, the possibility exists that they have overlapping functions. To address this, Ventura and colleagues deleted the clusters in mice, while preserving the expression of Mcm7 [73]. Singular deletion of miR-106a~363 and miR-106b~25 caused no obvious abnormalities and mice were viable and fertile. In contrast, mice lacking miR-17~92 died within minutes of birth, due to lung hypoplasia and cardiac ventricular septal defects. Compound knockout of miR-17~92 and miR-106b~25 and the triple knockout resulted in more severe defects, with death at mid-gestation.

Since the three clusters likely have overlapping target profiles, the differences in phenotype may be due to differences in the spatial and temporal expression of the clusters. In the case of miR-17~92 and miR-106b~25 their expression patterns and levels are fairly overlapping, however miR-106b~25 does not express any miR-19 or miR-18 family members, possibly explaining the difference in phenotype. The authors did not detect expression of miR-106a~363 in wildtype mice, but I have found that it is expressed at high levels in lymphoid tissues (Chapter 3). Considering the lack of phenotype of miR-106a~363 KO mice, it is likely that the miR-17~92 cluster compensates for loss of miR-106a~363. The severe early developmental defects caused by loss of miR-17~92 made later defects in immune system unassessable.

The *Xpcl1* miRNAs, as well as miRNAs from paralogous clusters, have been shown to be involved in regulating both cellular development and aging. During development, miR-17, miR-20a, miR-93 and miR-106a have been shown to be differentially expressed in mouse embryos. Within these cells the miRNAs regulate

expression of Stat3, an important suppressor of differentiation in ES cells, suggesting a mechanism through which they play a role in controlling cellular differentiation[74]. MicroRNAs from the paralogous clusters are also expressed during B cell and T cell development. During B cell development in the bone marrow, the three clusters were found to be sequentially expressed during different developmental stages, starting with miR-17~92 and ending with miR-106b~25 [75]. In knockout mice, the miR-17~92 cluster was also found to be essential for B cell development, with increased levels of Bim resulting from loss of the miRNAs, inhibiting it at the pro-B to pre-B transition[73]. During T cell development, miRNAs from the three paralogous clusters have been found to have specific expression patterns by both Neilson et al. and in work I have done[76]. In addition, miR-106a has been shown to regulate expression of an important immune system regulator, IL-10 [77]. IL-10 plays a variety of roles in the immune system including macrophage and dendritic cell maturation and activation, T cell activation and antibody production, with its dysregulation resulting in a variety of immunological diseases including cancer[78,79].

The high degree of conservation of the miR-106a~363 cluster and its paralogs throughout mammals suggests that they have important biological functions. The miRNAs from the clusters have been shown to be expressed both during embryonic and immune system development, strengthening this hypothesis. However, the key biological functions of the miRNAs during these events are unknown. The current dogma is that the seed sequence is the key determinant of miRNA targeting, which implies that the three clusters should have overlapping functions. The ability of miR-106b~25 to partially rescue the miR-17~92 knockout phenotype supports this view.

How closely the target profiles of highly similar miRNAs overlap will not be known until the rules of miRNA targeting are better understood, and large numbers of miRNA targets have been identified in vivo.

miR-106a~363 and paralogs as oncogenes and tumor-suppressors

In addition to their roles in normal development, a number of groups have found that miRNAs from the miR-106a~363 cluster as well as its paralogs are expressed in a variety of mouse and human cancers, as well as cancer cell lines, and function as both oncogenes as well as tumor-suppressors[80-85]. Overexpression of the miR-17~92 cluster has been shown to accelerate B cell lymphomas in Eμ-cMyc transgenic mice, and causes an immune lymphoproliferative disease[86,87]. Several miRNAs important for the oncogenic function of miR-17~92 have been identified. In Eμ-myc/miR-17~92 tumors miR-19a and miR-19b were shown to inhibit Myc induced apoptosis, by targeting PTEN[88]. In human fibroblasts miR-17~92 and miR-106a~363 may confer tumorigenicity by inhibiting Ras-induced senescence by targeting the CDK inhibitor, $p21^{Cip1}$ [89]. Members of the miR-17 family also target $p21^{Cip1}$ in breast cancer cells[90].

The miR-106a~363 cluster has not yet been validated as an oncogene. However, the miR-106a~363 cluster has been identified as a common integration site in a number of different retroviral insertional mutagenesis screens including in mice knocked out for the cell cycle inhibitors $p27^{Kip1}$, $p19^{Arf}$ and p53 [69,70,91,92]. In addition to their effects on Ras-induced senescence, the targeting of $p21^{Cip1}$ by miR-106a and 20b is also able to override a DNA-damage checkpoint[90]. Lastly, miR-106a has also been shown to induce anchorage independent growth, a trait often associated with oncogenes[93].

A number of miRNAs from the miR-17 family have also been found to possess tumor-suppressive functions. A feedback loop with miR-17 and miR-20a has been shown to regulate expression of cyclin D1 [94]. However, in breast cancer, expression of miR-17 and miR-20a is often reduced and is inversely correlated with cyclin D1 expression, removing a block to proliferation. When expression of the miRNAs was reconstituted, they were able to reduce proliferation and block colony formation by targeting cyclin D1. The miR-17 family members can also inhibit proliferation in breast cancer by targeting AIB1 and ERα[95,96]. In glioma, low miR-106a levels are correlated with high E2F1 levels and high-grade disease. When expression of miR-106a is restored it provides a tumor-suppressive effect by inhibiting E2F1 resulting in p53 mediated apoptosis and inhibition of proliferation through an unknown p53-independent mechanism[97].

In normal cells, all of the miRNAs from the miR-106a~363 cluster and paralogs are usually expressed as a group, although their relative expression levels vary. In some cases, the altered expression of miRNAs in cancer has been shown to be caused by the typical genetic and epigenetic mechanism that control mRNA expression[98,99]. Interestingly, the relative expression of individual miRNAs from within clusters are often altered, suggesting that there is an unknown mechanism for the post-transcriptional regulation of individual miRNAs. In the case of miR-17~92, this is of particular interest given that the miR-17 family member miRNAs act as tumor suppressors and the miR-19 family members function as oncogenes with both groups up-regulated or down-regulated in cancer accordingly. Although it is not known if this is also the case with miR-106a~363, since the oncogenic components of the cluster have not been identified,

it is interesting to note that miR-106a has also been shown to cause a tumor-suppressive effect[97].

T cell development

The process of T cell development primarily occurs in the thymus through a series of ordered stages that can be characterized by the status of T cell receptor rearrangement and cell surface protein expression (Fig. 1.3). T cells develop from a common lymphoid progenitor in the bone marrow that can also develop into B cells. The progenitors that develop into B cells remain in the bone marrow, while those destined to become T cells migrate to the thymus. The thymus can be divided into two main regions, the outer thymic cortex and the inner medulla. Throughout the thymus the thymic stroma, made up of a network of epithelial cells, creates a unique microenvironment necessary for T cell development. The cortex primarily consists of the immature thymocytes along with a few macrophage. Meanwhile, the medulla contains the mature thymocytes as well as dendritic cells and macrophages.

The different stages of thymocyte development can be characterized by expression of the cell surface proteins CD3, CD4 and CD8. When the lymphoid progenitors enter the thymus they lack expression of all T cell specific markers. Following an initial phase of development they begin to express Thy-1 and are called double negative thymocytes (DN) due to their lack of CD4 or CD8 expression. The double negative population consists of three separate sub-populations. The two minority populations, each making up about 20% of the double negatives, develop into γδ T cells and NK T cells. The majority population develops into α:β T cells. All double negative cells rearrange the β, γ and δ T cell receptor (TCR) loci, followed by

expression of the pre-TCR in complex with CD3 and the γ:δ TCR. Signaling through one of the receptors leads to down regulation of the other and lineage commitment of the thymocyte. Signaling through the pre-TCR induces proliferation and the thymocytes begin expressing CD4 and CD8. This population, called double-positive thymocytes (DP), is the majority thymocyte population, and approximately 80% of the total.

Once the double-positive thymocytes cease proliferating they rearrange the TCR α-chain. The T cell receptor α (TCR) loci consist of a series of gene segments organized into the variable (V) and joining (J) segments, and the constant (C) region (Fig. 3.6). The TCRα chain is rearranged from the TCRα/δ locus, which contains approximately 70 Vα and 60 Jα segments along with the constant region. Rearrangement occurs through rearrangement of V to J, with the first rearrangement excising the TCRδ region. The large number of V and J segments in the TCRα locus enables it to go through a series of rearrangements until it produces an α chain that efficiently pairs with the TCRβ chain the T cell is expressing.

Following TCR rearrangement, the thymocytes undergo positive selection where they must successfully recognize a self MHC molecule or they undergo apoptosis. The majority of thymocytes fail positive selection and die. The thymocytes that survive positive selection downregulate expression of either CD4 or CD8 and become single positive thymocytes. During and following the transition from double positive to single positive stage the thymocytes undergo negative selection during which thymocytes that react strongly to ubiquitous self-antigen are removed. Only approximately 2% of the starting double positive thymocytes survive passing through the selection stages to

become mature T cells, which then migrate from the thymus to peripheral lymphoid organs.

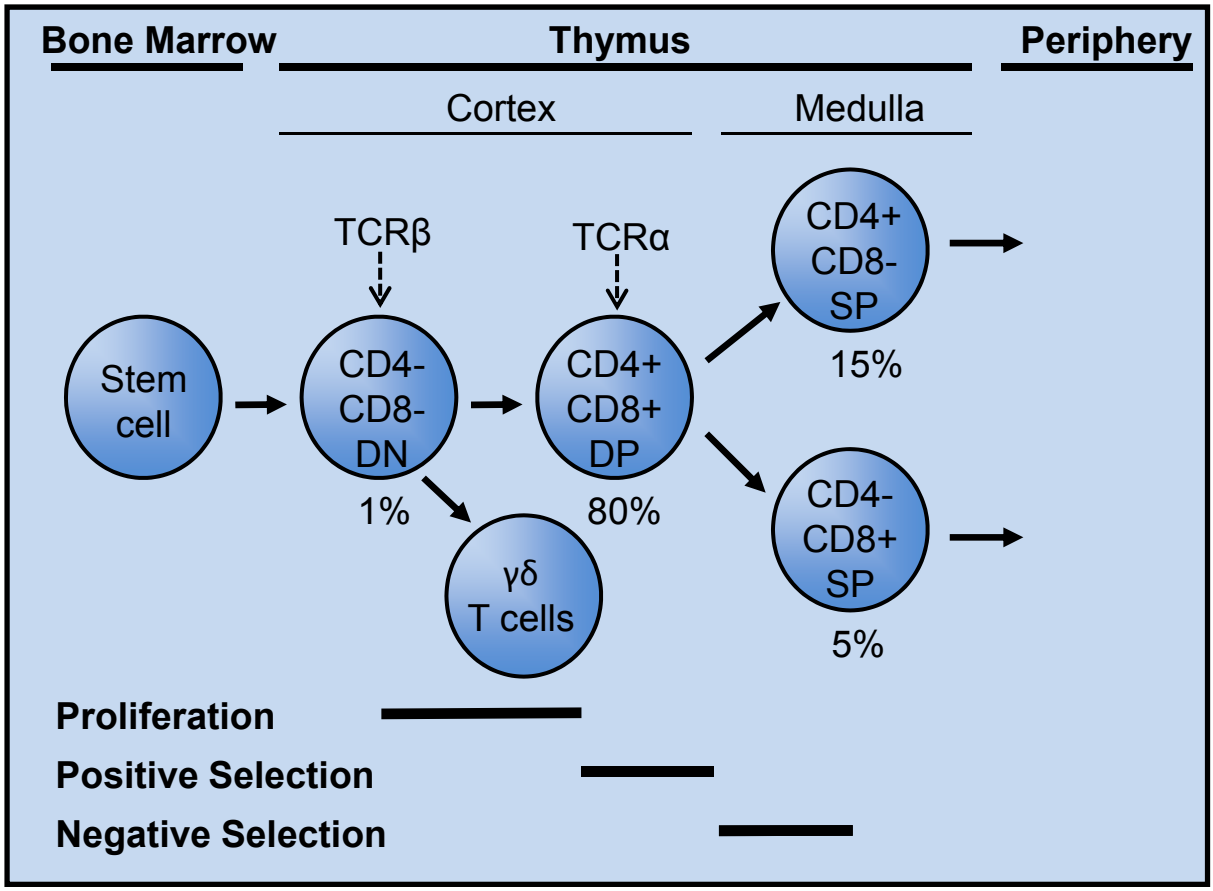

Figure 1.3 Thymic T cell development. T cells develop from common lymphoid progenitors, in the bone marrow, which migrate to the thymus to develop into T cells. The four main stages of T cell development within the thymus can be differentiated by expression of CD4 and CD8 on the cell surface. Each stage constitutes a widely varying proportions of the total thymocyte population. The T cell receptor (TCR) β chain rearranges during the $CD4^-/CD8^-$ (DN) stage and the TCRα chain rearranges during the $CD4^+/CD8^+$ (DP) stage. Positive and negative selection occurs primarily during the DP and single positive stages respectively. The γδ T cell lineage develops from the DN population. Only approximately 2% of the initial DP cells survive to develop into mature T cells which then leave the thymus and populate other lymphoid tissues.

The $p27^{Kip1}$ CDK inhibitor

The Cell Cycle

The eukaryotic cell cycle is a directional process punctuated by DNA replication and cellular division. Essential regulators of the cell cycle include cyclins and cyclin-dependent kinases (CDK). Cyclins and CDKs form heterodimeric protein complexes, wherein the cyclins act as regulatory subunits and CDKs function as the catalytic subunits. Cyclin expression oscillates throughout the cell cycle, and regulatory checkpoints control cyclin/CDK activity at crucial G1/S and G2/M transitions. The cyclins are classified according to sequence homology, and different classes of cyclins function at specific phases of the cell cycle. The D-type cyclins are expressed early in the cell cycle, in response to stimulation by extracellular growth factors. The Cyclin D/CDK complex targets Rb for phosphorylation which in turn activates the E2F transcriptions factors. This leads to expression of Cyclin E, Cyclin A and a variety of components of the DNA replication machinery. Cyclin E/CDK2 complexes then initiate the transition from G1 to S phase by targeting the negative regulators of the cyclin/CDK complex necessary for S phase, Cyclin A/CDK1,2. Cyclin A/CDK are responsible for initiating DNA replications. During M phase the final cyclin/CDK complex Cyclin B/CDK1 is activated and controls mitotic spindle formation and sister-chromatid pair alignment. Activity of the cyclins throughout the cell cycle is regulated by three mechanisms: increased protein degradation, decreased gene expression and by two families of CDK inhibitory proteins the cyclin-dependent kinase inhibitors (CKI).

$p27^{Kip1}$ regulation of the cell cycle

The CKIs fall within the Cip/Kip family ($p21^{Cip1}$, $p27^{Kip1}$ and $p57^{Kip2}$) and the INK4 family ($p15^{INK4b}$, $p16^{INK4a}$, $p18^{INK4c}$ and $p19^{INK4d}$). Both of these families regulate progression through the cell cycle by binding CDKs and cyclin/CDK complexes to inhibit their activity. The INK4 family binds to monomeric CDK4 and CDK6 during the G1 phase in response to growth inhibitory signals, thereby preventing their binding to Cyclin D. The Cip/Kip CKIs both inhibit and activate different cyclin/CDK complexes through binding of both the cyclin and the CDK. In the case of $p27^{Kip1}$ it inhibits the G1/S complex of Cyclin E/CDK2 and and the S phase complex of Cyclin A/CDK1,2 by interfering with the ATP-binding site and the active site of the CDK. Unlike the other cyclin/CDK complexes, during the G1 phase Cyclin D and CDK4,6 require additional proteins in order to bind to each other with high affinity. Assembly of the complex requires $p27^{Kip1}$ binding to both of the subunits.

Regulation of $p27^{Kip1}$ expression

Activation of the G1/S and S-phase cyclin/CDK complexes is an essential step for initiation of cellular replication. Therefore robust and tightly regulated inhibition of $p27^{Kip1}$ expression is essential to ensure cellular replication is initiated at the appropriate time and to prevent unregulated cellular proliferation. Regulation of $p27^{Kip1}$ occurs at the transcriptional, translational and post-translational levels in cancer and normal cells. While $p27^{Kip1}$ expression during the cell cycle is predominantly regulated post-transcriptionally, transcriptional regulation of $p27^{Kip1}$ has been described during development and in cancer.

A number of transcription factors have been found to regulate $p27^{Kip1}$ expression. The FoxO1, FoxO3a and FoxO4 transcription factors are positive regulators of $p27^{Kip1}$ expression. They also increase $p27^{Kip1}$ protein levels by decreasing Akt signaling[100,101]. ID3 and c-Myc function as negative regulators[102,103]. ID3 downregulates $p27^{Kip1}$ expression in lymphomas in mice and is required for regulation of $p27^{Kip1}$ during lck controlled T cell development. While c-Myc can transcriptionally regulate $p27^{Kip1}$, it mainly regulates $p27^{Kip1}$ through control of key proteins,Cks1 and Cul1, involved in its proteolysis[104,105]. Translation is also regulated through the 3'UTR with inhibition by Rho and CDK4 as well as three miRNAs, miR-221,miR-222 and miR-181a[106-111].

Ubiquitin-dependent $p27^{Kip1}$ degradation is mediated by a number of different mechanisms. The best characterized of these is polyubiquitination of $p27^{Kip1}$ by the SCF^{SKP2} E3 ubiquitin ligase complex. Efficient ubiquitination of $p27^{Kip1}$ by SCF^{SKP2} is dependent on $p27^{Kip1}$ phosphorylation at a number of sites by Cyclin E/CDK2, Cyclin A/CDK2, LYN, ABL and SRC[112-117]. Phosphorylation by KIS or MIRK results in the nuclear export of $p27^{Kip1}$, which also results in its proteolytic degradation[118-120].

$p27^{Kip1}$ in cancer

In mice, $p27^{Kip1}$ has been shown to be a haplo-insufficient tumor suppressor and loss of $p27^{Kip1}$ accelerates tumor development in Rb, Pten and Apc mouse tumor models[121-124]. In human malignancies $p27^{Kip1}$ does not function as a typical tumor suppressor, given that genetic mutation or deletion of both alleles of $p27^{Kip1}$ is rare. Instead, $p27^{Kip1}$ expression is commonly decreased through increased proteolysis, cellular mislocalization and miRNA mediated inhibition. Reduced expression of $p27^{Kip1}$ is a negative prognostic indicator in a variety of cancers including breast, colon, prostate

and lung cancer[125]. ELAVL, a negative regulator of $p27^{Kip1}$ translation, is often overexpressed in ovarian and colon cancer. Additionally, miR-221 and miR-222 are overexpression in a variety of tumors[80,107,108,126]. Increased proteolysis of $p27^{Kip1}$ in cancer is mediated through a number of oncogenic signaling pathways. In epithelial malignancies oncogenic activation of EGFR results in increased activation of SRC and Ras mediated degradation of $p27^{Kip1}$ through Rho[127]. In the case of hematopoietic malignancies, $p27^{Kip1}$ levels are reduced by BCR-ABL[128]. PTEN mutation also results in reduced $p27^{Kip1}$ levels through increased expression of Skp2 [129].

Chapter 2. The Impact of Xpcl1 Activation and $p27^{Kip1}$ Loss on Gene Expression in Murine Lymphoma

Introduction

A low level of $p27^{Kip1}$ expression in human cancers is frequently associated with a poor prognosis. However, the only type of spontaneous tumors that develop in $p27^{Kip1}$ knockout mice are *pars intermedia* pituitary adenomas. However, these mice display increased susceptibility to a variety of tumor types when exposed to mutagenic agents[121,130]. Several oncogenes and tumor suppressor genes have been shown to cooperate with *$p27^{Kip1}$* loss in the induction of breast, colon and prostate cancers in mouse models[124,130,131]. However, the biochemical mechanisms that underlie the cooperation between $p27^{Kip1}$ loss and oncogene overexpression in cancer development, is still not well understood.

One possible approach to identifying both cooperating and novel oncogenes is the use of retroviral insertional mutations. The Moloney Murine Leukemia Virus (M-MuLV) is one of a number oncogenic mouse retroviruses having been shown to cause tumors by driving expression of genes close to its insertion sites through the viral long terminal repeat (LTR)[132,133]. The LTR is the transcriptional regulatory region of the virus and contains many of the same elements found in eukaryotic promoters. Retroviral mutagenesis screens involve injecting neonatal mice with a retrovirus, which then randomly integrates into the mouse genome, and drives expression of neighboring genes. If a sufficient number of oncogenes are activated, then a tumor develops. Less commonly, a tumor suppressor gene may be inactivated, but this is less likely to cause tumors since mammalian cells are diploid. On average M-MuLV induced tumors contain 20 viral common insertion sites, insertion sites targeted in multiple tumors at a higher

frequency than expected by chance and therefore thought to contribute to tumorigenesis[134].

Moloney murine leukemia virus (M-MuLV) was previously used to induce lymphomas in $p27^{Kip1}$ knockout mice, in an attempt to identify oncogenes that cooperate with $p27^{Kip1}$ loss[69]. In this study, M-MuLV integrations were found to target the Myc family members, Jdp2, and Xpcl1 at a higher frequently in tumors induced in $p27^{Kip1}$ knockout mice vs. mice with wildtype $p27^{Kip1}$. At the time of the discovery it was not known that Xpcl1 encoded the miR-106a~363 miRNA cluster. However, expression of a non-coding RNA, AI464896 EST, which maps to the 3' end of this locus, and includes the miR-363 sequence, was increased in tumors with Xpcl1 integrations[69]. Xpcl1 is not exclusively targeted in mice with $p27^{Kip1}$ deletions; it has also been identified as a viral integration site in $p27^{+/-}$ mice, wildtype mice, and in mice with $p53^{-/-}$, $p19^{-/-}$, or $p16^{-/-}$ mutations[69,70,91,134]. Likewise, integrations of other retroviruses, RadLV and SL3-3, have been independently reported to map to the same X-chromosomal locus in murine lymphomas[70,92]. The RadLV integrations at this locus were associated with increased expression of multiple non-coding RNA splice variants located between the viral integration sites and the 5' end of the miR-106a~363 cluster. Because of a small gap between these proximal ESTs and AI464896, it was speculated that the proximal RNAs represented a different gene, and were named *Kis2* [70]. However, *Kis2* and *Xpcl1* overlap the two ends of the miR-106a~363 cluster, and thus probably represent two ends of a longer primary transcript. Uren *et al.* deep sequenced the viral insertions in $p53^{-/-}$ and $p19arf^{-/-}$ mice, enabling them to create an interaction network for genes that are frequent targets of viral insertions. In the case of *Xpcl1,* they found increased

numbers of co-integrations in combination with Zfhx1a, Pik3r5, Myc/Pvt1 and Smg6/Hic1/Ovca2. In contrast co-integration of *Xpcl1* and Flt3 occurred at reduced frequencies[91].

Many genes that are targeted by retroviruses in murine lymphomas have been well characterized. However, little was known about the global patterns of miRNA or protein-coding gene expression in the murine retroviral-induced lymphomas. In collaboration with Rosetta Inpharmatics, we used microarrays to characterize mRNA expression, and an RT-qPCR-based miRNA expression platform to characterize miRNA expression in M-MuLV lymphomas from $p27^{-/-}$ mice. The analysis included an assessment of global changes in miRNA expression within the tumors as well as identifying miRNA expression profiles associated with $p27^{-/-}$ genotype, or *Xpcl1* insertions. We also examined whether the global gene expression pattern in M-MuLV lymphomas is similar to lymphomas caused by other genetic mutations. To classify expression profiles associated with $p27^{-/-}$ and *Xpcl1* tumors, gene ontology terms enriched for genes associated with each tumor group were identified. Additionally, I validated four genes as targets of the miR-106a~363 cluster.

Results

Global miRNA expression in lymphomas vs. normal thymus

To measure global expression profiles of miRNAs in murine T-cell lymphomas, we utilized a miRNA qPCR platform developed by Rosetta Inpharmatics to quantify expression of 188 microRNAs from the original $p27^{Kip1}$ knockout M-MuLV screen.[135] The source material was frozen T-cell lymphomas with ($p27^{-/-}$) or without ($p27^{+/-}$ or $p27^{+/+}$) $p27^{Kip1}$ null mutations and for which the retroviral integration sites for Xpcl1 had been mapped (Table 2.1)[69]. Thymus from normal and $p27^{Kip1}$ knockout mice were used as controls. The abundance of specific microRNAs, calculated as copies per 10 pg total input RNA, varied over a wide range in both tumor and normal thymus (Fig. 2.1). Consistent with what has been reported in human cancers, when looking at the global miRNA expression profile we found that the majority of microRNAs were reduced in lymphomas relative to thymus based on total RNA input (Fig. 2.2 dashed red line as baseline)[136].

The normalization to total input RNA however fails to consider that proliferating tumor cells typically have a higher RNA content per cell than do normal tissues[137]. Since we did not know the cell numbers in our samples, I instead quantified the genomic DNA content of our samples. It is safe to assume that genomic DNA content is proportional to cell number, since others have shown that M-MuLV-induced lymphomas are near diploid[138]. Thus, I measured the RNA and DNA content in each tumor relative to tissue mass and made a similar assessment in normal thymus. On average, lymphomas contained 1.9-fold more RNA relative to genomic DNA abundance compared to normal thymus (Table 2.2). Standard curves

Table 2.1. The $p27^{Kip1}$ genotype and M-MuLV insertion status of tissues used to quantify mRNA expression in M-MuLV tumors

Mouse ID	Tissue	p27	Xpcl1	Myc	Jdp2
WT pool	Thymus	+/+	-	-	-
KO pool	Thymus	-/-	-	-	-
MM1-55	Thymus	-/-	-	-	-
K5-335	Tumor	+/+	-	+	-
K5-300	Tumor	+/+	-	+	-
K5-289	Tumor	+/+	-	-	+
K5-316	Tumor	+/+	-	-	-
K4-904	Tumor	+/+	-	-	-
K4-764	Tumor	+/-	+	+	-
K4-803	Tumor	+/-	+	-	-
K4-752	Tumor	+/-	+	-	-
K5-772	Tumor	-/-	+	+	-
K5-764	Tumor	-/-	+	+	-
K5-964	Tumor	-/-	+	-	-
K4-896	Tumor	-/-	+	-	-
K4-817	Tumor	-/-	+	-	-
K5-168	Tumor	-/-	-	+	+
K4-663	Tumor	-/-	-	+	+
K4-753	Tumor	-/-	-	+	-
K5-961	Tumor	-/-	-	-	-

For all analyses $p27^{+/+}$ and $p27^{+/-}$ were grouped together as non-null tumors

Table 2.2. Increased total RNA abundance in M-MuLV tumors compared to thymus when normalizing to genomic DNA

Tissue	RNA (µg)/ Tissue (mg)	DNA (µg)/ Tissue (mg)	RNA/DNA Ratio	Relative to Thymus
Tumor	8.10	9.23	0.88	1.93
Thymus	4.54	9.97	0.46	1

DNA and RNA was isolated from 10 tumors and 3 normal thymus

generated by 2-fold dilutions of lysed tissue demonstrated a high degree of linearity of my assay in DNA and RNA abundance relative to the mass of input tissue (R^2 = 0.985 for RNA, R^2 = 0.984 for DNA)(Fig. 2.2). When adjusting the total RNA content by 1.9x RNA per cell, I found that the number of miRNAs significantly increased in lymphomas is comparable to the number that are decreased (Fig. 2.2). Also, the total copies of miRNAs per cell in lymphomas was equivalent to normal tissue with a fold change of 1.08 ± 0.05 when comparing tumor vs. normal thymus. In other words, these tumors display an altered pattern of miRNA expression but not a global reduction in miRNA abundance.

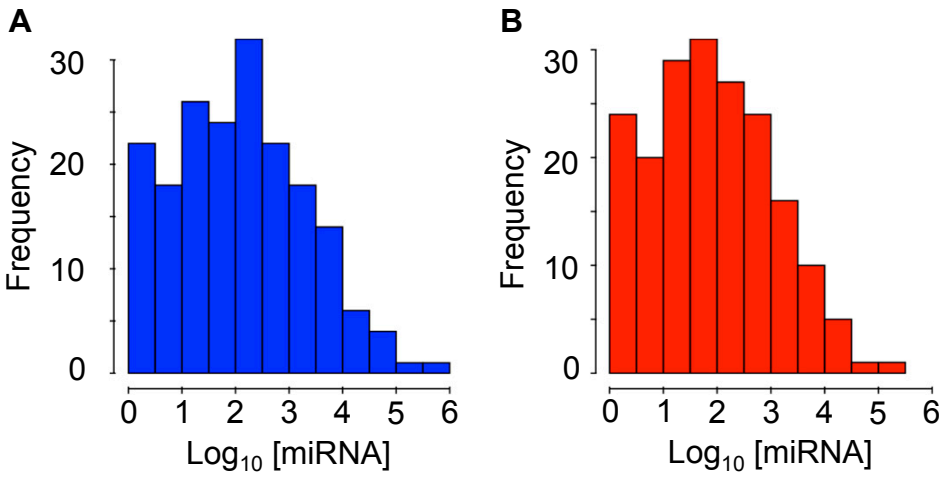

Figure 2.1 Distribution of miRNA abundance. The distribution of individual miRNA abundance in (A) normal thymus and (B) M-MuLV lymphomas based on concentration expressed as the number of copies per 10 pg of total RNA. Adapted from Kuppers *et al.*[147]

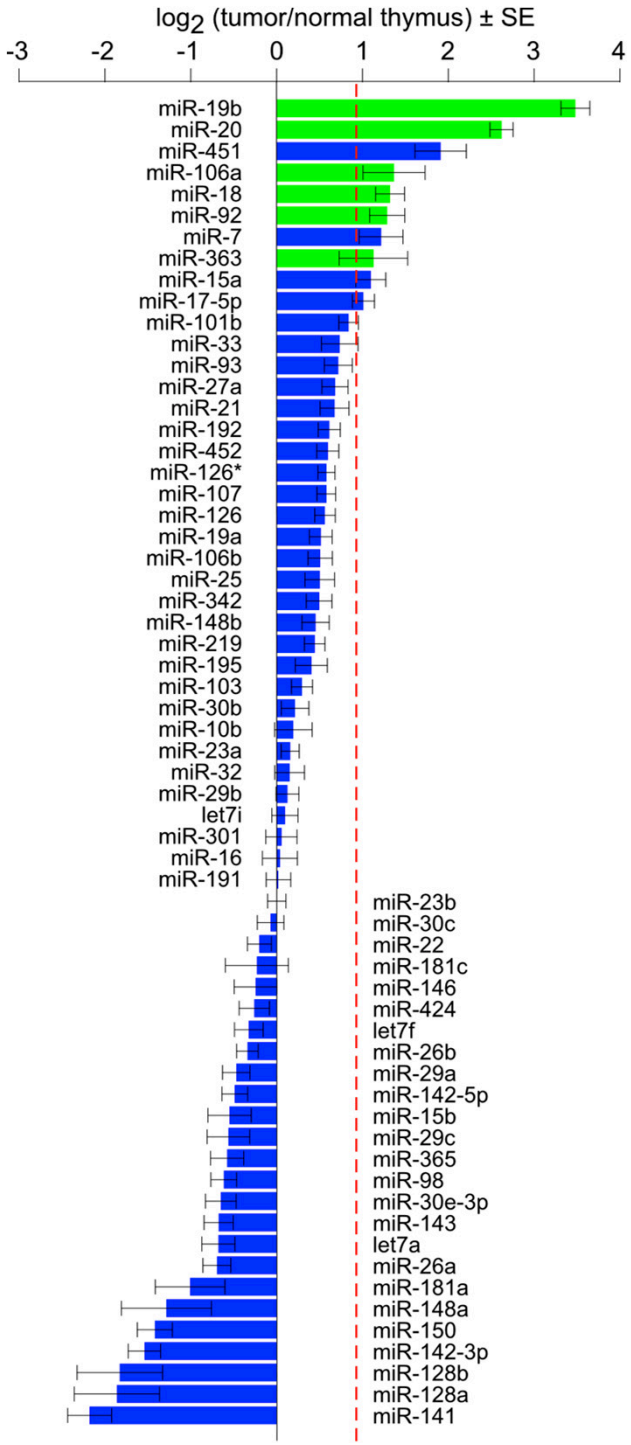

Figure 2.2 Altered miRNA expression in M-MuLV lymphomas. Change in expression of the 62 miRNAs with expression of at least 250 copies per cell when comparing tumor to normal thymus. The dashed red line represents the baseline expression level without normalization for differences in total RNA abundance in tumor and normal thymus. The miR-106a~363 miRNAs are represented in green. Adapted from Kuppers *et al.*[147]

miRNA expression profiles associated with Xpcl1 integration or deletion of p27^{Kip1}

Within the M-MuLV tumor samples, I compared the global microRNA expression profiles associated with p27^{Kip1} genotype (p27^{Kip1} null vs. wildtype), in addition to the presence or absence of viral integrations at *Xpcl1*. Unsupervised hierarchical clustering based on the abundance of individual miRNA did not strictly segregate tumor samples either by p27^{Kip1} genotype or by *Xpcl1* integration. This indicates that, for the majority of miRNA, neither of these factors are the major determinant of variability. Nonetheless, miRNAs in the mir-106a~363 cluster were among the most significantly increased in the tumors (Fig. 2.3A). We also assessed whether viral integrations at Xpcl1 are associated with expression of a distinct set of miRNA using a supervised analysis algorithm (PAM). This algorithm computed the false positive discovery rate (FDR) as a function of the number of significantly changed miRNA species. The median false positive discovery rate (FDR) was zero at 1 to 5 microRNAs but rose sharply at higher numbers. This indicates that there were only 5 microRNAs (miR-106a, miR-20b, miR-19b, miR-92, and miR-363), all members of the miR-106a~363 cluster, whose expression was associated with viral integration at *Xpcl1* (Fig. 2.3A). Expression of the sixth microRNA in the cluster, miR-18b, was not increased in Xpcl1^{+} tumors (Fig. 2.3A). In summary, viral integration at *Xpcl1* led to increased miR-106a~363 expression, but not overexpression of other miRNA.

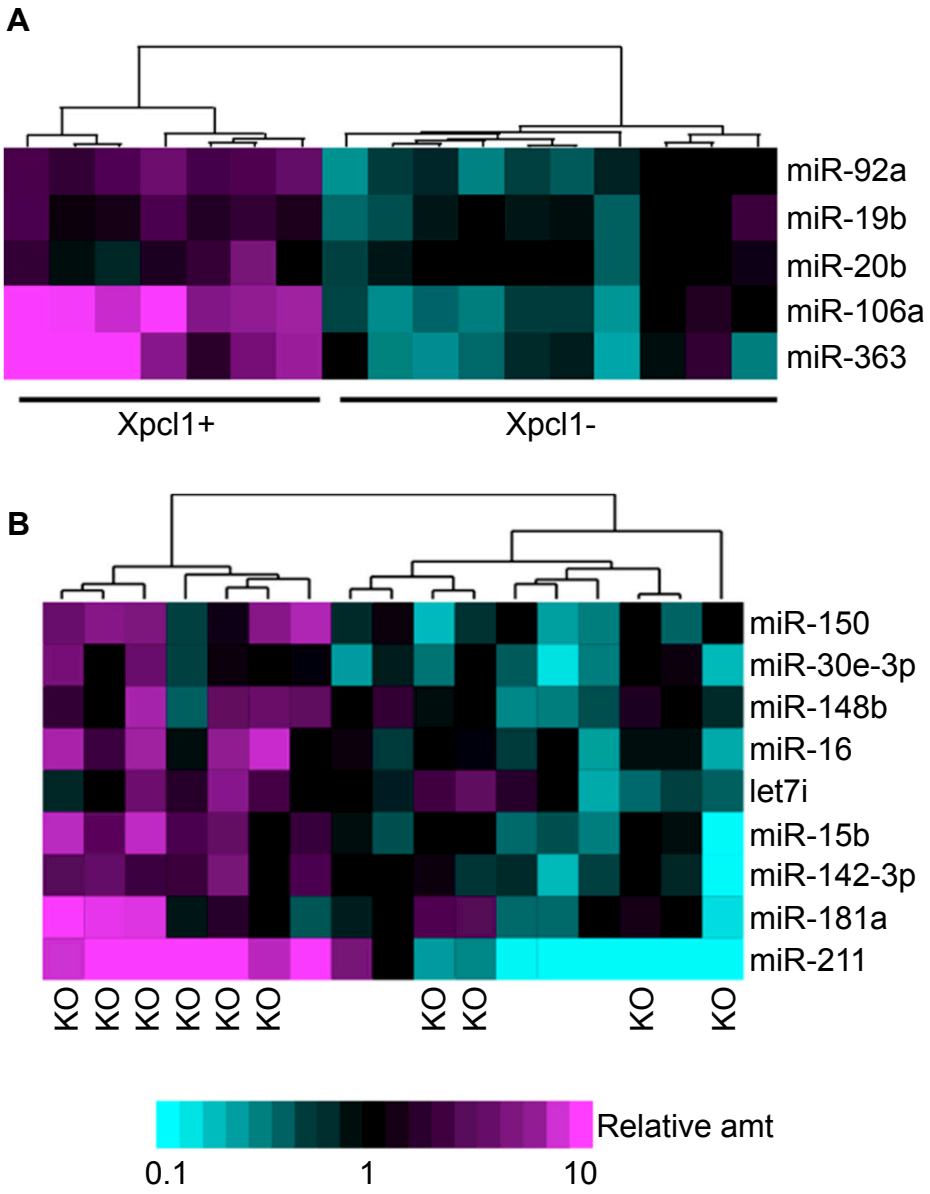

Figure 2.3 The miRNA expression profiles associated with Xpcl1 and p27$^{-/-}$ tumors. (A) A heat map of the 5 miRNAs with altered expression associated with Xpcl1 integrations utilizing a supervised analysis (PAM). The FDR was zero for the 5 miRNAs, all of which are members of the miR-106a~363 cluster and increased in expression. (B) The expression of the 9 miRNAs associated with loss of p27 in M-MuLV tumors by supervised analysis, although there was high variability among the tumors (FDR 30%). All 9 were increased expression and did not include any miR-106a~363 miRNAs. Adapted from Kuppers *et al.*[147]

One potential mechanism of cooperation between $p27^{Kip1}$ loss and *Xpcl1* integrations would be if $p27^{Kip1}$ deletion increased *Xpcl1* expression. This could occur through $p27^{Kip1}$ loss increasing the stability of the miRNA cluster at any stage from the pri- to mature miRNAs or by altering expression of genes associated with processing of the miRNA transcripts. To address this possibility we assessed whether $p27^{Kip1}$ loss was associated with altered miRNA expression in tumor samples. A supervised analysis suggests that 9 microRNAs are associated with the $p27^{Kip1}$ null genotype, although there is significant variability (FDR 30%)(Fig. 2.3B). However, these 9 miRNAs did not include any from the miR-106a~363 cluster. A second analysis, using only tumors without *Xpcl1* integrations, also does not identify an association between $p27^{Kip1}$ deletion and miR-106a~363 expression $p27^{Kip1}$ (data not shown). Thus, $p27^{Kip1}$ deletion did not increase miR-106a~363 expression in M-MuLV lymphomas, but it did alter the expression of other miRNAs.

Gene expression in M-MuLV induced tumors

Retroviral insertional mutagenesis in mice is a powerful tool to identify novel and cooperating oncogenes. However, no analyses have been done to determine how closely retroviral induced lymphomas mirror other T cell lymphomas, in general. More specifically, there are no prior reports of gene expression profiles for M-MuLV induced lymphomas. We therefore measured gene expression from the same experimental group of M-MuLV tumors, described above. Some of the samples were changed to meet more stringent RNA quality control guidelines for expression arrays. First, we compared the general pattern of gene expression in tumors compared to normal thymic tissue. The raw data was first normalized across all arrays as a function of the overall

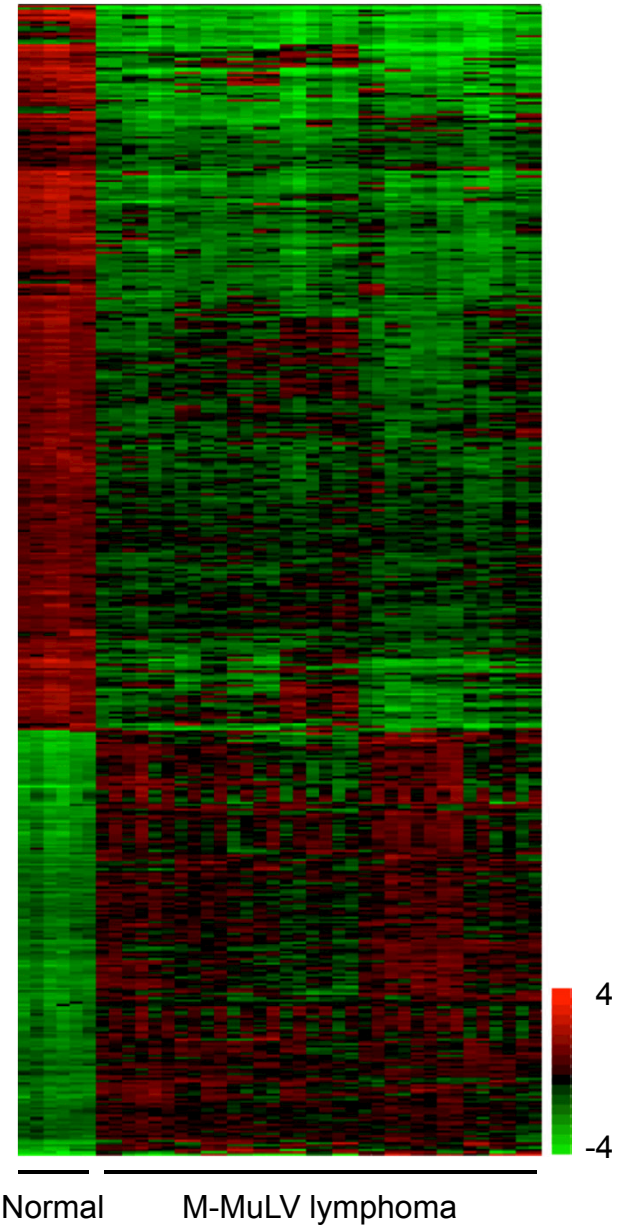

Figure 2.4 Gene expression in M-MuLV tumors and normal thymus. A heat map of mRNA expression for the top 5000 genes with altered expression in 22 M-MuLV tumors versus normal thymus. The expression levels are displayed on a Log_2 scale of microarray spot intensities with expression relative to gene-specific means. Tumors did not strictly segregate based on Xpcl1 insertions or p27 genotype. Increased expression is in red and decreased is in green. Adapted from Kuppers *et al.*[147]

intensity of individual features, and as a function of 2-dimensional feature locations using loess smoothing[139]. A supervised analysis (PAM) was used to identify genes differentially expressed in tumors compared to normal thymus. Several findings are immediately apparent in this analysis. The first is that there was a very large number of genes altered in tumors compared to normal thymus. The second finding is that gene expression in tumors was more heterogeneous than normal tissue (Fig. 2.4). In order to determine whether M-MuLV tumors have a gene expression pattern similar to other T-cell lymphomas, we compared the data to that previously reported for T-cell lymphomas induced by ß-catenin mutations in mice, and publically available in the Gene Expression Omnibus (GEO) database[140]. Since both studies included normal thymus, this was used as a common reference. In addition, to avoid platform specific bias, we compared expression ranks and calculated geometric means across the multiple samples (i.e. we did not assume a similar levels of sensitivity or Gaussian distribution of the raw sample data across the two platforms). When the gene expression rankings for the two data sets were compared a high degree of correlation was observed (Fig. 2.5). When plotted in two dimensions, the correlation is represented by the clustering of points in the upper right and lower left quadrants ($R^2 = 0.45$, $p < 2x10^{-16}$ Pearson correlation). If there was no correlation then the data points would be expected to be diffusely distributed across the entire plot.

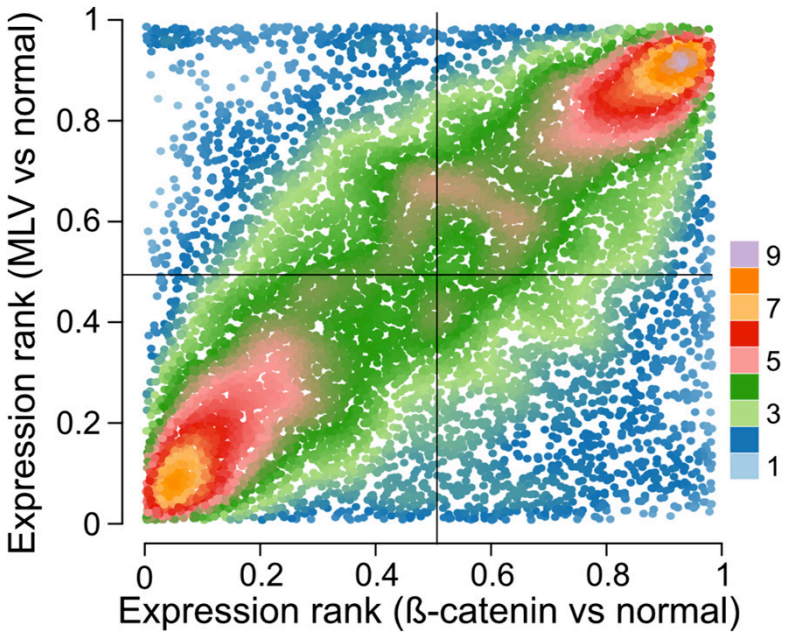

Figure 2.5 Comparison of gene expression in M-MuLV tumors versus β-catenin induced lymphomas. A comparison of expression rank of the 9804 genes with the highest level of change in expression in the M-MuLV tumors and β-catenin induced lymphomas. The density of points is color coded with genes decreased in expression clustered in the lower-left quadrant and those increased in expression in the upper-right quadrant. Adapted from Kuppers *et al.*[147]

To identify biological changes common to T cell lymphomas, ontologies for the 2500 genes with the highest PAM scores associated with lymphomas were determined. Genes with high levels of expression from both studies were enriched for the Gene Ontology biological function terms nucleic acid, protein metabolism and cell cycle (Table 2.3). In contrast, the terms T-cell function and inter- and intracellular signaling were enriched in genes with reduced expression in lymphomas (Table 2.3).

Table 2.3 Classification of genes with altered expression in M-MuLV tumors vs. normal thymus

Category	Biological Process	Observed	Expected	P-value
Tumors Down	Immunity and defense	225	95.45	9.26E-31
	Interferon-mediated immunity	39	6.08	4.97E-17
	T-cell mediated immunity	56	15.61	1.82E-13
	Cytokine mediated signaling pathway	53	17.18	4.40E-10
	Cell communication	142	83.07	1.11E-07
Tumors Up	Protein biosynthesis	59	10.6	1.26E-23
	Nucleoside metabolism	174	80.46	3.90E-22
	DNA replication	16	2.96	1.30E-05
	Cell cycle	42	24.04	1.31E-02
p27-/- Down	Immunity and defense	122	57	3.41E-13
	Complement-mediated immunity	14	2	1.12E-05
	Macrophage-mediated immunity	19	5	1.36E-03
	B-cell immunity	15	4	1.53E-02
p27-/- Up	Cell cycle	75	46.4	1.46E-03
	Protein phosphorylation	59	34.59	1.49E-02
	Cell cycle control	38	20.63	4.90E-02
Xpcl1 Down	Nucleoside, nucleotide metabolism	161	113	8.40E-05
	Cell cycle	55	33	1.19E-02
	Mitosis	26	12	6.51E-02
Xpcl1 Up	Immunity and defense	129	79	2.57E-06
	B-cell mediated immunity	18	6	1.91E-02
	T-cell mediated immunity	28	13	2.81E-02

This table contains select Biological Processes with the complete results available in Kuppers et al. 2011 Supporting Table 2 [151]. Genes with highest PAM scores were compared to the overall set of genes present on the array using Panther Biological Processes. For each tumor category the top 2500 genes associated with the tumor were analyzed. P-values are from the binomial test with Bonferroni correction for multiple testing.

Gene expression profiles of p27^{Kip1} null and Xpcl1^{+} tumors

To identify gene expression profiles associated with p27^{Kip1} loss or Xpcl1 integrations, within tumors, we excluded the normal thymus samples and compared the microarray expression profiles according to p27^{Kip1} genotype and *Xpcl1* integration status. In a supervised analysis, genes were ranked according to their PAM score and then tested for enrichment of gene ontology terms for the top 2500 genes altered in association with the p27^{Kip1} null genotype or with *Xpcl1* integration, using the Panther gene classification system[141]. In this analysis, statistical significance is a function of both the relative enrichment of classification terms and the size of the gene class, so we displayed results in circle plots showing all three parameters (Fig. 2.6). In the case of p27^{Kip1} null tumors, the classes of enriched genes (up: Cell cycle, down: Immunity) were similar to those enriched in tumors in general (Table 2.3, Fig. 2.6A,B). These results suggest that p27^{Kip1} loss enhances the general lymphoma phenotype, namely increased metabolism, proliferation and de-differentiation. Using the identical method, a separate analysis was done analyzing the pattern of gene expression associated with *Xpcl1* integrations. In this case, genes increased in association with *Xpcl1* were enriched for immune response, and genes exhibiting reduced expression included an excess of cell cycle genes (Table 2.3, Fig. 2.6C). In other words, similar classes of genes showed the opposite pattern of expression in association with *Xpcl1* integration compared to p27^{Kip1} deletion in tumors, or in comparison to the overall tumor phenotype. Among the tumors there was a partial overlap between *Xpcl1* insertions and p27^{Kip1} genotype, with 5 out of 8 Xpcl1^{+} tumors knocked out for p27^{Kip1}, and 4 out of 9 non-Xpcl1^{+} tumors lacking p27^{Kip1} (Table 2.3, Fig. 2.6B,C). Due to sample number limitations, we did not break

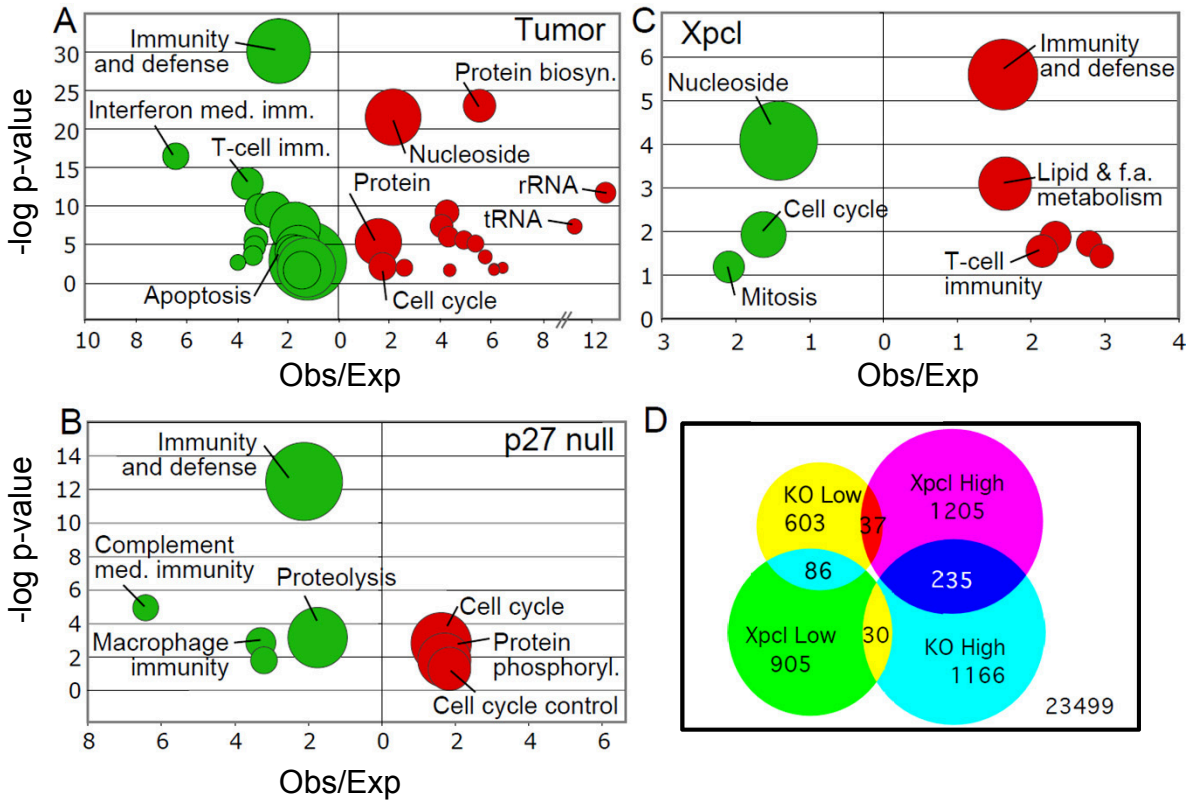

Figure 2.6 Altered gene expression associated with Xpcl1 and p27$^{-/-}$ tumors. (A) Biological function classes of the top 2500 genes associated with M-MuLV tumors vs. normal thymus are shown in a circle plot with statistical significance (P-values, binomial test with Bonferroni correction for multiple testing) plotted on the Y-axis and relative enrichment (observed/expected) plotted on the X-axis. Genes showing increased expression are shown in red and those with decreased expression are plotted in green. Circle diameters are proportional to the number of genes observed in each group. Within tumor samples, the functional classification of genes associated with (B) *p27^{Kip1}* knockout genotype or (C) *Xpcl1* integrations are shown. (D) The Venn diagram shows limited overlap amongst genes with decreased expression in association with tumors containing one mutation while simultaneously having increased expression in the other tumor type (ie. Xpcl Low vs. KO High). Adapted from Kuppers *et al.*[147]

the analysis down further and do pair-wise comparison's amongst all 4 p27^{Kip1}/Xpcl1 genotypes (i.e. p27null/Xpcl1^{+}, p27^{+}/Xpcl1^{+}, p27null/Xpcl1^{-}, and p27^{+}/Xpcl1^{-}), which could be compared 7 different ways. One could speculate that the opposite patterns of expression observed for p27null and Xpcl1^{+} tumors was due a specific set of genes

being highly altered in one of the overlapping groups, e.g. high levels of cell cycle gene expression in the $p27^{-/-}$; $Xpcl1^{-}$ tumors. We therefore determined the identities of the genes with altered expression with in association with $p27^{Kip1}$ deletion or Xpcl1 integration which were also functionally enriched. As is shown in the Venn diagram, the identities of genes associated with $Xpcl1^{+}$ or $p27^{-/-}$ were largely different from one another, despite having similar functional classifications (Fig. 2.7).

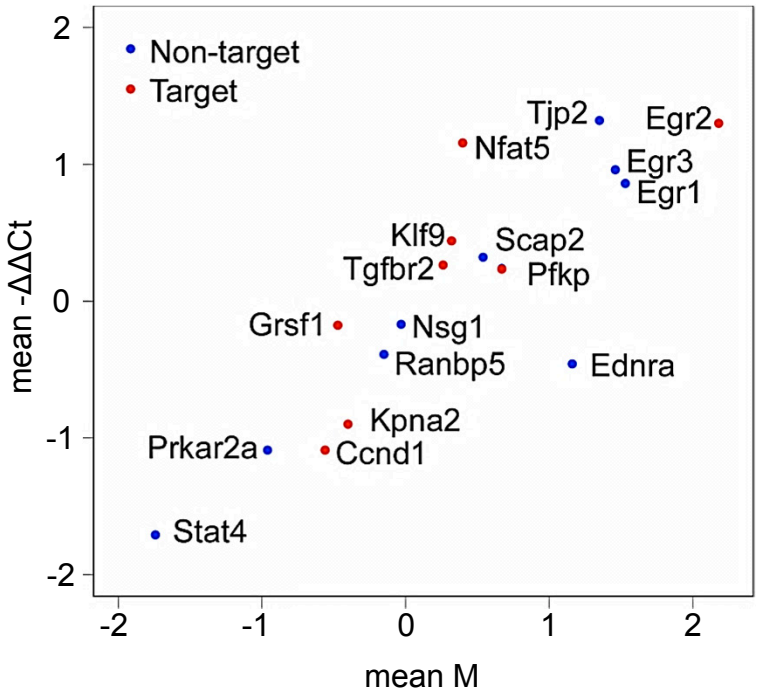

Figure 2.7 Correlation between gene expression changes on the M-MuLV microarrays and by qPCR. The expression of 17 genes altered to varying degrees on the microarrays, in association with *Xpcl1* insertions, were quantified by qPCR (mean –ΔΔCt). Expression measured by qPCR is plotted as the Ct difference between tumors with *Xpcl1* insertions versus those without insertions. Expression on the microarrays is plotted as the Log_2 change in expression of tumor versus normal thymus (mean M). Genes that are predicated targets of miR-106a~363 are in red. Adapted from Kuppers *et al.*[147]

In order to validate the accuracy of the array data, I quantified RNA expression levels of 17 genes by RT-qPCR (Fig. 2.8). The mean change in expression, with respect to *Xpcl1* integration status, varied widely and included both genes with increased and decreased expression. Eight of these genes are predicted targets of the miR-106a~363 miRNAs according to TargetScan algorithm. There was a strong correlation (R^2 = 0.91, p = $5x10^{-6}$, Pearson correlation) between mean expression levels determined by the microarrays and expression measured by the RT-qPCR assays. However, the predicted miR-106a~363 targets, included examples both of genes increased and of genes decreased in $Xpcl1^+$ tumors.

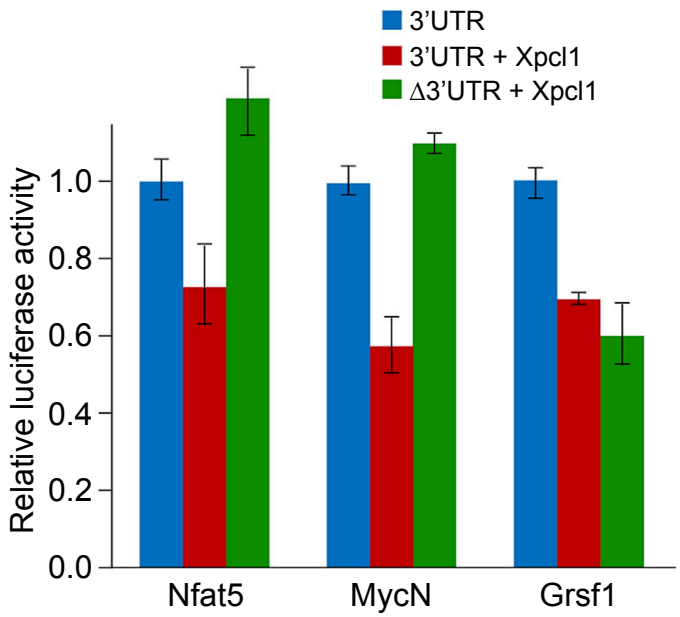

Figure 2.8 Validation of miR-106a~363 targets by luciferase reporter. Luciferase activity was measured for reporter constructs containing the 3' UTRs for Grsf1, Nfat5 or MycN. Each reporter was co-transfected with pCIG-vector or pCIG-Xpcl1 and pRL-TK as a transfection control. The predicted miRNA binding sites in the 3' UTRs were also mutated (Δ3' UTR). Adapted from Kuppers *et al.*[147]

Xpcl1 target gene expression

To identify potential miR-106a~363 miRNA targets relevant to tumorigenesis, we determined whether tumors with Xpcl1 integrations exhibited reduced expression of genes predicted to be targeted by the miRNAs. The TargetScan database contained approximately 2,000 potential gene targets of the miRNAs in the miR-106a~363 cluster. Within tumors, 500 miR-106a~363 target genes displayed reduced expression in association with *Xpcl1* integration. A gene analysis of predicted target genes reduced in association with *Xpcl1* integrations demonstrated a relative enrichment of genes with the biological functions terms Oncogenesis, and Cell Cycle (Table 2.4). On the whole, being a predicted target of a miR-106a~363 miRNA was not a good predictor of whether a gene was decreased in Xpcl1$^+$ tumors. Indeed, the majority of predicted targets exhibited increases or no change in expression in Xpcl1$^+$ lymphomas.

Table 2.4 Biological Process of miR-106a~363 targets with reduced expression in Xpcl1$^+$ tumors

Biological Process	Observed	Expected	P-value
Oncogenesis	21	9	2.20E-02
Cell cycle	35	20	5.20E-02

Panther biological process terms for the 500 miR-106a~363 predicted target genes with reduced expression in Xpcl1+ tumors relative to all genes present on the microarrays. Table is adapted from Kuppers et al. 2011[151].

The variability of target gene expression in Xpcl1^{+} tumors brings in to question the ability of TargetScan (or any bioinformatic algorithm) to predict biochemical changes *in vivo*. The alternative explanation is that biological systems, tumors in particular, are highly variable, and that a myriad of changes can occur through secondary effects. To address this issue, I selected four predicted targets whose expression displayed varying levels of expression with respect to *Xpcl1* insertions. Among these, N-myc and Grsf1 were reduced in association with *Xpcl1* viral integration, Tgfbr2 was unchanged, and Nfat5 was modestly increased. I cloned the 3'UTR, including the miRNA target sequences, of the four genes onto the 3' end of luciferase to generate reporter constructs. I then assayed the impact of miR-106a~363 cotransfection on the expression of these 3'UTR-luciferase reporters. In all cases, co-transfection of a 1 kb *Xpcl1* genomic fragment encompassing miR-106a~363 reduced expression of the 3'UTR reporter constructs (Fig. 2.9, 2.10). Additionally, mutation of seed sequences in the predicted 3' UTR miRNA binding sites prevented the inhibitory effect of miR-106a~363 on the expression of Nfat5 and N-myc, but not Grsf1 (Fig. 2.9). The failure to restore expression by mutating the Grsf1 reporter maybe due to the presence of non-canonical target-sites in the 3'UTR that were not identified by TargetScan. In the case of Tgfbr2, I also examined whether *Xpcl1* may have downstream effects on the signal transduction. Co-transfection of *Xpcl1* not only decreased the expression level of endogenous Tgfbr2, as assayed by RT-qPCR, it also decreased TGF-beta signaling as measured by the p3TP-Lux reporter construct (Fig. 2.9)[142].

N-myc has been shown to inhibit p27^{Kip1} expression in neuroblastoma through upregulation of the Skp2 ubiquitin ligase, which degrades p27^{Kip1} protein. Likewise, c-

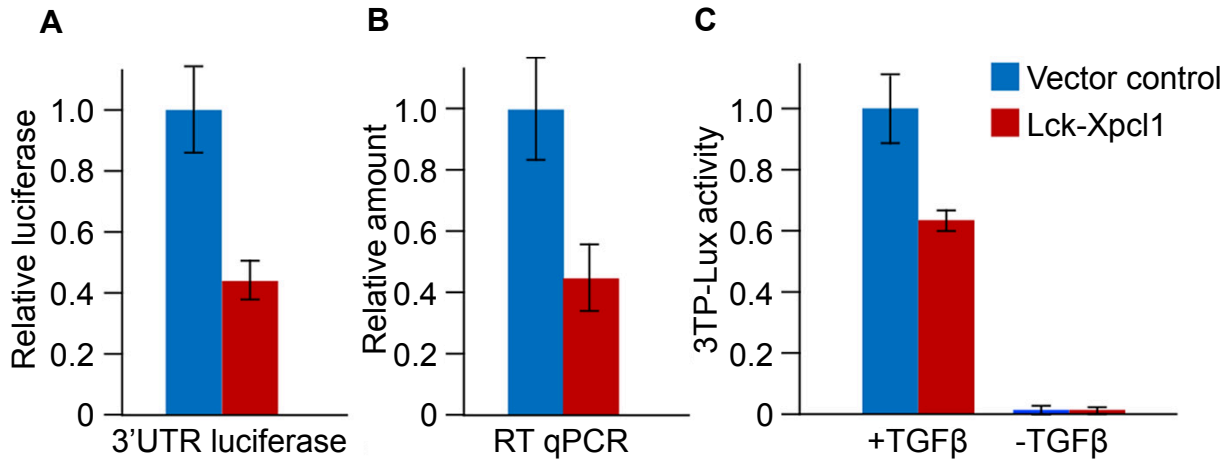

Figure 2.9 Regulation of Tgfbr2 by miR-106a~363. (A) Tgfbr2 expression measured by a 3' UTR luciferase reporter assay. (B) Expression of Tgfbr2 mRNA expression measured by qPCR with or without miR-106a~363 expression. (C) Downstream Tgfβ signaling, as measured by the 3T3-Lux reporter, with or without miR-106a~363 expression. Adapted from Kuppers *et al.*[147]

myc inhibits $p27^{Kip1}$ expression in a variety of contexts. I therefore tested the hypothesis that downregulation of N-myc might alter expression of $p27^{Kip1}$ in T-cells. I co-transfected a luciferase reporter containing the $p27^{Kip1}$ promoter along with either pCS2-N-myc or pBABE-cMyc into mouse SV40 T-cells (Fig. 2.10). In the case of cMyc, I was able to recapitulate the ability of the gene to inhibit $p27^{Kip1}$ expression. However, in the case of N-myc, rather than inhibiting $p27^{Kip1}$ expression, I observed a small increase in $p27^{Kip1}$ expression. These results do not support the hypothesis that inhibition of N-myc by miR-106a~363 enhances tumorigenesis in T-cells via reduced $p27^{Kip1}$.

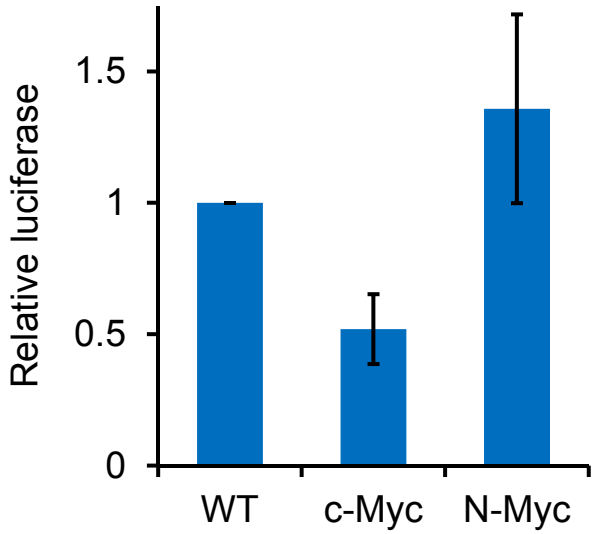

Figure 2.10 Regulation of p27 expression by c-Myc and N-Myc in T cells. Luciferase activity measured from the pGL2-p27 promoter luciferase reporter when co-transfected with pBABE-cMyc or pCS2-Nmyc into SV40-180 cells.

Identification of miRNA targets by Ago2 immunoprecipitation

Since, in the M-MuLV study, there was no correlation between expression of miR-106a~363 predicted targets on microarrays and the *Xpcl1* status of tumors, I was interested in developing a new approach to identify miRNA target genes. Ago2 HITS/CLIP employs immunoprecipitation of RNA cross-linked Ago2 followed by cDNA generation and high throughput sequencing. It has been utilized to identify global miRNA targets, but not to identify genes targeted by the overexpression of specific miRNAs[50]. Therefore my initial aim has been to validate that Ago2 HITS/CLIP can detect an enrichment of target genes when a miRNA of interest is overexpressed. The end goal is to utilize Ago2 HITS/CLIP to identify miR-106a~363 targets by comparing wildtype thymus to Lx^{+} thymus.

The initial HITS/CLIP protocol had a very low yield of material at the end to sequence, requiring extensive pre-sequencing amplification. The protocol utilizes UV crosslinking to stabilize the Ago2/mRNA/miRNA complex, which prevents modifications to the components which may alter the interaction. However, the downside to this method is that it produces very low yields of crosslinked material and can cause nicking of the RNA. To see if I could further optimize the crosslinking to increase product yields, I also tested out the use of paraformaldehyde. I crosslinked 293T cells extracts, transfected with either pSM30-Xpcl1 or pSM30-empty, with UV or varying concentrations of paraformaldehyde followed by Ago2 IP. I quantified the effectiveness of each crosslinking method by qPCR for miR-106a and miR-20b. In both cases, paraformaldehyde crosslinking resulted in 2-4 fold higher yields of the two miRNAs compared to UV versus the yield with no crosslinking (Fig. 2.11A).

To validate that overexpression of miR-106a~363 results in enrichment of target genes by HITS/CLIP, I performed the entire procedure short of Solexa sequencing utilizing 293T extracts as described for testing crosslinking. The yield of two validated miR-106a~363 targets, $p21^{Cip1}$ and Tgfbr2, was increased by 3.5-4 fold when the miRNA cluster was overexpressed (Fig. 2.11B). I also Sanger sequenced a number of random clones of the HITS/CLIP products to determine the quality of the final material. The yields were comparable to what has previously been reported with 57% of the sequences found within UTRs and 69% within coding genes (Fig. 2.11C)[50].

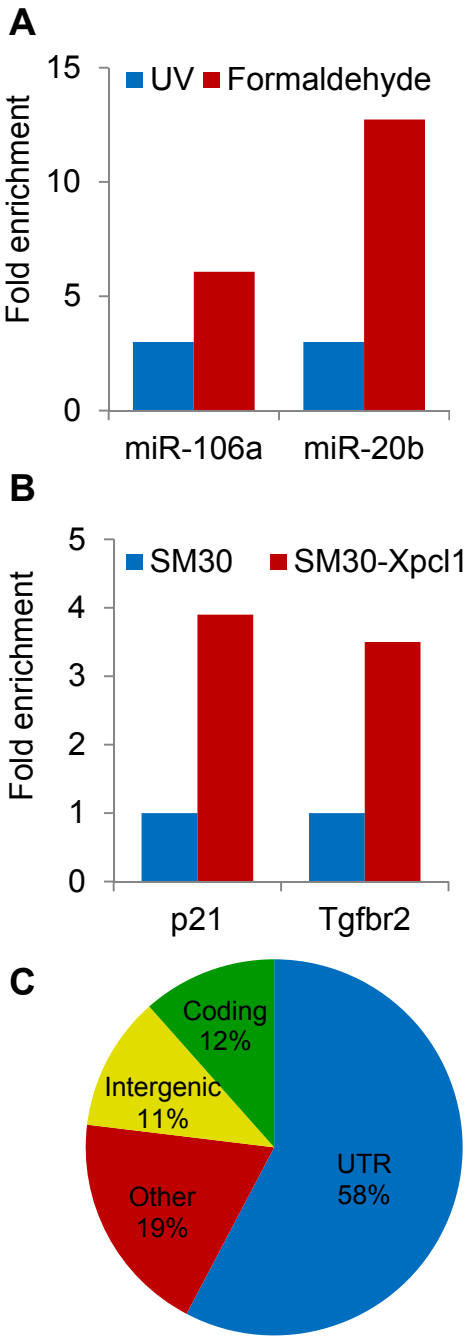

Figure 2.11 Optimization and validation of Ago2 HITS/CLIP for detection of miR-106a~363 targets. (A) Cell extracts from 293T cells transfected with pSM30-Xpcl1 were crosslinked with UV or 1% paraformaldehyde followed by Ago2 IP. Expression of miR-106a and 20b from the immunoprecipitated RNA was then quantified by RT-qPCR. Expression is presented as fold enrichment in paraformaldehyde versus UV. (B) The quantity of HITS/CLIP tags isolated for known miR-106a~363 targets was quantified by qPCR from samples with or without overexpression of the miR-106a~363 miRNAs. (C) A pie chart of the sequence origin of 22 random HITS/CLIP tags sequenced by Sanger sequencing.

Discussion

Retroviral mutagenesis in mice has been extensively used to identify novel oncogenes; yet no studies had previously examined global mRNA or miRNA expression profiles in the resulting lymphomas. The morphological, growth, and cell surface immunophenotypes of M-MuLV induced tumors characterizes them in the general category of high grade T-cell lymphomas. Still, it is unknown how closely these retroviral-induced lymphomas mirror tumors arising from targeted mutations or oncogene overexpression. We found a high concordance between the global pattern of gene expression between M-MuLV induced lymphomas and T-cell lymphomas induced by ß-catenin mutations (Fig. 2.5)[140]. Thus, we identified a large number of genes which appear to be generalized markers of high grade lymphomas. The functional classification of the genes altered in these tumors include up regulation of genes involved in nucleic acid and protein metabolism as well as the cell cycle, while genes involved in T cell immunity were down regulated. High rates of metabolism and altered cell cycle gene expression is expected in these tumors due to their high proliferation rate. The global reduction in immune gene expression is consistent with a de-differentiated phenotype, as one might expect with a lymphoid progenitor or embryonic cell type[143].

Others have reported reduced miRNA expression in tumors and some have taken this to be a general characteristic of cancer cells[136]. Along with this observation, it has been reported that cancer cells have reduced function of miRNA biosynthetic machinery, and that this reduction enhances the tumor phenotype[61,144]. However, it has long been known that proliferating cells, and many tumor cells often express an

increased amount of RNA compared to normal tissues[137,145]. Therefore, it was surprising to us, that the prior reports compared miRNA expression in cancers vs. normal tissue, relative to total RNA abundance and not on a per-cell basis. In the case of M-MuLV tumors compared to normal thymic tissue, I also found reduced global miRNA expression when normalized to total input RNA. However, in consideration of the likely changes in total RNA abundance of these highly proliferative T-cell lymphomas, I took additional steps to estimate the total RNA abundance on a per cell basis. Although counting cells is not feasible in frozen specimens, I was able to take advantage of the fact that M-MuLV tumors have a normal diploid chromosome number, and thus was able to estimate cell number per gram based by quantifying genomic DNA from each tumor sample. In M-MuLV lymphomas, when I quantified RNA on a per cell basis, I found that the tumor cells had twice the amount of total RNA compared to normal thymus. In contrast miRNA abundance was almost exactly the same as normal tissue. In other words the relative reduction of miRNA abundance in lymphomas is just an artifact of the comparatively high level of total RNA in these tumors. Even though the total miRNA abundance was unchanged in the tumors, the expression profile of specific miRNAs was significantly altered in tumors compared to normal thymus. Additionally, the ability of miRNAs to effectively inhibit expression of target genes may be reduced by a relative increase in global mRNA abundance. However, the reduction in miRNA/target RNA interactions is likely due to global increases in mRNA expression and not due to defects in miRNA biogenesis. Whether, this is a generalizable phenomenon, or is specific to these high grade lymphomas is unknown, but warrants further study.

While other retroviral studies have identified *Xpcl1* as a viral insertion site, global expression of miRNA has never been studied. The miRNA expression profile I found altered in association with Xpcl1 integration consists of only 5 miRNAs, all in the miR-106a~363 cluster. This clearly demonstrates that viral insertions at the Xpcl1 results in miR-106a~363 overexpression. A theoretical mechanism of cooperation between Xpcl1 insertions and $p27^{Kip1}$ loss, would be if loss of $p27^{Kip1}$ increases expression miR-106a~363, e.g. through altered RNA processing or stability. I found this not to be the case, with the miRNA expression profiles associated with $p27^{Kip1}$ loss, with or without $Xpcl1^{+}$ insertions, did not include the miR-106a~363 miRNAs.

Since $p27^{Kip1}$ loss does not directly affect miR-106a~363 expression, I hypothesized that the loss of $p27^{Kip1}$ and expression of the miRNAs impacted functionally similar pathways, such as cell cycle gene activation, augmenting the effects of one another. Alternatively, they may impact parallel processes which, in combination, increase the aggressiveness of the lymphomas, such as increased cell proliferation and reduced apoptosis. To test these hypotheses, I determined the functional classes of genes whose altered expression was characteristic of $p27^{Kip1}$ null lymphomas and compared this with the pattern of expression associated with Xpcl1 integration. It was perhaps not surprising that we observed an enrichment for cell cycle and metabolism genes amongst genes increased in association with $p27^{Kip1}$ deletion. With the additional finding of reduced expression of immunity genes the profile associated with $p27^{Kip1}$ deletion closely parallels that of tumors vs. normal thymus. This is consistent with the characterization of $p27^{Kip1}$ loss enhancing the tumor expression phenotype. Surprisingly, the pattern of gene expression associated with Xpcl1

integrations was opposite that of $p27^{Kip1}$ null tumors. In this case cell cycle genes were enriched amongst those exhibiting reduced expression whereas immunity genes were more abundant in those with increased expression (Fig. 2.7). Additionally, in both cases the altered genes contained a mixture of potential tumor suppressors and oncogenes. There are at least two different explanations as to why $p27^{Kip1}$ loss and Xpcl1 insertions induce gene expression profiles that mirror one another. The biological function terms do not distinguish between activators or inhibitors of the respective processes. Thus $p27^{Kip1}$ loss and Xpcl1 deletion might both promote cell cycle proliferation by different approaches. In the case of $p27^{Kip1}$ deletion there may be an abundance of cell cycle gene activators that are increased whereas Xpcl1 overexpression may induce repression of cell cycle inhibitors. However, inspection of the genes altered in each case does not reveal obvious examples of this. The second possibility is that miR-106a~363 has a mixture of oncogenic and tumor suppressive effects, and that $p27^{Kip1}$ loss helps to overcome the tumor suppressive effects of the miRNAs. As for the latter possibility, we have shown that Xpcl1 downregulates N-myc, a well-known oncogene[146]. Others have shown that members of the miR-106a~363 and miR-17~92 clusters have tumor suppressive functions in certain tumor types[94-97].The miR-106a~363 cluster is predicted to target over 2,000 genes, so its targeting a combination of oncogenes and tumor suppressors is not surprising.

One method of identifying genes targeted by the miRNAs in the lymphomas is to compare the list of miR-106a~363 predicted targets to those genes exhibiting decreased expression in association with *Xpcl1* integration. Based on those criteria, 52% of genes that are miR-106a~363 predicted targets were reduced in lymphomas.

However, a similar assessment of the expression of all the predicted target genes in the murine genome revealed a similar number exhibiting reduced expression in tumors. Therefore, it appears that reduction in expression of miRNA target genes is a general characteristic of lymphomas. The reason for this is unclear, but given that miRNAs are more likely to target certain classes of genes, their targets may, coincidentally, be those also reduced in highly proliferative tumor cells. The practical implication of this observation is that it calls in to question our ability to identify specific miR-106a~363 targets responsible for oncogenesis based on expression data alone.

Using a 3'UTR reporter assays, I was able to verify the ability of miR-106a~363 to directly inhibit expression of 4 predicted targets (N-myc, Grsf1, Nfat5 and Tgfbr2). Of these only 2 (N-myc and Grsf1) were reduced in association with *Xpcl1* integration in tumors, further illustrating the point made above. In part this discrepancy may be due to luciferase assays functioning at the protein level and thus measure the combined effects of miRNA on RNA stability as well as protein translation. In contrast, microarrays measure RNA abundance and thus may only pick up the effect of miRNAs on target RNA stability. Another issue is that gene expression is highly variable within tumor cells and can vary through a myriad of secondary effects. A luciferase reporter assay, in contrast, does not contain promoter or protein-coding sequences of the target gene and thus is relatively immune to secondary effects. The magnitude of the reduction in luciferase activity that I observed varied from 20-60%, which is consistent with what is commonly reported for miRNA gene targeting but which may not be easily observed on an expression microarray. In summary, the *Xpcl1* miRNAs are likely to have broad effects on gene expression, consistent with target gene predictions, but that these

effects are often quite limited and of questionable biological significance. The remaining challenge is to find the genes actively targeted by these miRNAs that are of functional significance.

Materials and Methods

Animals and tumor samples

Frozen tumor samples were previously taken from $p27^{Kip1}$ knockout mice ($p27^{-/-}$, $p27^{+/-}$, and $p27^{+/+}$) infected as neonates with Maloney Murine Leukemia Virus (M-MuLV), and have been previously surveyed for the M-MuLV proviral genomic integration sites. They were characterized for the presence or absence of M-MuLV integrations at the Xpcl1 locus and Myc family members[69]. The $p27^{Kip1}$ genotypes of the tumor samples were balanced with 9 of the samples being *$p27^{Kip1}$* null, and 8 of the samples containing *Xpcl1* viral integrations, 4 of which were both $p27^{Kip1}$ null and $Xpcl1^{+}$ (Table 2.1). Frozen whole thymus from uninfected animals, on the same 129S4 x C57BL/6J F1 hybrid strain background, was used for comparisons. The prior animal work was conducted according to national guidelines (OLAW) and approved by the IACUC of the Fred Hutchinson Cancer Research Center. Animals had been observed daily and were euthanized if they developed signs of morbidity, palpable tumors greater than 1 cm. diameter, or age > 1 year.

MicroRNA quantification and normalization

Expression of individual miRNAs was determined using a quantitative primer-extension PCR assay[135]. The miRNA is converted to cDNA using a miRNA specific primer that contains a tail on the end using SuperScript III reverse transcriptase. The

miRNAs are then quantified by SYBR green qPCR with a miRNA specific primer which contains LNA and a primer specific to the tail on the RT primer. Ct values were converted to copy numbers by comparison to standard curves generated using single stranded mature miRNAs to calculate miRNA copies per 10 pg of input RNA. The total RNA to DNA ratios of each tumor sample was determined by purifying total RNA and genomic DNA from weighed samples (<5mg) under non-saturating conditions on nucleic acid biding columns (RNeasy and DNeasy, QIAgen). The RNA and DNA were quantified using the ND-1000 (Thermo). The pamr software package for R (R-project.org, BioConductor.org) was used to identify miRNA associated with Xpcl1 integration and $p27^{Kip1}$ genotype[147]. The top miRNAs associated with $p27^{Kip1}$ genotype and Xpcl1 integration are shown in heat maps where quantities of individual miRNAs are displayed relative to the mean expression value of the same miRNAs across all samples. Hierarchical clustering was used to group samples post hoc using Cluster 3.0 software with Euclidean distance and complete linkage.

Microarray analysis

Tissues were split, weighed and then total RNA was isolated. RNA was prepared with Trizol (Invitrogen) following the protocol for miRNA isolation, which uses 1.5 volumes of isopropanol to increase the efficiency of miRNA precipitation. Trizol prepped total RNA was additionally treated with DNAseI (RNAse free, Roche) and purified with RNeasy mini columns (Qiagen). RNA was quantified using Ribogreen (Invitrogen) fluorescence. RNA was amplified and labeled with Cy5 and Cy3 as previously described[148]. Labeled RNA pooled from 17 tumor samples and 3 normal thymus formed a common reference and were co-hybridized vs. sample RNA in a two

color format on duplicate custom murine oligonucleotide arrays (Agilent, GEO accession GPL8525) (n=40 arrays).

$Log_{(2)}$ ratios of fluorescence intensities (experimental sample vs. pooled reference) were normalized by intensity-dependent Loess followed by 2-dimensional location-dependent loess using the marray Bioconductor package without local background subtraction or scaling[139]. Missing (software flagged features) values were imputed by the K-nearest neighbor method, and genes associated with tumors vs. normal were determined with the PAM algorithm, using the pamr BioConductor package[149]. We compared relative gene expression of tumors vs. normal, ranked by their PAM scores to similarly processed raw data for ß-catenin induced tumors obtained from the GEO repository[140]. Both studies included normal thymus so we used this as a common reference. Platform specific bias was avoided by comparing ranks of expression data (expressed as log tumor/normal) and calculating the geometric means across multiple samples. This approach is equivalent to the Rank Product (RP) method, which was shown to be robust for comparing gene expression profiles[150]. Likewise we analyzed our M-MuLV tumor data for genes associated with either Xpcl1 integration or $p27^{Kip1}$ genotype (PAM scores listed in Supporting Table 3 of Kuppers 2011[151]. Data processing was streamlined with custom wrapper functions contained in the ArrayFun package (available at http://labs.fhcrc.org/fero/R/ArrayFun.html). This package includes functions, (array.getGEO, array.readGEO), that downloads data from these 40 microarrays, along with the sample description table, from the GEO FTP site directly into R. Both MIAME compliant raw and normalized data are available at the GEO data repository (accession GSE16005)[152]. An R script that outlines obtaining raw data from

the GEO repository and recapitulates the data processing steps is included as Supporting data file 6 in Kuppers et al. 2011[151].

We used the “compare gene list” tool of the Panther Classification System (http://www.pantherdb.org) In order to determine the enrichment of biological function terms in genes of interest[141]. We input the top 2500 Entrez Gene IDs (ranked by PAM scores, above) and compared this to the entire set genes on the arrays. Terms over-represented in the genes of interest (p-values ≤ 0.05, binomial test) are shown in (Table 2.3). RT-qPCR validation of the microarray results was done using aliquots of the RNA run on the arrays. Reverse transcription was performed using 1 ug of total RNA with an oligo dT primer following the standard Superscript III (Invitrogen) protocol. SYBR Green qPCR was performed using primer pairs which spanned intron junctions using an ABI 7900 thermocycler.

MicroRNA target validation

129S4 mouse genomic Xpcl1 DNA was isolated from a phage library. A 1.04 kB fragment containing the entire miR-106a~363 miRNA cluster was subcloned into pCIG (courtesy of Andy McMahon) with the chicken B-actin promoter, the pSM30 vector (courtesy of Muneesh Tewari) and the p1026x vector with the Lck promoter (courtesy of Brian Iritani)[153-155]. Cloning of the vectors is described in greater detail in Chapter 3 Material and Methods under Mice. Genomic 3'UTR DNA segments for putative target genes (N-myc, Tgfbr2, Grsf1, and Nfat5) were PCR amplified from mouse 129S4 genomic DNA, cloned into pGL3-control (Promega), a luciferase reporter with the SV40 promoter, and verified by sequencing. Three or four bases of miRNA seed sequence, in the UTR of predicted target genes, were mutated using the QuickChange Mutagenesis

Kit (Agilent, #210513) with oligonucleotides, listed in Kuppers 2011 Table S4[151]. The $p27^{Kip1}$ promoter luciferase reporter has been previously described (courtesy of James Roberts)[103]. The pCS2-N-Myc vector and the pBABE-cMYC vector was provided by Robert Eisenman.

Wildtype and mutant 3' UTR reporter constructs were co-transfected (in triplicate) with pSM30-Xpcl1 vs. empty vector and pRL-TK (Promega) into 293T cells using Lipofectamine 2000 (Invitrogen). Tgfbr2 3'UTR luciferase assays compared pCIG-Xpcl1 vs. empty vector. Luciferase activity was assayed at 48 hrs. and adjusted for renilla activity. To quantify the effect on Tgfbr2 mRNA expression and Tgf-beta signaling, murine SV40-180 T-cells were transfected by electroporation with either p1026x–Xpcl1 or empty vector. RNA was isolated at 48h and Tgfbr2 qPCR was done, as described above. To measure Tgf-beta signaling the p3TP-Lux reporter of TGF-beta signalling (courtesy of William Grady) was additionally transfected. The cells were treated with porcine TGF-beta 1 (5 ng/mL, R&D Systems) starting at 24 hrs. post-transfection and luciferase activity was assayed at 48h[156]. The transfection of each construct and its controls were performed in triplicate or quadruplicate. To measure the effect of the myc proteins on $p27^{Kip1}$ expression the pGL2-$p27^{Kip1}$ vector was co-transfected with either pCS2-N-myc or pBABE-cMyc and pRL-TK in triplicate. Luciferase activity was assessed 48h post-transfection.

Chapter 3: The Role of miR-106a~363 in Mouse Development

Introduction

The role of miRNAs in T cell development is still largely not known. Utilizing high throughput sequencing of small RNAs, a global analysis of miRNA expression across the stages of T cell development identified a number of miRNAs that are differentially expressed[76]. Additionally, gene expression analysis found that targets of the miR-17 family and miR-92 were repressed in the late DN population[76]. These results suggest that miR-106a~363 and/or its paralogous clusters may play a role in regulating the developmental transition from DN to DP thymocytes.

Further evidence that miRNAs play an important role in T cell development comes from the conditional knockout of Dicer by Lck-Cre and CD4-Cre during early and late T cell development, respectively[157,158]. In the case of the Lck-Cre, total T cell numbers past the DN stage were reduced 10-fold due to a defect in αβ T cells, and increased cell death[157]. T cell development continued normally for those cells making it to the DP stage, and development of the γδ T cell lineage was relatively increased[157]. In contrast, when Dicer was knocked out by CD4-Cre, thymocyte development was largely unaffected, but, the number of peripheral T cells was significantly reduced. Furthermore, decreased proliferation and increased apoptosis was observed in CD4+ T cells[158]. The differences in the experimental results may be due to the timing of Dicer deletion in the respective model systems and, together, the studies indicate that miRNAs are important for T cell survival and proliferation.

The high degree of evolutionary conservation of miR-106a~363 implies that it has important biological functions. Elevated expression of the miRNAs in M-MuLV

lymphomas further suggests that they may be involved in regulating T cell biology. To address the role of miR-106a~363 in T cell development and lymphomagenesis, I determined the expression profile of the miRNAs during T cell development, and generated a transgenic mouse model forcing expression of the miRNAs in T cells. To identify other relevant tissues in which to study the function of miR-106a~363, I characterized its global expression and generated a transgenic mouse model globally expressing the miRNAs.

Results

Tissue specific expression of miR-106a~363 and paralogs

The pattern of tissue and cell-type expression of the miR-106a~363 miRNAs is not well characterized. To quantify expression of individual miRNAs of the miR-106a~363 cluster, as well as the paralogous miR-17~92 and miR-106b~25 clusters, I adapted a Taqman miRNA RT-qPCR assay for use with SYBR green[159]. This method utilizes a hairpin RT primer to minimize cross detection of longer pri-miRNA and pre-miRNAs, followed by qPCR with miRNA-specific primers. Shown in Figure 3.1A, is the expression of the 4 most highly expressed miR-106a~363 miRNAs in various tissues relative to their expression in thymus. MicroRNAs miR-18b and miR-363 are not included because I was only able to detect very low levels of expression. Expression of the two miR-106a~363 specific miRNAs (miR-106a and miR-20b) is 10-fold higher in thymus than any other tissue, indicating that the miRNA cluster is primarily expressed in T cells. Based on the previously reported expression profile for the miR-17~92 cluster,

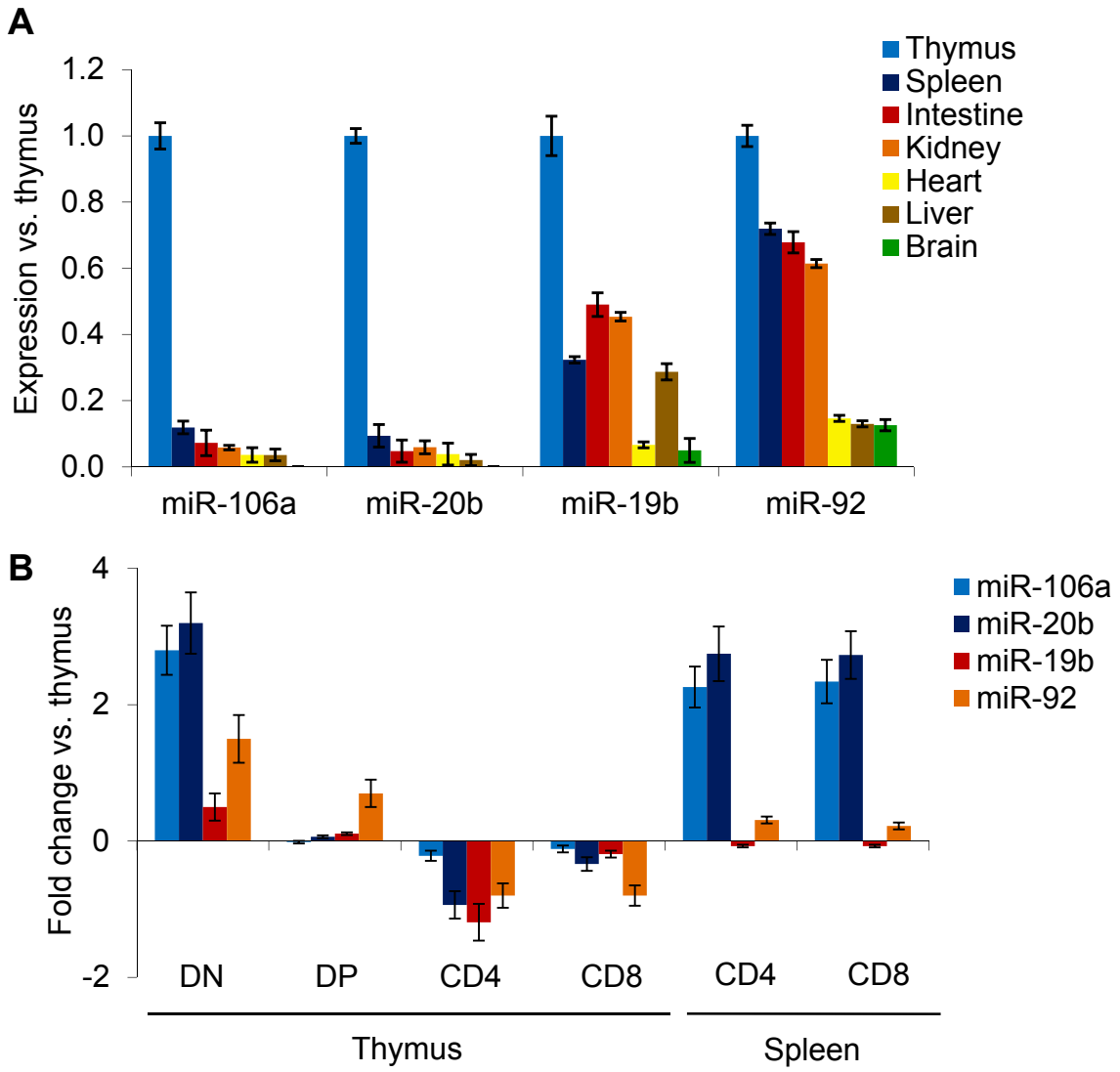

Figure 3.1 Tissue specific expression of the miR-106a~363 cluster in normal mice. (A) The expression levels of miR-106a~363 miRNAs in various tissues from 8-10 week old 129S4 mice. Expression of individual miRNAs was quantified by SYBR green qPCR that utilized a hairpin RT primer to reduced detection of the non-mature forms of the miRNAs. Expression of individual miRNAs is expressed as relative expression compared to thymus. (B) Thymocytes and splenic T cells from 8-10 week old mice were flow sorted into the 4 main CD4/CD8 thymocyte subsets and splenic $CD3^+/CD4^+$ and $CD3^+/CD8^+$ T cell populations. MicroRNA expression was quantified by RT-qPCR and miRNA levels are presented as fold change in expression relative to their expression in whole thymus.

elevated miR-19b and miR-92a expression in other tissues is likely from that cluster rather than miR-106a~363 [73].

To further characterize miR-106a~363 expression within thymocytes and peripheral T cell populations, I flow sorted T cells into the 4 main populations defined by CD4 and CD8 cell surface expression. Quantification of the miRNAs in these populations revealed differential expression of the miRNAs during T cell development (Fig. 3.1B). Expression of the miR-106a~363 miRNAs decreased between the CD4-CD8- (double negative, DN) to the $CD4^+CD8^+$ (double positive, DP) transition. This developmental stage follows T-cell receptor beta (TCRβ) rearrangement and increased signaling by the Lck tyrosine kinase. Interestingly, expression of the miRNA cluster remained low during maturation of thymocytes to $CD4^+$ or $CD8^+$ (single positive, SP) stages, but then increased again in mature CD4 SP and CD8 SP T cells purified from the spleen.

Generation of Lx^+ and Cx^+ mice

The expression profiling of miR-106a~363 indicated that it is differentially expressed in the T cells. In order to determine the importance of miR-106a~363 during T-cell development, and to generate a model that recapitulates the effect M-MuLV integration at *Xpcl1*, I generated transgenic mice with T-cell specific overexpression of miR-106a~363. The Lck-Xpcl transgene was generated by combining the Lck promoter with a 1.04 kb *Xpcl1* genomic DNA fragment, which contains approximately 100 bp of additional sequence 5' and 3' of the first and last miRNAs in the cluster (Fig. 3.2A). Mice containing the Lck-Xpcl transgene (Lx^+) were maintained as separate lines derived from two founders with equivalently high levels of thymic miR-106a~363 expression. Of

the six miRNAs in the cluster, only three displayed elevated levels of expression by RT-qPCR in transgenic thymi: miR-106a, miR-20b and miR-92a (Table 3.1). In contrast, expression of miRNAs from paralogous clusters was unchanged in the transgenics (Table 3.1). Expression of the miRNAs was elevated at equivalent levels during all stages of T cell development (Fig. 3.3).

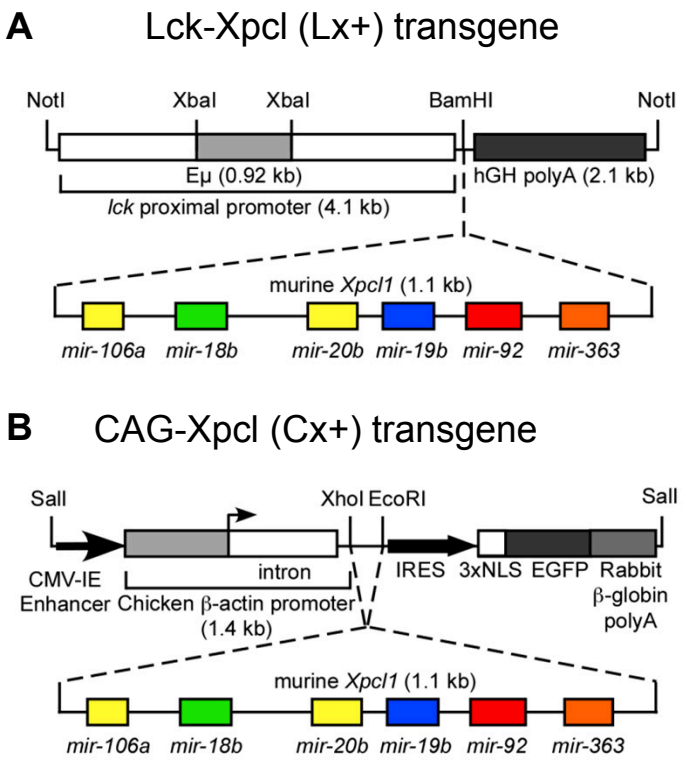

Figure 3.2 Diagrams of the Lck-Xpcl and the CAG-Xpcl transgenes. (A) To generate Lx^+ mice a 1.04 kb fragment of Xpcl1, containing the entire miR-106a~363 cluster, was inserted in the BamHI site of p1026x vector, which contains the Lck proximal promoter with an Eμ enhancer. (B) Cx^+ mice were generated by inserting the same Xpcl1 fragment downstream of the chicken β-actin promoter in the pCIG vector, which also expresses nuclear localized GFP.

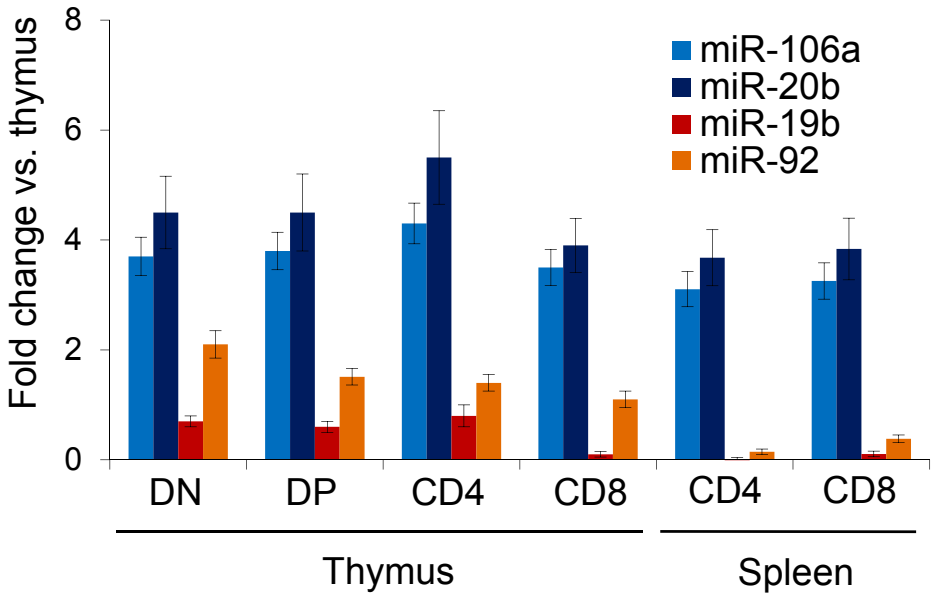

Figure 3.3 Expression of the Lck-Xpcl transgene in T cells. Expression of miR-106a~363 in flow sorted thymic T cell subsets and splenic $CD3^+/CD4^+$ and $CD3^+/CD8^+$ T cells from Lx^+ mice quantified by RT-qPCR. MicroRNA levels are expressed as fold change relative to their expression in wild type thymus.

To study the function of the miR-106a~363 miRNAs in a non-T cell context, I generated an additional transgenic mouse line with ubiquitous miR-106a~363 expression. To generate the transgene, I inserted a 1.04 kb *Xpcl1* genomic fragment into a vector containing the CMV enhancer/ chicken β-actin promoter (CAG), plus an IRES with nuclear localized EGFP (Fig. 3.2B). These CAG-Xpcl1-GFP mice (Cx^+) were maintained as separate lines from two different founders and successively backcrossed to wildtype 129S4 mice. miR-106a~363 miRNAs levels were elevated in all of the tissues that I tested, except thymus (Table 3.2). The lack of thymic expression conveniently enabled us to study the miRNAs in a pattern of expression opposite that of Lx^+ mice, i.e. largely free of effects in T cells. Interestingly, the miRNAs whose

Table 3.1 Increased expression of miR-106a~363 in thymus from Lck-Xpcl1 mice

	mir-106a	mir-20b	mir-19b	mir-92	mir-363	miR-17	miR-19a	miR-20a	miR-106b	miR-93	miR-25
WT	25.19	23.65	16.70	18.71	22.48	25.48	29.15	30.40	27.94	24.29	22.88
Lck-Xpcl1	22.12	19.57	16.84	17.20	22.41	25.85	29.08	30.10	27.96	24.34	22.80
ΔCt	3.07*	4.09*	-0.14	1.51*	0.07	-0.37	0.07	0.29	-0.02	-0.05	0.08

*p-value < 0.05 vs WT. Samples were pools of 5 WT or 5 Lck-Xpcl1 thymus with the values the average of 2 replicates.

Table 3.2 Increased expression of miR-106a~363 in tissues from CAG-Xpcl1 mice

	Spleen			Brain			Heart			Intestine			Thymus		
miRNA	Wt	Cx+	Δ Ct	Wt	Cx+	Δ Ct	Wt	Cx+	Δ Ct	Wt	Cx+	Δ Ct	Wt	Cx+	Δ Ct
miR-106a	31.31	26.91	**4.40**	32.77	28.09	**4.68**	32.91	26.30	**6.62**	31.45	26.84	**4.62**	28.42	27.68	**0.74**
miR-20b	29.05	24.17	**4.88**	30.23	25.02	**5.22**	30.64	23.27	**7.37**	29.20	23.81	**5.39**	26.58	24.99	**1.59**
miR-19b	24.63	23.19	**1.44**	26.37	23.87	**2.50**	26.69	23.37	**3.31**	23.93	23.05	**0.88**	23.80	23.13	**0.67**
miR-92a	28.55	26.96	**1.59**	31.06	28.82	**2.24**	30.84	27.26	**3.58**	28.63	26.98	**1.65**	28.07	27.31	**0.76**
miR-363	19.41	19.36	**0.05**	19.42	19.32	**0.10**	19.31	19.35	**-0.04**	20.08	19.42	**0.66**	19.44	19.27	**0.16**

Values are the average of tissues from 2 Wt or Cx+ mice

expression was increased by the CAG-Xpcl transgene differed from the Lck-Xpcl transgene, namely miR-19b and miR-92a demonstrated higher levels of expression. Cx^+ mice had normal sized litters and were equal in size to wildtype littermates. Additionally, they had no overt developmental phenotypes.

T cell developmental phenotype in Lx^+ mice

In order to determine the effect of overexpression of miR-106a~363 on T cell development, I examined thymus and splenic size as well as the flow cytometry profiles of thymocytes and splenic T cells from Lx^+ mice. Since Xpcl1 integrations by M-MuLV were increased in $p27^{-/-}$ mice, I bred the Lx^+ mice to $p27^{Kip1}$ knockout mice in order to directly test for cooperation between these two different mutations. At 8-weeks, thymuses in wildtype and Lx^+ mice were of equal size (60 ± 20 mg for both genotypes) as was the spleen (Table 3.3). The $p27^{-/-}$ mice had enlarged thymi compared to wildtype mice (110 ± 30mg vs. 60 ± 20mg) consistent with previously reported thymic hyperplasia[160-162]. Thymus size in $Lx^+;p27^{-/-}$ mice was equivalent to $p27^{-/-}$ mice (110 ± 30mg vs. 120 ± 30mg) as were total body weight and spleen size (Table 3.3). Therefore overexpression of miR-106a~363 did not alter the size of the thymus or spleen, nor did it augment thymic or splenic hyperplasia caused by $p27^{Kip1}$ deletion.

Table 3.3 Weight of whole animal, thymus and spleens in Lck-Xpcl1 and p27 knockout mice

Genotype	Mouse (g)†	Thymus (g)†	Spleen (g)†
WT	21.1±1.9	0.06±0.02	0.05±0.01
Lck-Xpcl	21.8±1.5	0.06±0.02	0.07±0.01
p27-/-	26.1±3.5*	0.11±0.03*	0.12±0.04*
Lck-Xpcl;p27-/-	25.9±3.2*	0.12±0.03*	0.16±0.03*

† Mean ± SD, *p< 0.05 vs. WT

WT n=34, Lck-Xpcl n=34, p27-/- n=8, Lck-Xpcl;p27-/- n=8

In order to determine whether forced expression of miR-106a~363 alters T cell development, I analyzed thymocyte and splenic T cell populations by flow cytometry. I observed no difference in the $CD3^+/CD4^+$ and $CD3^+/CD8^+$ splenic T cell populations in either the Lx^+ or $Lx^+;p27^{-/-}$ mice (Fig. 3.4A). However, Lx^+ mice exhibited an increase in the proportion of DP thymocytes, along with decreased proportions of both CD4 and CD8 SP thymocytes (Fig. 3.4B). While $p27^{-/-}$ mice have enlarged thymuses, the proportions of the thymocyte subsets is unchanged (Fig. 3.4B)[160-162]. The combination of Lck-Xpcl1 expression and $p27^{Kip1}$ deletion ($Lx^+;p27^{-/-}$) caused a cell surface phenotype identical to that observed in Lx^+ mice, yet the thymuses were also 2x the normal size and cellularity, identical to $p27^{-/-}$ mice. The γδ T cell population was unchanged in Lx^+ mice compared to wildtype. In summary, Lx and p27 mutations caused two independent phenotypes in murine thymocytes. The former caused a shift in the composition of T-cell subsets, whereas the latter effected overall cellularity.

There are two different explanations that could account for a shift in T-cell subsets in Lx^+ mice. One possibility is that the primary defect is an accumulation of DP thymocytes, e.g. due to a maturation block. The second explanation is that the primary defect is at the level of CD4 SP (and to a lesser extent the CD8 SP cells) wherein there is more rapid progression through the CD4 cell compartment. In the latter case, the apparent accumulation of DP cells would be to the change in relative proportioning of cells within the thymus. Considering that the overall cell number of the thymus was unchanged, either of these explanations is possible.

Following TCRβ rearrangement within DN thymocytes, the TCRβ/CD3 complex is expressed on the cell surface activating cellular signaling required for the progression to

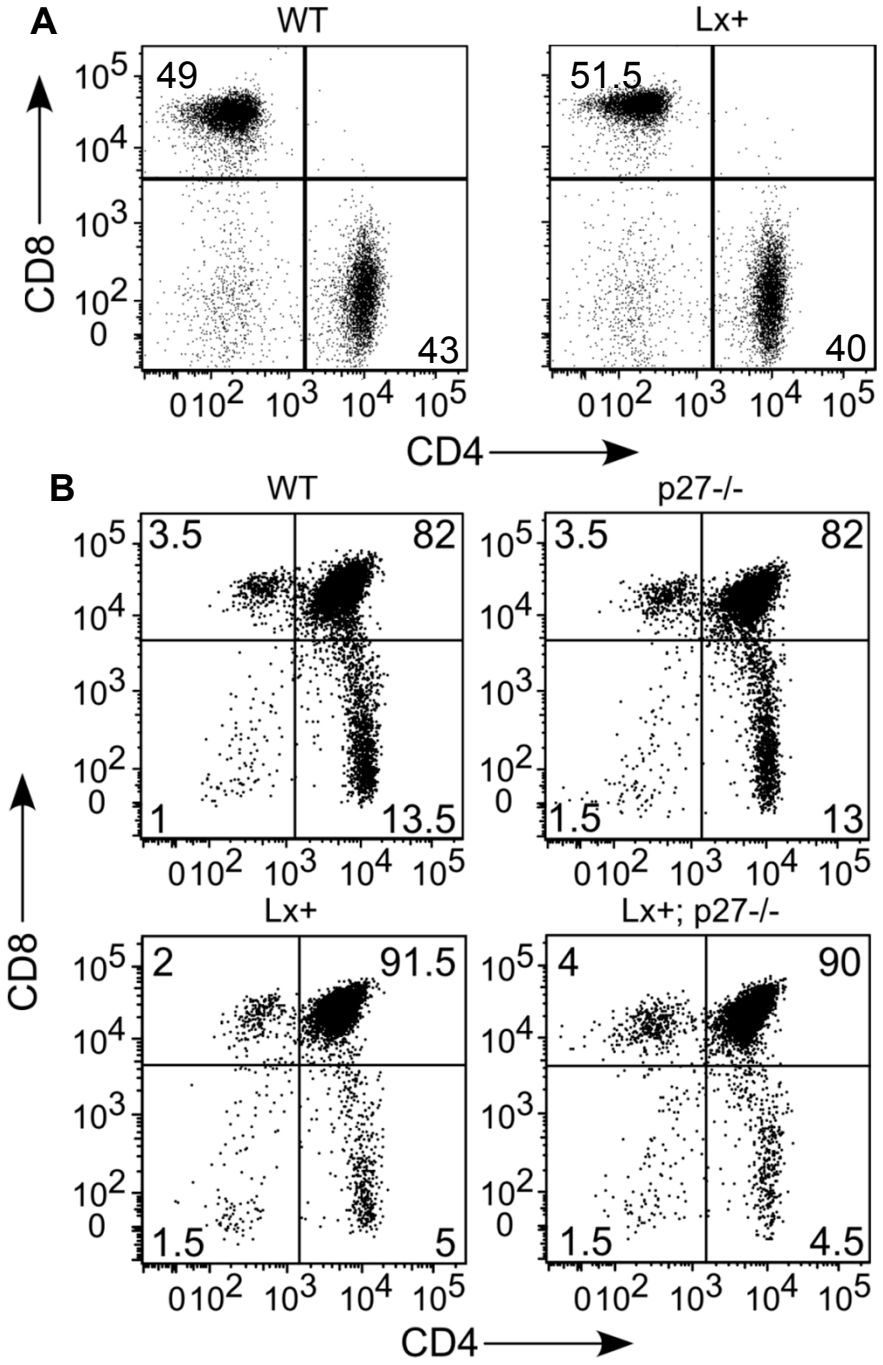

Figure 3.4 Splenic and thymic T cell subpopulations in Lx^{+} mice.
(A) Splenocytes from 8-10 week old wildtype and Lx^{+} mice were analyzed by flow cytometry for CD4 and CD8 expression on CD3+ gated cells. The numbers indicate the proportion of the CD3+ gated cells that fall within the particular quadrant. (B) Representative flow cytometry profiles for CD4 and CD8 on thymocytes from 8-10 week old wildtype, Lx^{+}, p27$^{-/-}$ and Lx^{+};p27$^{-/-}$ mice. As thymocytes mature they progress from the lower left DN quadrant to the upper right DP quadrant and finally develop into one of the SP populations. The DN population also contains γδ T cells which make up approximately 0.1% of all thymocytes.

the DP stage. To determine if the accumulation of DP cells might be due to a defect in TCR development, I examined the expression of CD3 and TCRβ on thymocytes. In the Lx^+ mice, I observed a global reduction in CD3 expression compared to wild type mice. This is manifested as a shift to the left of the CD3 fluorescent intensity when plotted as a histogram (Fig. 3.5A). In addition, I observed reduced numbers of the CD3 high population, which is explained by the reduced numbers of SP thymocytes (Fig. 3.5A). A failure to rearrange the TCRβ will prevent its surface expression and normally arrest the cells at the DN stage. If miR-106a~363 deregulates TCR signaling, then the thymocytes could potentially reach the DP stage without a functional TCRβ chain. In Lx^+ mice, I also observed a global decrease in TCRβ cell surface expression, comparable to the decrease in CD3 expression (Fig. 3.5B). Since TCRβ and CD3 are complexed together on the cell surface, it is expected that a reduction in CD3 expression would

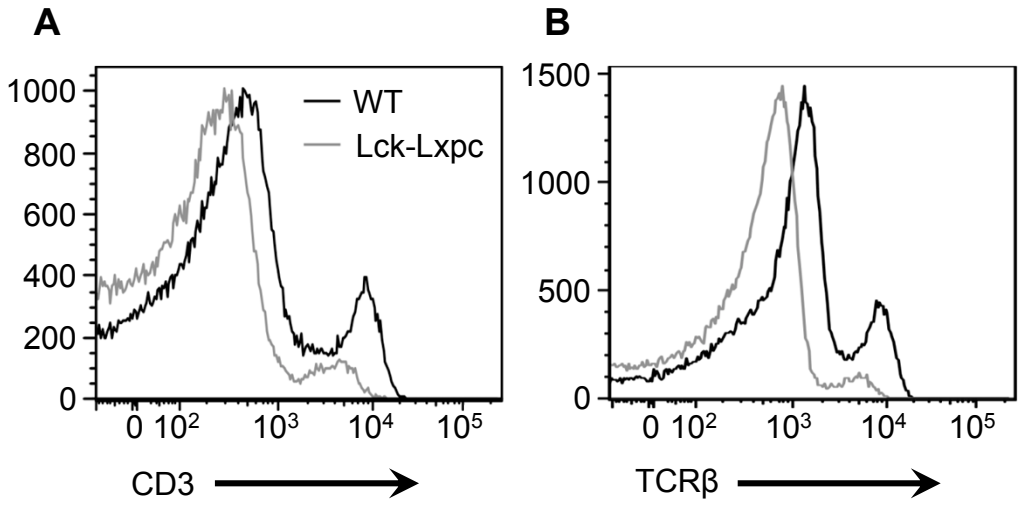

Figure 3.5 Reduced CD3 and TCRβ cell surface expression in Lx^+ thymocytes. (A) Flow cytometry for CD3 expression on wildtype (black) and Lx^+ (grey) thymocytes from 8-10 week old mice. (B) TCRβ expression measured by flow cytometry on 8-10 week old wildtype (black) and Lx^+ (grey) thymocytes. Thymocytes were incubated at 37°C for 4 hours in RPMI+10% FBS prior to antibody staining in order to enhance TCRβ surface expression[165].

result in reduced TCRβ expression. The expression of TCRβ indicates that β chain rearrangement is occurring normally.

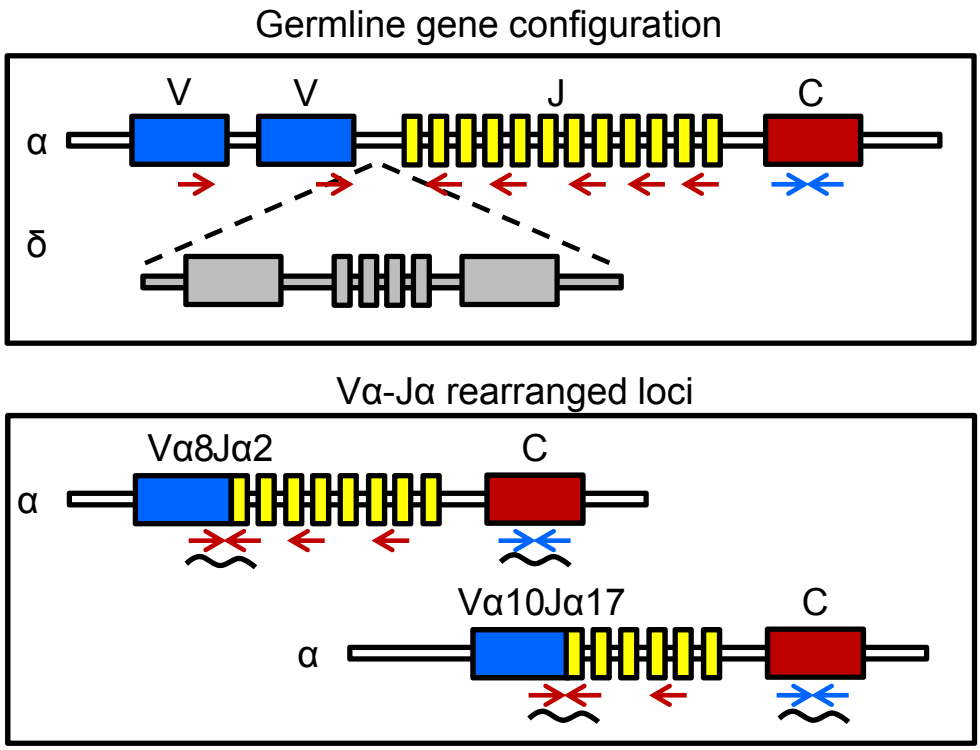

Figure 3.6 TCRα rearrangement qPCR. The TCRα loci consist of a series of gene segments which undergo rearrangement to form function chains of the TCR. The segments are organized into the variable (V) and joining (J) segments, and the constant (C) region. The TCRα chain is rearranged from the TCRα/δ locus which in addition to the TCRδ segments contains approximately 70 Vα and 60 Jα segments along with the constant region. TCRα rearrangement occurs through rearrangement of V to J with all TCRα chains utilizing the same constant region. The qPCR strategy to detect TCRα rearrangement utilizes a PCR primer pair (red arrows) for a given Vα and Jα combination in along with a common primer pair targeting the constant region (blue arrows) for normalization. Due to the large size of the TCRα locus only rearranged loci will produced PCR product (black wavy line).

Another possible explanation for the accumulation of DP thymocytes is that miR-106a~363 expression causes a defect in TCRα rearrangement. Rearrangement of the TCRα chains occurs following an arrest in DP thymocyte proliferation and a defect would reduce the number of thymocytes that successfully reach the single positive stage. The proportion of TCRα chains which rearrange at specific Vα-Jα splice junctions can be measured by qPCR, since only rearranged V-J pairs form small enough products to amplify (Fig. 3.6). I measured 10 different Vα-Jα genomic DNA splice forms in flow sorted DP thymocytes from Lx^+ and wildtype mice (Fig. 3.7). The frequency of recombination for all of the pairs was unchanged in the Lx^+ thymocytes compared to wild type DP thymocytes. Therefore, it appears that the accumulation of DP thymocytes in Lx^+ transgenics is not primarily due to a defect in TCRα rearrangement.

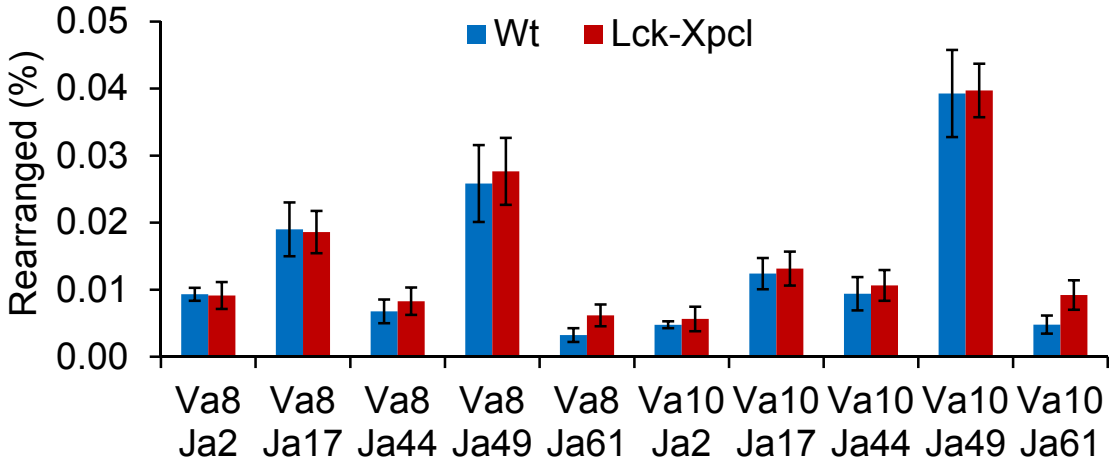

Figure 3.7 TCRα rearrangement in wildtype and Lx^+ mice. The frequency of TCRα chain rearrangement was quantified by qPCR for specific VαJα pairs using genomic DNA from flow sorted CD4+CD8+ thymocytes. The frequency of rearrangement of a particular V-J pair relative to the constant region was calculated using the formula, $1.9^{-V}/1.9^{-C}$, where C is the Ct for the constant region of the TCRα chain and V is the Ct for a particular TCRα chain V-J pairing.

A marker of the completion of positive selection is the up regulation of the CD69 cell surface receptor. It has been shown that CD69 regulates the rate of egress of SP thymocytes to the periphery. CD69 is a predicted target of all of the miRNAs in the miR-106a~363 cluster, with the exception of miR-18b. To determine whether CD69 expression was altered in Lx^+ transgenics I measured CD69 expression by flow cytometry. The number of DP thymocytes with high CD69 expression in Lx^+ mice was significantly reduced (1.73 ± 0.13% vs. 7.65 ± 0.26%, p-value <1E-03) and the total number of CD69 positive thymocytes was also reduced (2.41±0.1% vs. 13.9±1.18%, p-value <1E-03)(Fig. 3.8A). The mRNA level of CD69 in Lx^+ thymus was also reduced compared to wildtype thymus and a further reduction was observed in Lx^+;$p27^{-/-}$ mice compared to $p27^{-/-}$ thymus (Fig. 3.8B). There was no difference in CD69 expression observed between wildtype and $p27^{-/-}$ mice (data not shown). To demonstrate that decreased CD69 was not a secondary effect of the miRNAs, I tested the ability of miR-106a~363 miRNAs to directly target CD69 using a 3'UTR-luciferase reporter assay. Co-transfection of SM30-Xpcl1 reduced CD69 3'UTR reporter activity by more than 50% compared to empty vector control (Fig. 3.8C). Taken together, this data demonstrates that CD69 expression is inhibited by miR-106a~363 expression, and that this results in a loss of CD69 expression in Lx^+ mice. This is an important finding because overexpression of CD69 has been shown to block thymocyte egress from the thymus, and inhibition of CD69 function causes an phenotype that closely resembles Lx^+ thymocyte populations[163].

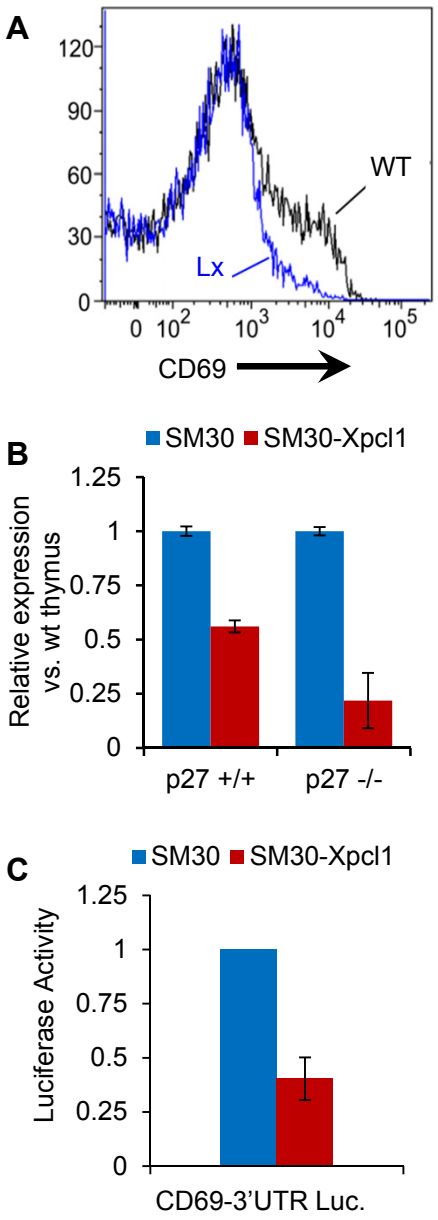

Figure 3.8 CD69 expression in Lx^{+} thymocytes. (A) Flow cytometry for CD69 expression on wildtype (black) and Lx^{+} (blue) DP thymocytes from 8-10 week old mice. (B) CD69 mRNA levels in wildtype, Lx^{+}, p27$^{-/-}$ and Lx^{+};p27$^{-/-}$ thymus quantified by qPCR. (C) Relative luciferase activity from a dual reporter assay of a luciferase reporter with the CD69 3' UTR co-transfected with either control pSM30 vector or pSM30-miR-106a~363 in SV40-180 mouse T cells.

Discussion

The tissue specific expression profiles of the miR-17~92 and 106b~25 clusters have been previously reported[73]. The expression of both clusters largely overlapped with their highest levels of expression found in lung, testis, intestine, spleen and thymus. Select miRNAs from the clusters were also elevated in heart, brain and kidney. I found expression of the miR-106a~363 cluster is limited primarily to the thymus and mature T cell lineages. I also detect miR-106a and miR-20b expression in the pre-B cell and pro-B cell populations, but not in mature B cells (data not shown). Expression of miR-106a~363 also diverges from expression of the paralogous clusters during T cell development. Expression of miR-17~92 decreases after the DN stage and remains low in all subsequent T cell populations[76]. While miR-106a~363 also decreases following the DN stage, I found that it subsequently increases in peripheral T cell populations. The differential expression of miR-106a~363 and its paralogs during T cell development suggests that they play a role in regulating the process. The T cell developmental phenotype I observed in the Lck-Xpcl1 supports this hypothesis.

Transgenic expression of miR-106a~363 in T cells resulted in shift in thymocyte subsets characterized by an accumulation of DP thymocytes and reduced numbers of SP thymocytes. Despite this change, there was no change in mature T cell numbers and no apparent immune deficiency. In contrast, others have reported that transgenic expression of miR-17~92 in T cells did not have a significant effect on T cell development except to increase the number of the early DN cells[87]. The developing thymocyte immunophenotype appears not to be due to a defect in TCRα rearrangement, but in theory another mechanism impairing positive selection could

account for the reduced number of thymic SP cells. Alternatively, an accelerated rate of egress of mature SP cells from the thymus could also account for a reduction of the number of SP cells.

Egress from lymphoid tissue is regulated through the sphingosine 1-phosphate receptor (S1P1) and its negative regulator CD69, a transmembrane C-Type lectin. Low levels of S1P are maintained in lymphoid organs while S1P is abundant in lymph, blood and likely egress associated epithelium[164,165]. Egress is mediated through S1P1 driving migration of lymphocytes toward higher concentrations of S1P and S1P1 cell surface expression is negatively correlated to S1P levels[165]. CD69 regulates S1P1 activity by interacting with the protein on the cell surface and causing its internalization and transgenic overexpression of CD69 impairs thymocyte egress[163,166,167]. Up regulation of CD69 is one of the two markers of the completion of positive selection, functioning to inhibit thymocyte egress until the thymocyte successfully undergoes negative selection. CD69 is a predicted target of the majority of the miR-106a~363 miRNAs and I observed reduced CD69 surface expression by flow cytometry and reduced CD69 RNA levels in Lx^+ thymocytes. CD69 has previously been shown to be a target of miR-20a from the miR-17~92 cluster in a 3' UTR reporter assay and I further validated CD69 as a target of the miR-106a~363 cluster. These results suggest a model where the T cell developmental phenotype is caused by an accelerated rate of egress from the thymus of the single positive thymocytes.

Materials and Methods

miRNA qPCR primer and RT design and RNA isolation

Quantification of miRNA was performed using a stem-loop RT primer, followed by qPCR as previously described, using oligonucleotide sequences listed in Table 3.5 [159]. The assays used Power SYBR Green PCR Master Mix (ABI) and the ABI 7900 Real-Time PCR System. The qPCR primers that provided the greatest specificity for each assay were experimental determined by testing primers with 10-14 bp of homology to the mature miRNA against synthetic oligonucleotide standards representing each mature miRNA sequence with which it might cross-react. Results are expressed as relative amounts compared to whole thymus. The efficiency of amplification was quantified with standard curves based on 2-fold serial dilutions synthetic oligonucleotides. Adjustments were made for primer sets that exhibit less than perfect 2-fold amplification by interpolation of the PCR cycle number of samples compared to the standard curve. Total RNA was isolated with Trizol (Invitrogen) using an increased concentration of isopropanol (0.75 mL), to improve yield of miRNA. Total RNA concentration was measured using a Nanodrop ND-1000 (Thermo).

Table 3.4 miRNA hairpin RT primers and SYBR green qPCR primers

Hairpin RT Primers	
mmu-miR-106a, 20b, 17, 93, 20a*	GTCGTATCCAGTGCAGGGTCCGAGGTATTCGCACTGGATACGACTACCTG
mmu-miR-19b, 19a*	GTCGTATCCAGTGCAGGGTCCGAGGTATTCGCACTGGATACGACTCAGTTTTGCAT
mmu-miR-92a	GTCGTATCCAGTGCAGGGTCCGAGGTATTCGCACTGGATACGACCAGGCC
mmu-miR-363	GTCGTATCCAGTGCAGGGTCCGAGGTATTCGCACTGGATACGACTTACAG
mmu-miR-106b	GTCGTATCCAGTGCAGGGTCCGAGGTATTCGCACTGGATACGACATCTGC
mmu-miR-25	GTCGTATCCAGTGCAGGGTCCGAGGTATTCGCACTGGATACGACTCAGAC
miRNA qPCR Primers	
mmu-miR-106a	CTGTGAAGAGGCAAAGTGCTAAC
mmu-miR-106b	CTGTCAAGTGGTAAAGTGCTGAC
mmu-miR-17	CTGTCAAGTGGCAAAGTGCTTAC
mmu-miR-20a	CTGTCAAGTGGTAAAGTGCTTAT
mmu-miR-20b	CTGTCAAGTGGCAAAGTGCTCAT
mmu-miR-19b	CGGCTGTGCAAATCCATGCAA
mmu-miR-19a	CGGCTGTGCAAATCTATGCAA
mmu-miR-92a	GTCTGGTATTGCACTTGTCC
mmu-miR-93	TGTCAAGTGGCAAAGTGCTGTTC
mmu-miR-25	GTCTGGCCATTGCACTTGTCT
mmu-miR-363	GTCTCATTGCACGGTATCCATCTGTA

*Due to the high homology between many of the miRNAs, a single RT primer generates cDNA for multiple miRNAs

Animals

The Lck-Xpcl1 transgene was generated by inserting a 1.04 kb fragment of the miR-106a~363 cluster, containing the region 82 bp 5' of miR-106a to 134 bp 3' of miR-363, into the BamHI site of the p1026x vector, as previously described[151,153]. Lx^+ transgenic mice were generated by injecting a 6 kb NotI fragment of pLck-Xpcl1 DNA into C57/B6xCBA F2 zygote pronuclei. Two founder mice expressed increased Xpcl1 miRNA in T-cells, and were maintained as independent lines through backcrosses to wildtype 129S4 mice. Genotyping was performed on genomic DNA using primers DK-2 (5'-GGCAGGGGAGTTGTAATGAA-3') and DK-4 (5'-GCAGCTCAAAAACATCCACA-3'). The β-actin-Xpcl1 transgene was generated by inserting the 1.04 kb fragment of the miR-106a~363 cluster used in the Lx^+ mice, into the XhoI and EcoRI sites of the pCIG vector. Cx transgenic mice were generated by injecting a 4.7 kb SalI fragment of pCIG-Xpcl1 DNA into C57/B6xCBA F2 zygote pronuclei. Two founder mice expressed increased Xpcl1 miRNA in the majority of tissues tested, and were maintained as independent lines through backcrosses to wildtype 129S4 mice. Genotyping was performed on genomic DNA using primers DK-7 (5'-TTTGAAACTTGTGCCGTTCA-3') and DK-9 (5'-GCAACGTGCTGGTTATTGTG-3'). Both Lx^+ and Cx^+ transgenic mice were bred to mice carrying a knockout allele of the $p27^{Kip1}$ gene (p27L-, referred to as $p27^{+/-}$), resulting in Lx^+; $p27^{+/-}$ mice[168]. These were further crossed to $p27^{+/-}$ mice to generate transgenic animals with homozygous $p27^{Kip1}$ deletions (Lx^+; $p27^{-/-}$). A cohort of 41 Cx mice were observed until one year of age or signs of morbidity (primarily loss of balance from pituitary adenomas in mice knocked out for $p27^{Kip1}$). Necropsies were performed to determine the gross cause of morbidity for each animal and this was

confirmed by histologic specimens taken of all grossly visible tumor masses. All mouse studies were performed under protocols approved by the FHCRC Institutional Animal Care and Use Committee.

Flow cytometry

Single cell suspensions of thymi were prepared from 6 to 10-week old mice in PBS by mashing whole thymus between the ends of two glass slides. Cells were incubated (1:100 v/v PBS) with monoclonal rat anti-mouse CD3, CD4, CD8, γδTCR, TCRβ, or CD69 (BD Bioscience). Thymocytes stained for TCRβ, were first incubated at 37°C in RMPI with 10% FBS for 4 hours to enhance TCR signal[169]. Flow cytometry was performed using Canto or LSRII cytometers and flow sorting was performed on a FACSAria cell sorter (BD Biosciences). Data was analyzed using FlowJo software (TreeStar, Inc.).

TCR qPCR

Genomic DNA was purified from $CD4^+CD8^+$ DP thymocytes from Lx^+ mice and wildtype littermates. The qPCR was run as previously described using Power SYBR Green PCR Master Mix (ABI) in a 384-well format and the ABI 7900 Real-Time PCR System using the SDS 2.3 software[170]. The amount of TCRα rearrangements was calculated as the frequency of rearrangement of a particular V-J pair relative to the constant region using the formula, $1.9^{-V}/1.9^{-C}$, where C is the Ct for the constant region of the TCRα chain and V is the Ct for a particular TCRα chain V-J pairing.

Chapter 4: Cooperation Between miR-106a~363 and $p27^{Kip1}$ Loss in Tumorigenesis

Introduction

The Xpcl1 locus was originally identified as a locus targeted by M-MuLV at an increased frequency in $p27^{Kip1}$ knockout mice[69]. This suggests cooperation between $p27^{Kip1}$ loss and miR-106a~363 overexpression in lymphomagenesis. A confounding factor to this observation is that tumors induced by M-MuLV average approximately two dozen viral integrations into their genome. This raises the possibility that many other genetic events, in addition to $p27^{Kip1}$ loss and Xpcl1 activation are required for tumor formation. Therefore, further validation is needed to determine whether this interaction contributes to lymphomagenesis and whether cooperation is independent of the additional mutations. The large number of insertion sites also makes it unclear if miR-106a~363 is a potent oncogene. Increased expression of miR-106a~363 in other tumors types suggests that it may be oncogenic in non-lymphoid tumors as well. To determine the oncogenic potential of miR-106a~363, I observed the two previously described miR-106a~363 transgenic mouse models to look for tumor development. I also bred the mice to $p27^{-/-}$ mice to look for an altered tumor phenotype, indicating cooperation between the two.

In addition to looking at the interaction of $p27^{Kip1}$ loss and miR-106a~363 expression in lymphomagenesis, I studied the normal regulation of $p27^{Kip1}$ during thymocyte development. The reason for this is that despite nearly two decades of research on $p27^{Kip1}$ its regulation during thymocyte development is still poorly characterized. Early studies, using immunofluorescent microscopy, noted a qualitative reduction in $p27^{Kip1}$ expression and a rise in cyclin A expression in DN thymocytes at a

stage coinciding with TCRβ selection and cell proliferation[171]. Likewise forced overexpression of $p27^{Kip1}$ in Lck-$p27^{Kip1}$ transgenic mice led to cell cycle and developmental arrest at this stage[172]. Mice deficient for $p56^{Lck}$, a tyrosine kinase activated by TCRβ selection, also display a developmental block at this stage[173]. Regulation of $p27^{Kip1}$ expression by $p56^{Lck}$ has been found to occur through Id3, which inhibits $p27^{Kip1}$ transcription[103]. Mice deficient for $p27^{Kip1}$ develop thymic hyperplasia but otherwise T cell development occurs normally[161,162]. This indicates that while $p27^{Kip1}$ can block progression of T cell development, its regulation of thymocyte proliferation is not essential.

In mature T cells, $p27^{Kip1}$ has been found to be an important regulator of cellular proliferation. Induction of proliferation by antigen receptor signaling, co-stimulatory molecules, and growth factors, is an essential aspect of the T cell immune response, driving both clonal expansion and effector T cell differentiation. IL-2 induces an important co-stimulatory signal in activated T cells, which leads to a reduced $p27^{Kip1}$ expression and cell proliferation[174-176]. Additionally, T cells from $p27^{Kip1}$ knockout mice have an enhanced response to IL-2, which stimulates the phosphatidylinositol 3-kinase (PI3K) pathway and leads to the activation of Akt[162,177]. Phosphorylation of the FoxO proteins by Akt results in their export from the nucleus and reduced expression of their transcriptional target genes. Akt is linked to $p27^{Kip1}$ expression through the FoxO family of transcription factors (FoxO1, FoxO3a, and FoxO4), which have been determined to be positive regulators of $p27^{Kip1}$ expression in T cells. Thus, there is strong evidence that activation of mature T-cells is accompanied by reduced $p27^{Kip1}$ transcription. Less is known about other mechanisms of $p27^{Kip1}$ regulation in activated T-cells. However in

fibroblasts, a larger body of work has implicated post-transcriptional mechanisms of $p27^{Kip1}$ regulation, including translational regulation, ubiquitination and proteolysis[112-115,118-120]. Currently, the mechanism of $p27^{Kip1}$ regulation in developing thymocytes remains undetermined.

Results

Cx^+ mice survival

I observed a cohort of Cx^+ mice, until 1-year of age, for the development of spontaneous tumors. Cx^+ mice did not exhibit significantly reduced survival compared to wildtype littermates (87.5% vs. 100% at 52 weeks) (Fig. 4.1). Mice with the combination of Cx^+ and $p27^{-/-}$ mutations developed pituitary tumors at the same rate as mice with the $p27^{-/-}$ mutation alone (Fig. 4.1). Necropsies demonstrated that the single Cx^+ mouse that died before one year of age, and three of those surviving till the end of the study had significantly enlarged hearts (0.59 ± 0.24 g vs. 0.21 ± 0.03 g, p-value <9.6E-05) and spleens (0.15 ± 0.02 g vs. 0.09 ± 0.02 g, p-value <8.6E-06). These animals also exhibited pale extremities prior to necropsy (Table 4.1). This is a constellation of findings consistent with chronic anemia with compensatory splenic erythroid cell hyperplasia and cardiomegaly. However, a source of internal bleeding was not identified. One of the four mice also displayed pulmonary hemorrhages (Table 4.1). Additionally, one Cx^+ mouse and one $Cx^+;p27^{-/-}$ mouse had intestinal tumors (Table 4.1).

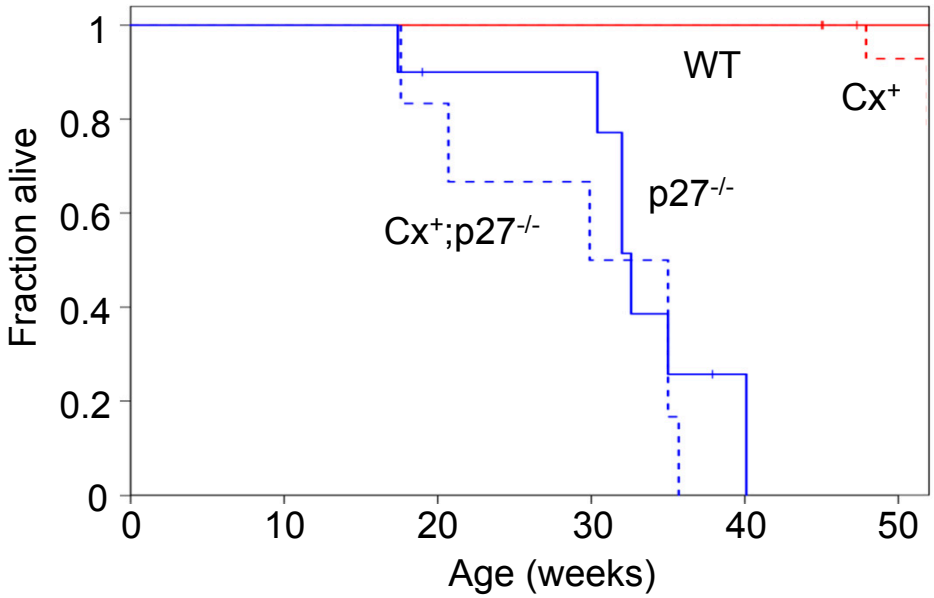

Figure 4.1 Survival of CAG-Xpcl1 transgenic mice. Cohorts of wildtype, Cx^{+}, $p27^{-/-}$ and Cx^{+};$p27^{-/-}$ mice were followed for 52-weeks. Mice were necropsied when they showed signs of morbidity. The cause of death for the Cx^{+} mouse was not determined, however no overt tumors were observed.

Table 4.1 Cause of morbidity in Cx^{+} and $p27^{-/-}$ mice

Genotype	Pituitary tumor	Intestinal tumor	Unknown*
Wildtype	0	0	0
Cx^{+}	0	0	1/1 (100%)
$p27^{-/-}$	7/7 (92%)	0	0
Cx^{+}; $p27^{-/-}$	5/6 (83%)	1/6 (17%)	0

Necropsies were performed on 14 animals from the observational cohort which displayed significant morbidity before one year of age. *Cause of death was non-malignant but otherwise undetermined.

Lx^+ and Lx^+; $p27^{-/-}$ mouse survival

To test the propensity of miR-106a~363 mice to develop spontaneous lymphomas, I observed cohorts of wildtype and Lx^+ mice up to 52-weeks of age. Additionally, I followed cohorts of $p27^{-/-}$ mice with or without the lck-Xpcl1 transgene, to determine whether $p27^{Kip1}$ loss cooperates with miR-106a~363 in lymphomagenesis. By one year of age 46% (13/28) of the Lx^+ mice had died compared to 7% (1/17) of the wildtype mice (Fig. 4.2). The cause of death was determined by necropsy, with T-cell lymphomas being the cause of morbidity in 79% (10/13) of the sick Lx^+ mice (Table 4.2). In comparison, the cause of death of the wildtype mouse was not determine but was not a lymphoma and none of the wildtype mice sacrificed at one year had developed pathologically enlarged lymph nodes or thymi (Table 4.2).

Lymphomas also developed in the Lx^+; $p27^{-/-}$ mice, and the combined mutations decreased both survival and time to death. In contrast to the Lx^+ mice, by 28 weeks of age 94% (16/17) of the Lx^+; $p27^{-/-}$ had died from T-cell lymphomas versus 15% (4/27) of the Lx^+ mice (Fig. 4.2, Table 4.2). A fraction (18%) of the Lx^+;$p27^{-/-}$ mice had concurrent pituitary tumors, which was expected based on prior reports for $p27^{-/-}$ mice (Table 4.2) [160-162]. However, in nearly all cases, the lymphoma was judged to be the principal cause of morbidity, based on its size and the behavior of the mouse. The $p27^{-/-}$ mice died exclusively from pituitary tumors, without any spontaneous lymphoma development. If there is no cooperation between the Lx^+ and $p27^{-/-}$ mutations on lymphomagenesis one would expect a simple additive effect of mortality rates of the individual mutations. Thus, at 25 weeks of age, the expected odds of mortality in compound Lx^+; $p27^{-/-}$ mutants was 0.25:1 (live:dead) (Table 4.3). However, the actual odds of death that was

observed in these animals was 4.5:1, at 25 weeks. Thus, the combination of Lx^{+} and $p27^{-/-}$ increased the odds of mortality by a factor 18 over the expected (additive) effects of the individual mutations.

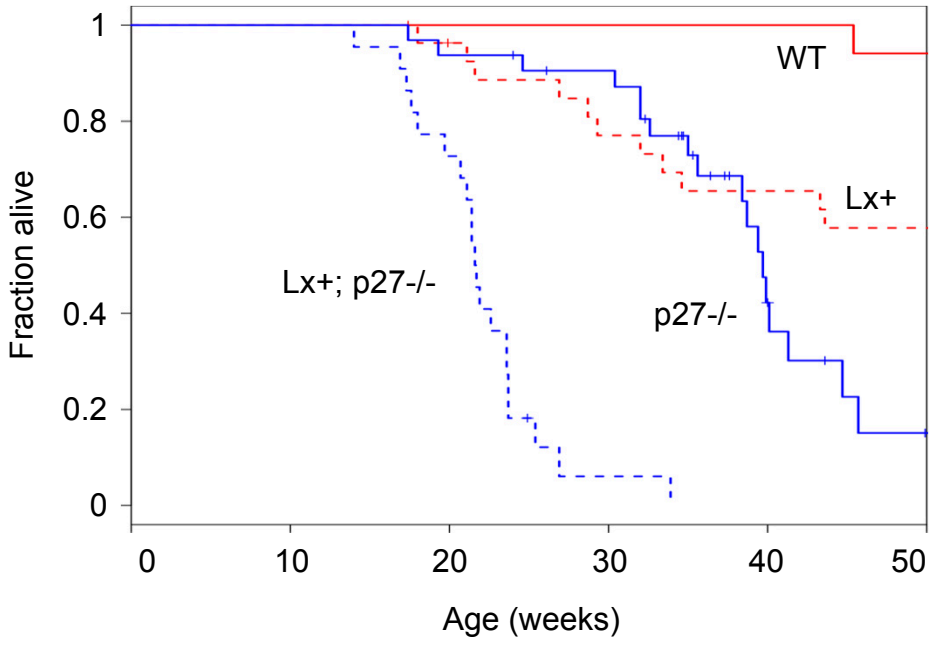

Figure 4.2 Cooperation with $p27^{Kip1}$ loss in miR-106a~363 induced lymphomagenesis. Cohorts of wildtype, Lx^{+}, $p27^{-/-}$ and Lx^{+};$p27^{-/-}$ mice were followed for 52-weeks. Mice were necropsied when they showed signs of morbidity. Approximately 20% of Lx^{+};$p27^{-/-}$ mice also developed pituitary tumors, however the primary cause of death in most cases was determined to be from a T cell lymphoma.

Table 4.2 Cause of morbidity in Lx^{+} and $p27^{-/-}$ mice

Genotype	Pituitary tumor	T-cell lymphoma	Non-malignant*
Wildtype	0	0	1/1 (100%)
Lx^{+}	0	10/13 (77%)	3/13 (23%)
$p27^{-/-}$	11/12 (92%)	0	1/12 (8%)
Lx^{+}; $p27^{-/-}$	3/17 (18%)†	16/17 (94%)	0

Necropsies were performed in 43 animals from the observational cohort which displayed significant morbidity before one year of age. *Non-malignant causes of morbidity included skin lesions, uterine prolapse and gastrointestinal bleeding. †2/3 mice had concurrent T-cell lymphomas.

Table 4.3 Additive survival odds at 25 weeks for Lx^+ and $p27^{-/-}$ mice

Genotype	Alive	Dead	Odds of mortality
Lx^+	0.89	0.11	**0.13**
$p27^{-/-}$	0.91	0.10	**0.10**
$Lx^+;p27^{-/-}$	0.18	0.82	**4.50**

Odds of mortality = dead/alive

Histological characteristics of Lx^+ lymphomas

I determined the immunophenotype of 23 lymphomas arising in either Lx^+ or $Lx^+;p27^{-/-}$ mice by flow cytometry and/or immunohistochemistry. The majority of tumors (87%), were DP ($CD4^+,CD8^+$) and the remainder (3/23) were CD4 single positive; paralleling the subset distribution of Lx^+ thymocytes. However, there was some anatomical and histological variation within the tumors. Whereas the majority of the tumors caused massive thymic enlargement, 20% of tumors involved primarily the spleen and lymph nodes (Fig. 4.3B). Furthermore, the majority of tumors had a high-grade, diffuse histological appearance on H&E staining (Fig. 4.3B). A smaller number of tumors contained larger cells with more abundant cytoplasm and reactive macrophage infiltration (Fig. 4.3C). Lx^+ tumors had a high proliferation rate, measured by Ki67 immunostaining (66 ± 9.4%, mean ± SEM), and a low rate of apoptosis (31 ± 14 caspase-3 cells/hpf) (Fig. 4.3D,E). However, the differences in Ki67 (73 ± 5%) or caspase-3 staining (47 ± 21 cells/hpf) were not significant enough to account for the differences in survival between Lx^+ and $Lx^+;p27^{-/-}$ mice.

Circulating miRNAs in serum have been identified as potential cancer biomarkers for a number of human cancers and in xenograft mouse models[178]. The regulation of miRNA release into the blood is still not understood; however, two populations of

circulating miRNAs have been identified. The majority of circulating miRNAs are bound within Ago2 protein complexes and a minority are found within vesicles[179]. To test the hypothesis that serum miR-106a~363 miRNAs might serve as biomarkers for the presence of a lymphoma, I collected serum from mice with lymphomas, prior to necropsy. The serum levels for miR-106a, miR-20b and miR-92a were elevated in the

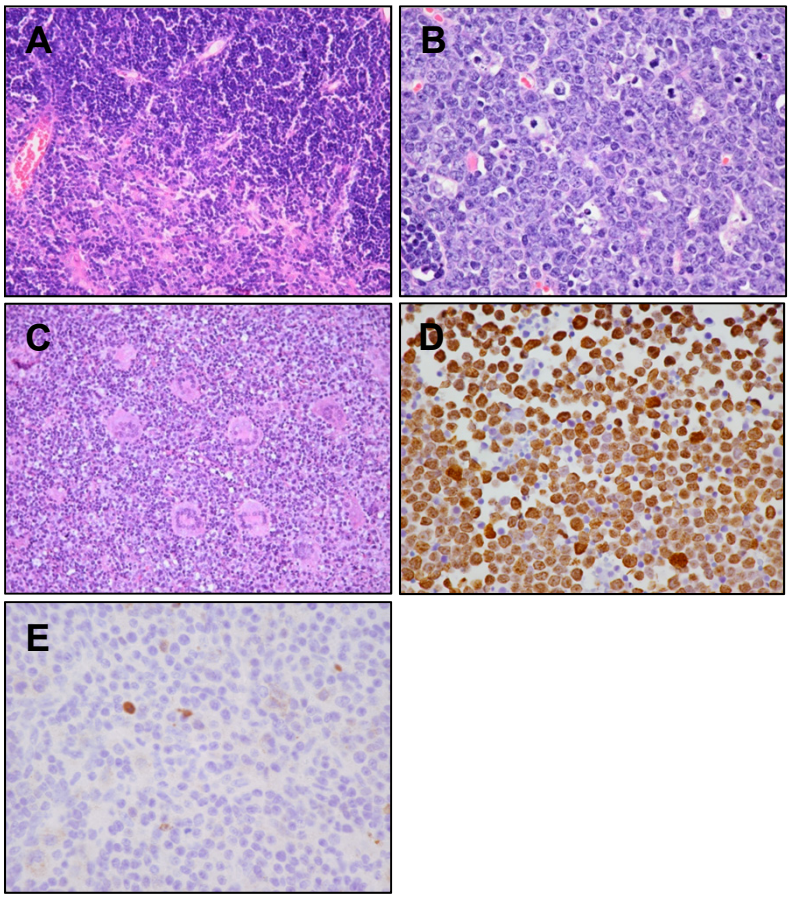

Figure 4.3 Histological characterization of the Lx^{+} lymphomas. (A) H&E of wildtype thymus showing clearly delineated cortex (dark blue) and medulla (pink and blue). (B) H&E showing the typical high-grade, diffuse appearance of the lymphomas. (C) Representative H&E of one of the tumors which contained larger cells and infiltration by reactive macrophage. (D) Ki-67 indicated the high level of proliferation within the tumors. (E) Low levels of caspase-3 staining indicate a low level of apoptosis within the tumors.

mice with tumors compared to healthy age matched Lx^+ mice (Fig. 4.4). The healthy Lx^+ mice were necropsied to ensure the absence of disease. Surprisingly the serum levels of miR-19b were also elevated even though its expression is unaltered by the transgene (Fig. 4.4 and Fig. 3.3). The increased expression of miR-19b suggests that the tumor cells may be releasing increased levels of miRNAs into the blood in general and is particularly notable since serum levels of miR-19b are among the highest of any miRNA[178].

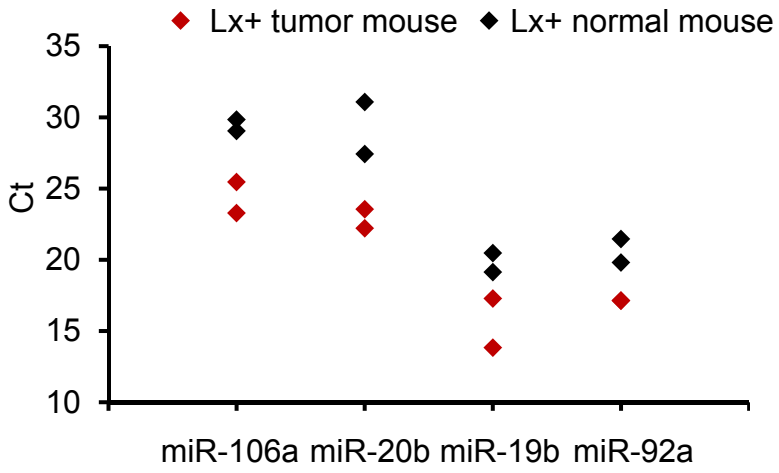

Figure 4.4 Elevated serum levels of miR-106a~363 miRNAs in mice with T cell lymphomas. MicroRNAs were isolated from the serum of morbid approximately 30-week old Lx^+ mice and age matched healthy Lx^+ littermates. Expressions of individual miRNAs were quantified by RT-qPCR. The majority of miR-106a~363 miRNAs are detectable in serum from healthy humans, with miR-19b and miR-92 expression within the top 10 highest expressed[174].

Cell cycle gene expression

In order to determine whether the synergistic effect of miR-106a~363 overexpression and $p27^{Kip1}$ loss may result from altered cell cycle gene expression, I compared thymic RNA expression from healthy 8-week old Lx^{+} and wildtype mice. I quantified the expression of Rb, p107, p130, E2F3, E2F5, Cyclin D1,2,3, $p21^{Cip1}$ and p57 by RT-qPCR. With the exception of Cyclin D3, all of these genes are predicted targets of one or more miR-106a~363 miRNAs (Fig. 4.5). No significant alterations were detected for any of these genes, with the exception of p57, which demonstrated a modest increase (<2-fold increase) in the Lx^{+} mice. Surprisingly, expression of $p27^{Kip1}$ was increased in Lx^{+} whole thymus by 2-3 fold on both the RNA level and protein level as measured by qPCR and by quantitative western blots (Fig. 4.6 A,B).

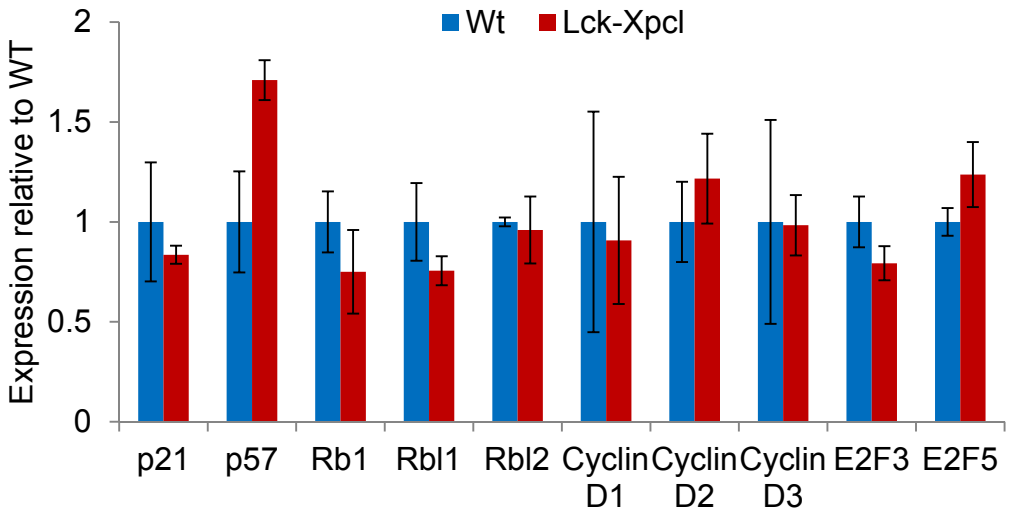

Figure 4.5 Expression of cell cycle genes in wildtype and Lx^{+} thymus. The expression of a variety of cell cycle genes in 4 wildtype and 4 Lx^{+} thymi was quantified by qPCR. All of the tested genes, with the exception of Cyclin D1, are predicted targets of the miR-106a~363 miRNA cluster.

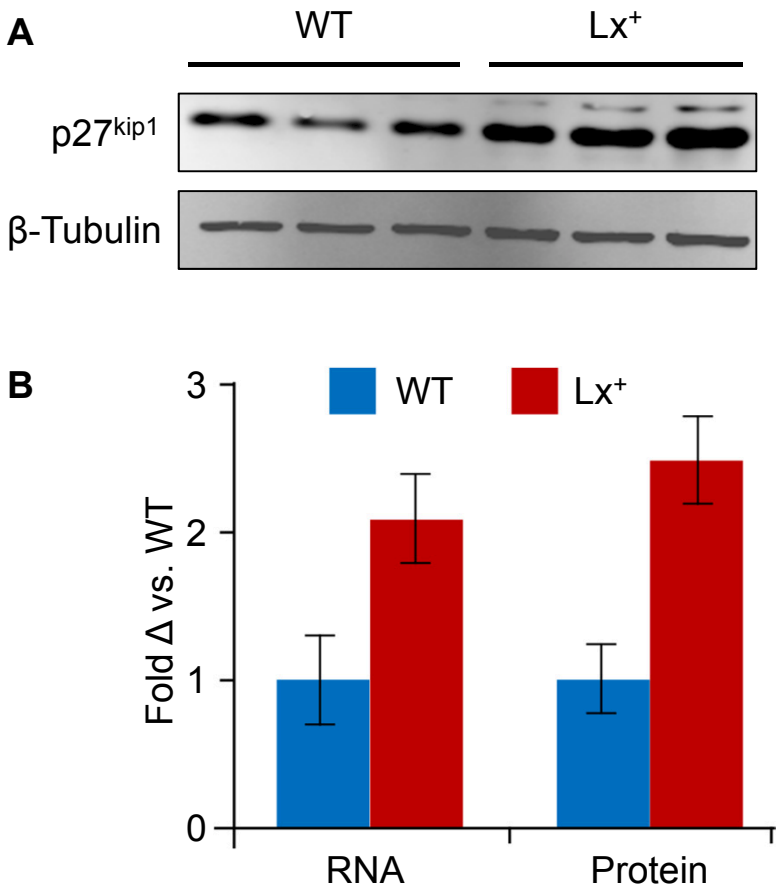

Figure 4.6 Elevated $p27^{Kip1}$ expression in Lx^+ thymus.
(A) A representative western blot of $p27^{Kip1}$ expression in wildtype and Lx^+ thymus. (B) The average $p27^{Kip1}$ mRNA expression level in 5 wildtype and 6 Lx^+ mice quantified by RT-qPCR. Quantification of $p27^{Kip1}$ protein expression from 7 wildtype and 7 Lx^+ mice was done using the Odyssey system as previously described.

Mechanism of p27^{Kip1} regulation by miR-106a~363

There are a number of mechanisms by which miR-106a~363 might regulate p27^{Kip1} expression in Lx^{+} thymus. These include altering expression of genes that regulate p27^{Kip1} protein or RNA stability, or altering the transcriptional or post-transcriptional regulation of p27^{Kip1} expression. To compare p27^{Kip1} protein and RNA stability in Lx^{+} thymocytes to wildtype thymocytes, I arrested protein and RNA synthesis with Actinomycin D and cyclohexamide. Cells were collected at a series of time points over 16 hours and protein and RNA levels quantified. In the Lx^{+} thymocytes, both protein (0.87 Pearson correlation) and RNA (0.86 Pearson correlation) stability was very similar to that in the wildtype thymocytes (Fig. 4.7A, B). This data does not support the hypothesis that miR-106a~363 regulates p27^{Kip1} at the post-transcriptional level.

To determine whether miR-106a~363 might regulate p27^{Kip1} at the level of transcription, I quantified FoxO3a, FoxO4, and Id3 in transgenic thymocytes (Fig. 4.8A). In addition to the three transcription factors whose expression I measured in T cell subsets, I also quantified the expression of miR-181a, miR-221 and miR-222 (Fig. 4.8B). If one of the miRNAs was regulating p27^{Kip1} expression, I would expect to see a decrease in its expression. Rather I observed either no significant change or in the case of miR-221 a slight increase in expression, ruling out the miRNAs as the regulatory mechanism (Fig. 4.8B). In the case of the transcription factors, I detected increased FoxO3a and FoxO4 expression in the Lx^{+} thymocytes. This finding supports the hypothesis that FoxO3a and FoxO4 are regulating p27^{Kip1} expression during T cell development.

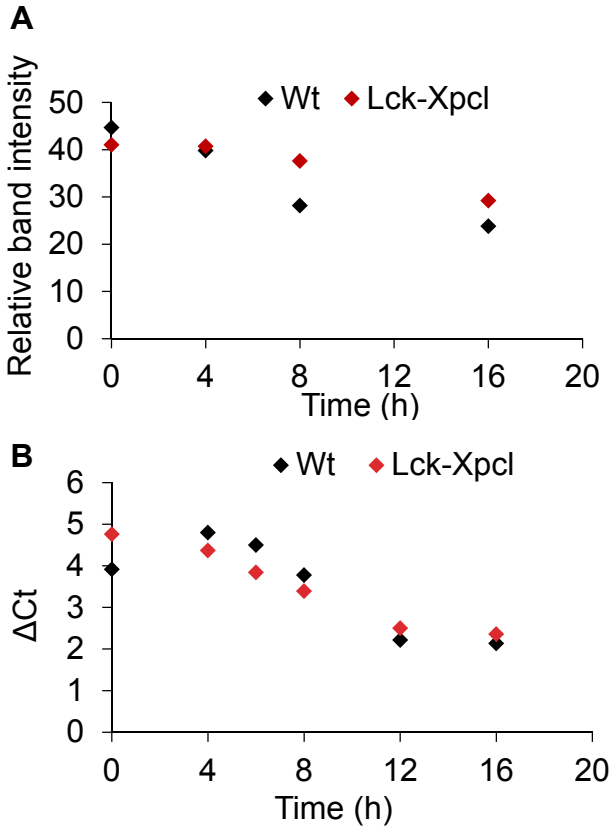

Figure 4.7 $p27^{Kip1}$ protein and RNA stability in Lx^{+} mice. (A) Protein synthesis was blocked in thymocytes from wildtype and Lx+ mice, pools of 2 mice, by cyclohexamide treatment. At the indicated time points protein was isolated from the cells. The abundance of $p27^{Kip1}$ at the various time points was quantified by western blot using the Odyssey system. Protein amount is plotted as the relative band intensity measured by the Odyssey software. There was strong correlation between protein stability in both samples (r=0.86 Pearson correlation, $p < 3x10^{-4}$).(B) RNA synthesis was blocked by actinomycin D treatment from the same thymocyte pools used to measure $p27^{Kip1}$ protein stability. At the indicated time points RNA was isolated from the cells. The $p27^{Kip1}$ RNA abundance was quantified by RT-qPCR and samples were normalized based on cell counts from which the RNA was isolated. There was strong correlation between RNA stability in both samples (r=0.87 Pearson correlation, $p < 2x10^{-3}$)

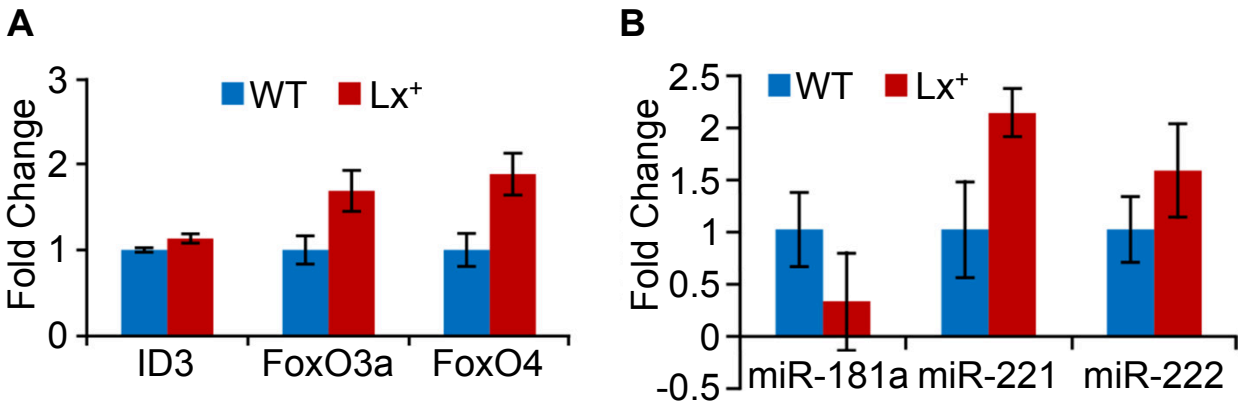

Figure 4.8 Expression of $p27^{Kip1}$ transcriptional and post-transcriptional regulators in Lx^+ thymus. (A) Expression of transcription factors that regulate $p27^{Kip1}$ expression were quantified in the samples previously used to measure $p27^{Kip1}$expression in Lx^+ thymus. Expression is presented as fold change compared to WT thymus (B) The expression of miRNAs known to regulate $p27^{Kip1}$ expression were quantified by RT-qPCR with expression presented as fold change versus WT thymus.

Validation of $p27^{Kip1}$ regulation by miR-106a~363

To further investigate the mechanism through which miR-106a~363 regulates $p27^{Kip1}$, I looked at $p27^{Kip1}$ expression in the SV40-180 and LGY-6871 mouse T cell lines. Transient expression of miR-106a~363 caused an increase in p27 protein levels in SV40-180 and $p56^{lck}$ cells (Fig. 4.9A). Overexpression of miR-106a~363 also resulted in approximately 2-fold increases in $p27^{Kip1}$, FoxO3a and FoxO4 RNA expression in the SV40-180 T cells (Fig. 4.9B). These results further support the model that miR-106a~363 induced $p27^{Kip1}$ expression is occurring at the transcriptional level through the FoxO3a and FoxO4 transcription factors.

To demonstrate that the FoxO transcription factors are regulating $p27^{Kip1}$ through direct binding of its promoter, I utilized a luciferase reporter containing a 2.2 kb fragment of the $p27^{Kip1}$ promoter[103]. When miR-106a~363 is expressed the reporter activity increased (Fig. 4.10A). However, when the promoter was truncated to remove the

FoxO binding site the ability of miR-106a~363 to activate the reporter was eliminated (Fig. 4.10A). Furthermore, when FoxO3a or FoxO4 expression was inhibited by shRNAs the effect of miR-106a~363 expression on the reporter was also reduced (Fig. 4.10B). These results demonstrate that miR-106a~363 induced expression of $p27^{Kip1}$ is due to transcriptional regulation of $p27^{Kip1}$ by the FoxO TFs.

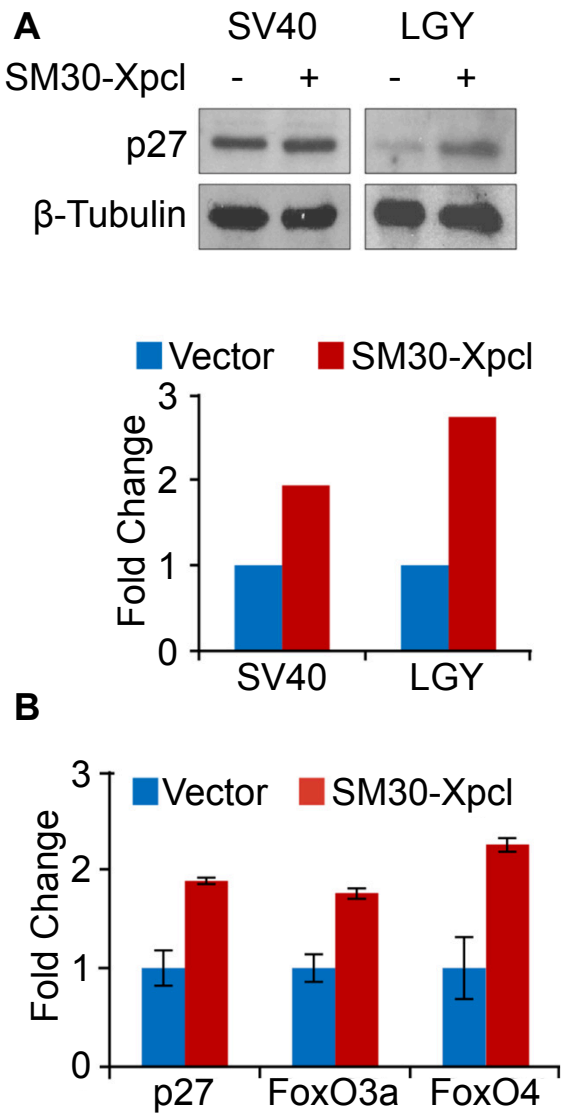

Figure 4.9 Regulation of $p27^{Kip1}$ and the FoxO TFs by miR-106a~363 in vitro. (A) Western blots of $p27^{Kip1}$ expression in LGY-6871 and SV40-180 cells transiently transfected with control vector or pSM30-Xpcl1. Cells were flow sorted 48h post transfection for GFP. The western blots were quantified using ImageJ software. (B) RT-qPCR quantified expression levels of $p27^{Kip1}$, FoxO3a and FoxO4 in the SV40-180 cells transiently transfected with control vector or pSM30-Xpcl1.

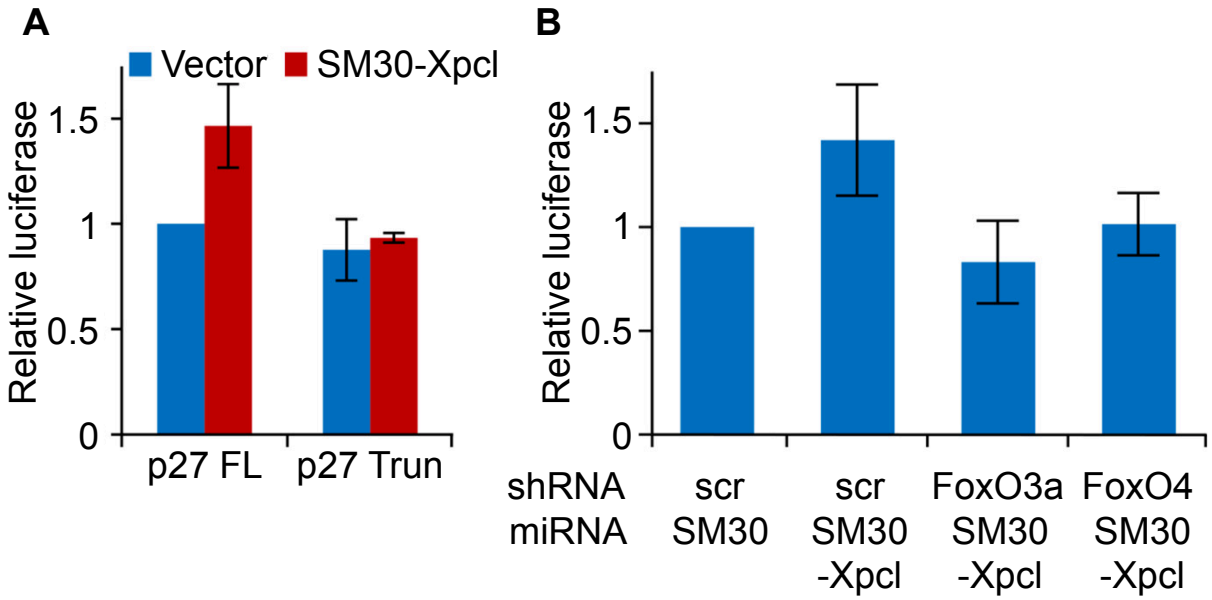

Figure 4.10 Regulation of a p27^{Kip1} promoter reporter by miR-106a~363 expression is mediated by the FoxO TFs. (A) Relative luciferase activity from a dual reporter assay of a luciferase reporter with the p27^{Kip1} promoter or a truncated p27^{Kip1} promoter, lacking the FoxO TF binding sites, co-transfected with either control vector or pSM30-Xpcl1 in SV40-180 mouse T cells. (B) p27^{Kip1} promoter luciferase activity in response to miR-106a~363 expression and shRNA inhibition of FoxO3a and FoxO4.

Regulation of p27^{Kip1} expression during T cell development

Since p27^{Kip1} levels were elevated in Lx^{+} thymus, I wanted to determine whether p27^{Kip1} is normally differentially expressed during T cell development as well, and if its expression correlates with that of miR-106a~363. I flow sorted thymocytes into subsets based on CD4/ CD8 expression and assayed p27^{Kip1} protein and RNA expression. Both p27^{Kip1} protein and RNA levels were differentially expressed, with the lowest levels in DN thymocytes, and the highest levels in DP thymocytes (Fig. 4.11A,B). Expression of miR-106a~363 and p27^{Kip1} do not correlate during T cell development, ruling out the miRNAs as regulators of p27^{Kip1} expression (Fig. 3.1 vs. Fig. 4.11B). To identify the transcriptional regulator of p27^{Kip1} in T cells, I quantified expression of three

transcription factors (FoxO3a, FoxO4, and Id3) which have previously been shown to regulate $p27^{Kip1}$ expression in mature T cells (Fig. 4.12). The expression pattern of the FoxO3a and FoxO4 transcription factors correlated with $p27^{Kip1}$ expression during T cell development suggesting that they are regulating $p27^{Kip1}$ expression (Fig. 4.12 compared to Fig. 4.11B).

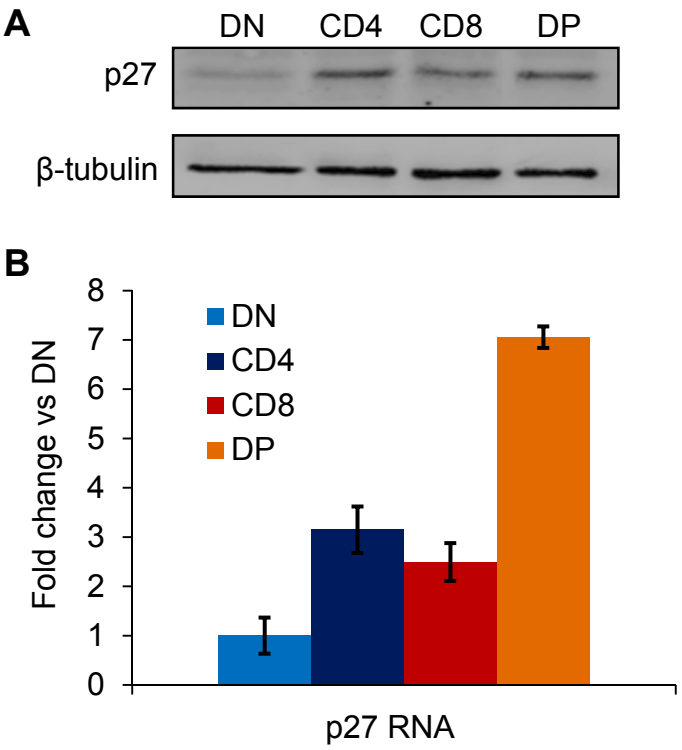

Figure 4.11 Differential expression of $p27^{Kip1}$ in thymocyte subsets. Thymocytes from 6 8-week old wildtype mice were flow sorted based on CD4 and CD8 expression, the sorted cells pooled and RNA and protein isolated. (A) Western blot of $p27^{Kip1}$ expression in the four main thymocyte subsets. The protein levels of $p27^{Kip1}$ were quantified using the Odyssey fluorescent western blot system with normalization to β-tubulin as a loading control. (B) Quantification of $p27^{Kip1}$ mRNA in thymocyte subsets by qPCR. Samples were normalized using S16 as an internal control.

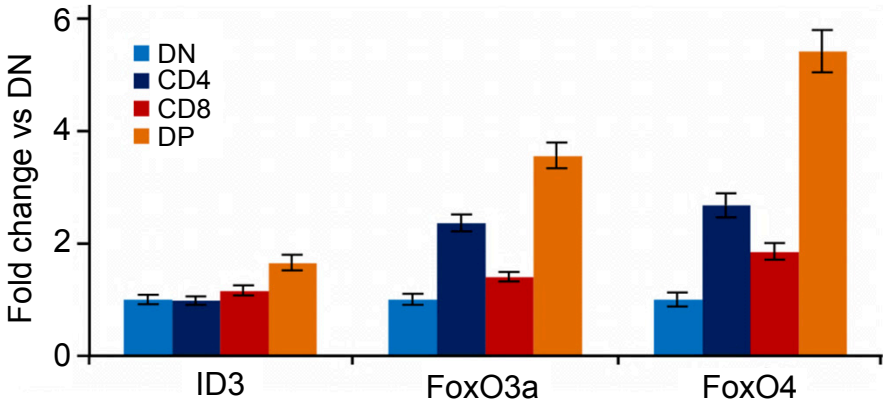

Figure 4.12 Expression of $p27^{Kip1}$ transcriptional regulators in thymocyte subsets. The mRNA expression levels of ID3, a negative regulator, and FoxO3a and FoxO4, positive regulators, was quantified by RT-qPCR. The source RNA was the same used to quantify $p27^{Kip1}$ expression in thymocyte subsets.

Discussion

The two paralogues of miR-106a~363, miR-17~92 and miR-106b~25, display a similar pattern of expression in vivo[73]. The idea that miR-17~92 and miR-106b~25 have compensatory functions is further supported by the observation that the embryonic lethality caused by knocking out miR-17~92, is accelerated by the additional deletion of miR-106b~25. Knockout of miR-17~92 results in hypoplastic lungs while transgenic overexpression results in a lethal phenotype due to hypercellularity from increased proliferation of the lung epithelium[180].

Since miR-106a~363 expression has been reported in a variety of cancer types, I hypothesized that ubiquitous expression of *Xpcl1* in transgenic mice would be oncogenic. I further posited that increased levels of miR-106a~363 miRNA would alter expression of genes normally regulated by miR-17~92 and miR-106b~25 and thus lead to developmental defects. However, I found that widespread expression of miR-

106a~363 in Cx^{+} transgenic mice did not induce severe developmental defects nor did it induce cancer at a high frequency. One of the mice did develop intestinal tumors, which is intriguing given the prior reports of elevated miR-106a levels in colon cancer[81]. The lack of more frequent tumor development may simply be a shortcoming of the limited time span of a mouse study. A more rigorous test of the oncogenic potential of CAG-Xpcl would require that the transgene be bred under a variety of scenarios in which tumors are expected at a measurable frequency. This could include addition of chemical carcinogens, the *Sleeping Beauty* transposon, or defined gene mutations such as Apc or Wnt.

Several of the other older mice displayed signs of anemia, pale paws, and had enlarged spleens with elevated amounts of erythropoiesis. While histology was not performed to look for occult intestinal tumors, cardiomegaly plus splenic erythroid hyperplasia is a typical manifestation of chronic blood loss due to G.I. tumors in mice. Alternatively, the animals may have developed anemia from other causes such as hematopoietic defects or hemolysis. Although these observations are preliminary, they are important clues that indicate that miR-106a~363 overexpression may promote gastrointestinal carcinogenesis, or hematological malignancies such as myelodysplasia or acute leukemia.

The *Xpcl1* gene, which encodes the miR-106a~363 miRNA cluster, was originally identified as a common integration site of M-MuLV in $p27^{Kip1}$ knockout mice. Subsequently, expression of miRNAs from the miR-106a~363 cluster and paralogous clusters has been observed in variety of human cancers[80-85]. To validate the miR-106a~363 cluster as an oncogene in lymphoid tissues, I generated Lx transgenic mice

which targets overexpression of the miRNAs to T lymphocytes starting at the DN stage. The Lx transgene alone was sufficient to induce spontaneous T cell lymphomas in 50% of the mice compared to none in wildtype littermates (Fig. 4.2). In addition, I observed a significant acceleration in lymphoma development through the deletion of $p27^{Kip1}$. These studies prove that miR-106a~363 is a potent oncogene in T cell lymphomas, and confirm the cooperation between *Xpcl1* and p27 loss in lymphomagenesis.

It is interesting to note that spontaneous lymphoma development has not been reported from overexpression of miR-17~92. Rather an autoimmune lymphoproliferative disease which resulted in the death of 92% of transgenic mice by 55-weeks[87]. Loss of PTEN or Bim has been shown to cause autoimmunity and lymphomas in mice and are targets of the miR-17~92 miRNAs[181,182]. Thus, it has been proposed that the autoimmune disease in miR-17~92 transgenic mice was a result of reduced PTEN and Bim expression[87]. In contrast, I did not observe reduced expression of either PTEN or Bim in M-MuLV tumors in association with *Xpcl1* integrations, nor was their expression reduced in primary Lx^{+} thymocytes (data not shown). This strongly suggests alternative targets of miR-106a~363 in lymphomagenesis.

Given the strong synergy of *Xpcl1* and $p27^{Kip1}$ deletion in lymphomas, I hypothesized that the biochemical mechanism involved the targeting of additional cell cycle inhibitors by the miRNAs. In support of this hypothesis, $p21^{Cip1}$ was previously reported to be targeted by the miR-17 family members and we observed a decrease in expression of cell cycle genes in $Xpcl1^{+}$ M-MuLV lymphomas (Fig. 2.6C)[90]. Furthermore, TargetScan predicts that the miR-106a~363 miRNAs target an array of cell cycle regulators including Rb, p107, p130 and p57. Thus it is surprising that I

observed equivalent RNA expression of all of these genes when comparing Lx^+ and wildtype thymuses (Fig. 4.5). It is possible that miR-106a~363 inhibits expression of these genes to some extent. Measuring RNA levels does not rule out translational effects, as might be detected in 3'UTR reporter assays. Also, compensatory mechanisms may increase transcription of these genes to normal levels. Nonetheless, my data suggests that miR-106a~363 overexpression does not have a potent, durable effect on the expression of these cell cycle genes.

Surprisingly, I did observe an increase in expression of $p27^{Kip1}$ at both the RNA and protein level, in Lx^+ thymus (Fig. 4.6B). The stability of $p27^{Kip1}$ protein and RNA was unchanged in Lx^+ thymocytes compared to wildtype thymocytes, indicating that $p27^{Kip1}$ was being transcriptionally regulated (Fig. 4.7). Transcriptional regulation of $p27^{Kip1}$ by a variety of mitogens has been described, with the various mechanisms of regulation being cell type specific[183]. In the case of T cells, the FoxO transcription factors have been identified as positive regulators and ID3 as a negative regulator. Expression of the FoxO transcription factors were also increased in Lx^+ thymus, suggesting that the miRNAs were upregulating their expression resulting in the elevated $p27^{Kip1}$ levels. I recapitulated the effect of miR-106a~363 on $p27^{Kip1}$ expression in two mouse T cell lines. Transient expression of miR-106a~363 caused increased $p27^{Kip1}$ protein levels and in the SV40-180 cells $p27^{Kip1}$, FoxO3a and FoxO4 RNA levels increased (Fig. 4.9). Since miRNAs can potentially target hundreds of genes, the increase in FoxO expression might be a secondary effect not directly related to elevated $p27^{Kip1}$ levels. To validate that the FoxO transcription factors were mediating expression of $p27^{Kip1}$ by the miRNAs, I demonstrated that deletion of the FoxO binding site from the $p27^{Kip1}$ promoter

or shRNA knockdown of FoxO3a and FoxO4 blocked increased expression of $p27^{Kip1}$ in a luciferase reporter assay (Fig. 4.10A, B). Therefore the miR-106a~363 induced increase in $p27^{Kip1}$ expression is due to transcriptional regulation of $p27^{Kip1}$ by FoxO3a and FoxO4. At this point it is difficult to hypothesize what the mechanism might be connecting the miRNAs to regulation of FoxO transcription, since little is known about their transcriptional regulation.

The elevated $p27^{Kip1}$ expression in Lx^{+} thymocytes suggests that the synergy between the miRNAs and $p27^{Kip1}$ loss is not due to $p27^{Kip1}$ loss enhancing the miR-106a~363 tumor phenotype. Rather, the synergy is due to $p27^{Kip1}$ loss overcoming an anti-oncogenic effect of the miRNAs. A number of oncogenes also cause anti-oncogenic effects. One example is c-Myc which induces both cellular proliferation and cell death[184]. Cancer cells overcome the apoptotic effects of c-Myc by inactivating the effectors of c-Myc induced apoptosis, p53 and Arf[185,186]. In the case of miR-106a, it has already been described to have a tumor suppressive function in glioma where it inhibits cell growth by targeting E2F1[97]. Here I am proposing that miR-106a~363 cause an additional anti-oncogenic effect, the upregulation of $p27^{Kip1}$. The upstream component of the mechanism, which directly involves the miRNAs, is unclear at this point but it is possible to hypothesize two potential mechanisms. The first is that the miRNAs are directly targeting an inhibitor of FoxO transcription and an indirect consequence is the upregulation of $p27^{Kip1}$. Alternatively, the miR-106a~363 miRNAs may target genes whose repression promotes proliferation and $p27^{Kip1}$ is upregulated as a compensatory mechanism.

I observed differential expression of miR-106a~363 miRNAs during normal T cell development, suggesting that they are involved in regulating T cell development. I therefore asked whether miR-106a~363 might be an important regulator of $p27^{Kip1}$ during T cell development, since its forced expression upregulates $p27^{Kip1}$ expression. A large body of literature has demonstrated that $p27^{Kip1}$ can be regulated by a variety of transcriptional and post-transcriptional mechanisms. However, these studies were mostly conducted in cultured fibroblasts or mature lymphocytes. To our knowledge, the only data on $p27^{Kip1}$ expression in developing thymocytes comes from a qualitative assessment using immunofluorescence and confocal microscopy[171]. To quantify $p27^{Kip1}$ at various stages of thymocyte development, both at the RNA and protein level, I flow sorted wildtype T cells into CD4 and CD8 subsets. Interestingly, both $p27^{Kip1}$ RNA and protein were differentially expressed. This is important because it points to transcription as the primary mode of regulation of $p27^{Kip1}$ during T cell development. However, expression of endogenous miR-106a~363 and $p27^{Kip1}$ did not correlate with one another during T cell development (Fig. 4.11 compared to Fig. 3.1B). Therefore the miR-106a~363 are not involved in regulation of $p27^{Kip1}$ during T cell development. The pattern of $p27^{Kip1}$ expression does inversely correlate with proliferation in thymocyte subsets; the lowest level of $p27^{Kip1}$ was detected in DN thymocytes and expression was elevated in all other subsets (Fig. 4.11).

Since the data pointed to transcription as the primary mode of regulation, I quantified the expression of FoxO3a, FoxO4 and ID3 in thymocyte subsets. I found that ID3 expression was largely unchanged. However, the expression of the FoxO3a and FoxO4 transcription factors largely mirrored that of $p27^{Kip1}$ expression, indicating that

they are likely regulating $p27^{Kip1}$ expression. At the protein level, the FoxO transcription factors are regulated through the Akt signaling pathway[187]. The Akt signaling pathway has also been shown to have critical roles in T cell development, so it is likely that FoxO protein levels are being regulated through Akt signaling in thymocytes[188]. The mechanism by which the FoxO transcription factors are transcriptionally regulated in T cell development is unclear, since their transcriptional regulators of are still largely unknown. The only known regulator is FoxO3a, which can stimulate expression of FoxO1 and FoxO4[189]. The data indicates that the FoxO transcription factors are likely to be key regulators of $p27^{Kip1}$ expression during T cell development. What role other mechanisms play in $p27^{Kip1}$ regulation remains to be elucidated.

Materials and Methods

miRNA qPCR from serum

Mice were terminally bled and serum was collected from 500ul of blood. Total RNA was isolated as previously described, without the use of *C. elegans* miRNA spike-ins[190]. The RNA was eluted into a final volume of 100ul water. The reverse transcription and SYBR green qPCR reactions are almost the same as for RNA isolated from cells, with the exception being the amount of RNA used per RT reaction. Since the concentration of RNA from serum is too low to quantify, a fixed volume of 3.05µl of serum RNA was used per RT reaction for each sample. Each sample was quantified with RT technical duplicates as well as qPCR technical duplicates.

Western blotting

Tumors and normal thymi from 8-week old animals were homogenized in RIPA buffer with protease inhibitors (10mM NaPO4, 0.3M NaCl, 0.1% SDS, 1% NP40, 1% Deoxycholate, 2mM EDTA, 10 µg/ml Leupeptin, 10 µg/ml Aprotinin, 2mM PMSF). Samples were sonicated and protein quantified with the Bio-Rad protein assay. Western blots for $p27^{Kip1}$ were performed using a rabbit anti-mouse polyclonal antibody (1:1000 v/v) followed by goat anti-rabbit HRP and ECL chemiluminescence[168]. For protein quantitation, we used secondary antibodies, goat anti-rabbit IgG-IRDye800 (Rockland), or goat anti-mouse IgG Alexa Fluor 680 (BD-Molecular Probes), and scanned blots with an Odyssey Imager (Li-Cor Biosciences). Sample loading was normalized with concurrent murine anti-β-tubulin immunostaining (1:10,000, T-0198, Sigma). Images were quantified with ImageJ software (NIH Research Services Branch).

Protein and RNA stability

Thymocytes from 8-week old wildtype and Lx^{+} mice were harvested and pooled by genotype. 5 million cells per time point and treatment were plated in 1ml of RPMI+10% FBS. The cells were treated with either Actinomycin D in DMSO at 10ng/µl or Cyclohexamide at 10ng/µl. The control samples were treated with equal volumes of DMSO (Actinomycin D) or filtered ddH_20 (Cyclohexamide). Samples were collected at the indicated time points and the cells washed twice with PBS. One ml of Trizol (Invitrogen) was added to the Actinomycin samples and RNA was prepared using the standard Trizol protocol. The Cyclohexamide samples had 250µl of RIPA buffer including protease inhibitors added and were incubated on ice for 5 mins, sonicated and

the cellular debris pelleted with a high speed spin. Detection of $p27^{Kip1}$ protein and RNA by western blot and RT-qPCR was done as described above.

Tissue culture

SV40-180 and LGY-6871 mouse T cells lines were grown in RPMI containing 10% fetal bovine serum, 100 μM β-mercaptoethanol, 50 U/ml penicillin and 50 μg/ml streptomycin at 37°C. Both cell lines were transfected by electroporation using 10 million cells/ml in 100 μl RPMI with 10% FBS, 50 mM trehalose and up to 20 μg DNA in a 0.2 cm cuvettes at 150V, 975 μF. Following transfection the cells were grown in 60-mm dishes containing complete RPMI. When using 0.4 cm cuvettes the total volume was scaled to 250 μl with the amount of used DNA scaled proportionally to the number of cells used and the electroporation conditions changed to 270V, 975 μF.

Luciferase assays

The mouse pGL2-$p27^{Kip1}$ promoter vector (courtesy of James Roberts) contains a 2.2 kb fragment of the $p27^{Kip1}$ promoter and has been previously described[103]. The truncated $p27^{Kip1}$ promoter was generated by cutting the pGL2-$p27^{Kip1}$ vector with BamHI and SpeI to generate a 1.7 kb promoter fragment. The pRL-TK-CX6x CD69 3' UTR Renilla reporter (courtesy of Phillip Sharp) has been previously described[76]. The FoxO3a and FoxO4 GIPZ Lentiviral shRNAmir vectors were obtained from Open Biosystems (V3LHS_375386, V3LHS_358494). To quantify the effect of miR-106a~363 on $p27^{Kip1}$ expression and the role of the FoxO transcription factors in the process the pGL2-$p27^{Kip1}$ vector was transfected along with pSM30-Xpcl or pSM30-empty, one of the GIPZ FoxO vectors or scramble control, and pRL-TK (Promega, Renilla control) into SV40-180 cells by electroporation or transfected either pGL2-$p27^{Kip1}$ or pGL2-p27Trun

along with pSM30-Xpcl or pSM30-empty and pRL-TK into SV40-180 cells by electroporation . The CD69 3' UTR Renilla reporter was transfected along with pSM30-empty or pSM30-Xpcl and pGL3 control (Promega, for transfection normalization) into SV40-180 cells. Luciferase and Renilla activity was assayed 48h post-transfection using the Dual-Luciferase Reporter Assay System (Promega).

Histology

Specimens were divided and either fixed in 10% neutral buffered formalin, or snap frozen in OCT. Fixed specimens were paraffin processed and cut in 4 μm sections and rehydrated. To assay proliferation and apoptosis IHC was performed on paraffin sections for the Ki67 antigen and caspase 3, respectively. Parallel sections were either stained with hematoxylin and eosin, or immunohistochemistry. IHC was conducted as previously described, using a Dako Autostainer[191]. Briefly, slides were rehydrated in Dako Wash Buffer (Carpinteria, CA), endogenous peroxide activity was blocked with 3% H_2O_2 for 8 min, followed by the Avidin/Biotin Blocking Kit (Vector Laboratories). Sections were blocked with Tris-buffered saline plus 1% BSA, 15% donkey serum, and 5% mouse serum for 10 min. Primary antibodies were applied for 30-min. followed by a wash and then incubation with biotinylated donkey anti-goat (Jackson ImmunoResearch) x30 min. Color development was achieved with Vectastain Elite ABC R.T.U. (Vector Laboratories), with a hematoxylin counterstain. IHC for the cell surface markers (CD4 and CD8, BD Bioscience) was done on frozen sections, cut at 5 μm and fixed by brief immersion in ice cold acetone. Isotype antibodies were run in parallel on each tissue sample, as negative controls.

Chapter 5: Conclusions

The work in this dissertation utilized transgenic mouse models to overexpress *Xpcl1* in order to study the oncogenic function and developmental roles of the miR-106a~363 miRNAs. I have shown that miR-106a~363 is a potent oncogene based on the high penetrance of lymphomas in the Lx^+ transgenic mice. This is the first time that the miR-106a~363 cluster, or any of its paralogs, has been found to spontaneously induce tumors. In contrast, overexpression of the miR-17~92 cluster resulted in immune lymphoproliferative disease in B cells rather than tumor development[87]. Over expression of the cluster had been show to accelerate tumorigenesis in Eμ-Myc mice suggesting an oncogenic effect[86]. However further studies determined that its oncogenic function in B cells was to inhibit apoptosis, which alone may not be sufficient to induce tumorigenesis but may promote survival of auto-reactive B cells[88].

Similarly, I did not observe a high incidence of tumors in Cx^+ mice despite widespread expression of miR-106a~363. One mouse did develop intestinal tumors, which is intriguing given the prior reports of elevated miR-106a levels in colon cancer[81]. The lack of more frequent tumor development may indicate that expression of the miRNAs is associated with later stages of tumorigenesis and as a result their expression does not alter rates of tumor initiation. Recently, a number of studies have identified functions of miR-106a~363, and paralogous clusters, that predict tumor suppression[94-97]. Therefore the miRNAs maybe functioning as tumor suppressors in Cx^+ mice; a phenotype that would not be detectable from a survival study of mice with only the miRNA transgene. A more sensitive study of the oncogenic potential or tumor suppressive function of the miRNAs in Cx^+ mice will require a system that predisposes

the mice to developing tumors; for example through the addition of chemical carcinogens or defined gene mutations.

To determine the expression changes associated with miR-106a~363 overexpression or $p27^{Kip1}$ loss in tumorigenesis, we examined the global mRNA or miRNA expression profiles in the lymphomas induced by M-MuLV. Our initial hypothesis was that *Xpcl1* viral integrations and $p27^{Kip1}$ deletion would have overlapping or complementary expression profiles. Consistent with this we identified a large number of genes which appear to be generalized markers of high grade lymphomas. The functional classification of the genes upregulated in these tumors include nucleic acid and protein metabolism, as well as the cell cycle, whereas genes involved in T cell immunity were down regulated. Surprisingly, while $p27^{Kip1}$ loss enhanced the expression profile associated with the general tumor phenotype, *Xpcl1* insertions were associated with the opposite pattern of expression, even though *Xpcl1* insertions were often found in $p27^{-/-}$ tumors. The genes with altered expression within the nucleic acid, protein metabolism, cell cycle and T cell immunity functional categories were mostly non-overlapping between the $Xpcl1^{+}$ and $p27^{-/-}$ tumors. The data suggests two possible mechanisms to account for the interaction between $p27^{Kip1}$ loss and *Xpcl1*; either deletion of $p27^{Kip1}$ counters an anti-oncogenic pattern of gene expression induced by *Xpcl1* or they have complementary oncogenic functions.

Even though the gene expression analysis of the M-MuLV did not identify a clear link between $p27^{Kip1}$ deletion and miR-106a~363, the initial M-MuLV study did implicate them as potential cooperating mutations. In this work I have shown unambiguously that loss of $p27^{Kip1}$ is strongly synergistic with oncogenic activity of miR-106a~363 in T cells.

Further, I have shown that miR-106a~363 induces $p27^{Kip1}$ expression, which is an anti-oncogenic, tumor suppressive effect. Prior studies have shown that the tumor suppressor effect of $p27^{Kip1}$ is gene-dose dependent. As a result, the level of $p27^{Kip1}$ protein expression directly determines the rate of tumor formation. Thus, deletion of $p27^{Kip1}$ from the mouse genome completely overcomes this anti-oncogenic effect of miR-106a~363, and allows the other oncogenic activities of the miRNA to function unopposed by a rise in $p27^{Kip1}$. These results confirm our initial hypothesis, from the M-MuLV expression study, that $p27^{Kip1}$ loss counters an anti-oncogenic function of miR-106a~363. My data indicates that the miR-106a~363 miRNAs mediate an increase in $p27^{Kip1}$ expression indirectly, by increasing expression of the FoxO3a/FoxO4 transcription factors. The mechanism through which the miRNAs induce the transcription factors is unclear, since they are not predicted to target any of the known regulators of FoxO3a/FoxO4 expression. An in-depth study of miR-106a~363 targeting using methods such as HITS/CLIP may identify targets that are not computationally predicted and help to elucidate the mechanism.

The aberrant immunophenotype of thymocytes in Lx^{+} mice indicates that the miR-106a~363 cluster regulates T cell development. Full elucidation of the role of the miRNAs in developing T cells will require further study of thymocyte DN subsets, e.g. those with the highest miR-106a~363 expression. Nonetheless, I have demonstrated that an important effect of the miRNA is to directly target, and reduce the expression, of the CD69 cell surface protein. CD69 is an important regulator of thymocyte emigration. by increasing the amount of time SP cells remain in the thymus, and effects the relative proportions of SP vs. DP thymocytes. Thus loss of CD69 may be the primary reason for

the reduction in SP, and concurrent rise in DP thymocytes, in Lx^{+} transgenic mice. Additionally, I observed a reduction in surface expression of TCR and CD3. Reduced expression of the TCR complex has been associated with inhibition of positive selection, which may also account for the altered thymocyte populations by reducing the number of DP cells that successfully develop to the SP stage.

Understanding the biology of miR-106a~363 and how it interacts with other genetic events has important implications for the diagnosis and treatment of cancers in which it is aberrantly expressed. These studies highlight the oncogenic effects of miR-106a~363, its interaction with cell cycle regulatory molecules, and its pivotal role in normal T cell development.

Bibliography

1. Lee, R. C., Feinbaum, R. L. & Ambros, V. The C. elegans heterochronic gene lin-4 encodes small RNAs with antisense complementarity to lin-14. *Cell* **75,** 843-854 (1993).

2. Reinhart, B. J., Slack, F. J., Basson, M., Pasquinelli, A. E., *et al.* The 21-nucleotide let-7 RNA regulates developmental timing in Caenorhabditis elegans. *Nature* **403,** 901-906 (2000).

3. Fire, A., Xu, S., Montgomery, M. K., Kostas, S. A., *et al.* Potent and specific genetic interference by double-stranded RNA in Caenorhabditis elegans. *Nature* **391,** 806-811 (1998).

4. Hamilton, A. J. & Baulcombe, D. C. A species of small antisense RNA in posttranscriptional gene silencing in plants. *Science* **286,** 950-952 (1999).

5. Zamore, P. D., Tuschl, T., Sharp, P. A. & Bartel, D. P. RNAi: double-stranded RNA directs the ATP-dependent cleavage of mRNA at 21 to 23 nucleotide intervals. *Cell* **101,** 25-33 (2000).

6. Bernstein, E., Caudy, A. A., Hammond, S. M. & Hannon, G. J. Role for a bidentate ribonuclease in the initiation step of RNA interference. *Nature* **409,** 363-366 (2001).

7. Yang, D., Lu, H. & Erickson, J. W. Evidence that processed small dsRNAs may mediate sequence-specific mRNA degradation during RNAi in Drosophila embryos. *Curr Biol* **10,** 1191-1200 (2000).

8. Hammond, S. M., Bernstein, E., Beach, D. & Hannon, G. J. An RNA-directed nuclease mediates post-transcriptional gene silencing in Drosophila cells. *Nature* **404,** 293-296 (2000).

9. Elbashir, S. M., Lendeckel, W. & Tuschl, T. RNA interference is mediated by 21- and 22-nucleotide RNAs. *Genes Dev* **15,** 188-200 (2001).

10. Griffiths-Jones, S., Saini, H. K., van Dongen, S. & Enright, A. J. miRBase: tools for microRNA genomics. *Nucleic Acids Res* **36,** D154-D158 (2008).

11. Clurman, B. E. & Hayward, W. S. Multiple proto-oncogene activations in avian leukosis virus-induced lymphomas: evidence for stage-specific events. *Mol Cell Biol* **9,** 2657-2664 (1989).

12. Tam, W., Ben-Yehuda, D. & Hayward, W. S. bic, a novel gene activated by proviral insertions in avian leukosis virus-induced lymphomas, is likely to function through its noncoding RNA. *Mol Cell Biol* **17,** 1490-1502 (1997).

13. Eis, P. S., Tam, W., Sun, L., Chadburn, A., *et al.* Accumulation of miR-155 and BIC RNA in human B cell lymphomas. *Proc Natl Acad Sci U S A* **102,** 3627-3632 (2005).

14. Kluiver, J., Poppema, S., de Jong, D., Blokzijl, T., *et al.* BIC and miR-155 are highly expressed in Hodgkin, primary mediastinal and diffuse large B cell lymphomas. *J Pathol* **207,** 243-249 (2005).

15. Lee, Y., Kim, M., Han, J., Yeom, K. H., *et al.* MicroRNA genes are transcribed by RNA polymerase II. *EMBO J* **23,** 4051-4060 (2004).

16. Cai, X., Hagedorn, C. H. & Cullen, B. R. Human microRNAs are processed from capped, polyadenylated transcripts that can also function as mRNAs. *RNA* **10,** 1957-1966 (2004).

17. Lee, Y., Ahn, C., Han, J., Choi, H., *et al.* The nuclear RNase III Drosha initiates microRNA processing. *Nature* **425,** 415-419 (2003).

18. Denli, A. M., Tops, B. B., Plasterk, R. H., Ketting, R. F. & Hannon, G. J. Processing of primary microRNAs by the Microprocessor complex. *Nature* **432,** 231-235 (2004).

19. Gregory, R. I., Yan, K. P., Amuthan, G., Chendrimada, T., *et al.* The Microprocessor complex mediates the genesis of microRNAs. *Nature* **432,** 235-240 (2004).

20. Yi, R., Qin, Y., Macara, I. G. & Cullen, B. R. Exportin-5 mediates the nuclear export of pre-microRNAs and short hairpin RNAs. *Genes Dev* **17,** 3011-3016 (2003).

21. Lund, E., Güttinger, S., Calado, A., Dahlberg, J. E. & Kutay, U. Nuclear export of microRNA precursors. *Science* **303,** 95-98 (2004).

22. Hutvágner, G., McLachlan, J., Pasquinelli, A. E., Bálint, E., *et al.* A cellular function for the RNA-interference enzyme Dicer in the maturation of the let-7 small temporal RNA. *Science* **293,** 834-838 (2001).

23. Grishok, A., Pasquinelli, A. E., Conte, D., Li, N., *et al.* Genes and mechanisms related to RNA interference regulate expression of the small temporal RNAs that control C. elegans developmental timing. *Cell* **106,** 23-34 (2001).

24. Ketting, R. F., Fischer, S. E., Bernstein, E., Sijen, T., *et al.* Dicer functions in RNA interference and in synthesis of small RNA involved in developmental timing in C. elegans. *Genes Dev* **15,** 2654-2659 (2001).

25. Chendrimada, T. P., Gregory, R. I., Kumaraswamy, E., Norman, J., *et al.* TRBP recruits the Dicer complex to Ago2 for microRNA processing and gene silencing. *Nature* **436,** 740-744 (2005).

26. Haase, A. D., Jaskiewicz, L., Zhang, H., Lainé, S., *et al.* TRBP, a regulator of cellular PKR and HIV-1 virus expression, interacts with Dicer and functions in RNA silencing. *EMBO Rep* **6,** 961-967 (2005).

27. Förstemann, K., Tomari, Y., Du, T., Vagin, V. V., *et al.* Normal microRNA maturation and germ-line stem cell maintenance requires Loquacious, a double-stranded RNA-binding domain protein. *PLoS Biol* **3,** e236 (2005).

28. Liu, J., Rivas, F. V., Wohlschlegel, J., Yates, J. R., *et al.* A role for the P-body component GW182 in microRNA function. *Nat Cell Biol* **7,** 1261-1266 (2005).

29. Meister, G., Landthaler, M., Patkaniowska, A., Dorsett, Y., *et al.* Human Argonaute2 mediates RNA cleavage targeted by miRNAs and siRNAs. *Mol Cell* **15,** 185-197 (2004).

30. Okamura, K., Ishizuka, A., Siomi, H. & Siomi, M. C. Distinct roles for Argonaute proteins in small RNA-directed RNA cleavage pathways. *Genes Dev* **18,** 1655-1666 (2004).

31. Grimson, A., Farh, K. K., Johnston, W. K., Garrett-Engele, P., *et al.* MicroRNA targeting specificity in mammals: determinants beyond seed pairing. *Mol Cell* **27,** 91-105 (2007).

32. Lal, A., Navarro, F., Maher, C. A., Maliszewski, L. E., *et al.* miR-24 Inhibits cell proliferation by targeting E2F2, MYC, and other cell-cycle genes via binding to "seedless" 3'UTR microRNA recognition elements. *Mol Cell* **35,** 610-625 (2009).

33. Shin, C., Nam, J. W., Farh, K. K., Chiang, H. R., *et al.* Expanding the microRNA targeting code: functional sites with centered pairing. *Mol Cell* **38,** 789-802 (2010).

34. Tay, Y., Zhang, J., Thomson, A. M., Lim, B. & Rigoutsos, I. MicroRNAs to Nanog, Oct4 and Sox2 coding regions modulate embryonic stem cell differentiation. *Nature* **455,** 1124-1128 (2008).

35. Chendrimada, T. P., Finn, K. J., Ji, X., Baillat, D., *et al.* MicroRNA silencing through RISC recruitment of eIF6. *Nature* **447,** 823-828 (2007).

36. Liu, J., Carmell, M. A., Rivas, F. V., Marsden, C. G., *et al.* Argonaute2 is the catalytic engine of mammalian RNAi. *Science* **305,** 1437-1441 (2004).

37. Behm-Ansmant, I., Rehwinkel, J., Doerks, T., Stark, A., *et al.* mRNA degradation by miRNAs and GW182 requires both CCR4:NOT deadenylase and DCP1:DCP2 decapping complexes. *Genes Dev* **20,** 1885-1898 (2006).

38. Piao, X., Zhang, X., Wu, L. & Belasco, J. G. CCR4-NOT deadenylates mRNA associated with RNA-induced silencing complexes in human cells. *Mol Cell Biol* **30,** 1486-1494 (2010).

39. Thomas, M., Lieberman, J. & Lal, A. Desperately seeking microRNA targets. *Nat Struct Mol Biol* **17,** 1169-1174 (2010).

40. Friedman, R. C., Farh, K. K., Burge, C. B. & Bartel, D. P. Most mammalian mRNAs are conserved targets of microRNAs. *Genome Res* **19,** 92-105 (2009).

41. Krek, A., Grün, D., Poy, M. N., Wolf, R., *et al.* Combinatorial microRNA target predictions. *Nat Genet* **37,** 495-500 (2005).

42. John, B., Enright, A. J., Aravin, A., Tuschl, T., *et al.* Human MicroRNA targets. *PLoS Biol* **2,** e363 (2004).

43. Kertesz, M., Iovino, N., Unnerstall, U., Gaul, U. & Segal, E. The role of site accessibility in microRNA target recognition. *Nat Genet* **39,** 1278-1284 (2007).

44. Miranda, K. C., Huynh, T., Tay, Y., Ang, Y. S., *et al.* A pattern-based method for the identification of MicroRNA binding sites and their corresponding heteroduplexes. *Cell* **126,** 1203-1217 (2006).

45. Selbach, M., Schwanhäusser, B., Thierfelder, N., Fang, Z., *et al.* Widespread changes in protein synthesis induced by microRNAs. *Nature* **455,** 58-63 (2008).

46. Rajewsky, N. microRNA target predictions in animals. *Nat Genet* **38 Suppl,** S8-13 (2006).

47. Sethupathy, P., Megraw, M. & Hatzigeorgiou, A. G. A guide through present computational approaches for the identification of mammalian microRNA targets. *Nat Methods* **3,** 881-886 (2006).

48. Lim, L. P., Lau, N. C., Garrett-Engele, P., Grimson, A., *et al.* Microarray analysis shows that some microRNAs downregulate large numbers of target mRNAs. *Nature* **433,** 769-773 (2005).

49. Tan, L. P., Wang, M., Robertus, J. L., Schakel, R. N., *et al.* miRNA profiling of B-cell subsets: specific miRNA profile for germinal center B cells with variation between centroblasts and centrocytes. *Lab Invest* **89,** 708-716 (2009).

50. Chi, S. W., Zang, J. B., Mele, A. & Darnell, R. B. Argonaute HITS-CLIP decodes microRNA-mRNA interaction maps. *Nature* (2009).

51. Katoh, T., Sakaguchi, Y., Miyauchi, K., Suzuki, T., *et al.* Selective stabilization of mammalian microRNAs by 3' adenylation mediated by the cytoplasmic poly(A) polymerase GLD-2. *Genes Dev* **23,** 433-438 (2009).

52. Ozsolak, F., Poling, L. L., Wang, Z., Liu, H., *et al.* Chromatin structure analyses identify miRNA promoters. *Genes Dev* **22,** 3172-3183 (2008).

53. Corcoran, D. L., Pandit, K. V., Gordon, B., Bhattacharjee, A., *et al.* Features of mammalian microRNA promoters emerge from polymerase II chromatin immunoprecipitation data. *PLoS One* **4,** e5279 (2009).

54. Saito, Y., Liang, G., Egger, G., Friedman, J. M., *et al.* Specific activation of microRNA-127 with downregulation of the proto-oncogene BCL6 by chromatin-modifying drugs in human cancer cells. *Cancer Cell* **9,** 435-443 (2006).

55. Lujambio, A., Ropero, S., Ballestar, E., Fraga, M. F., *et al.* Genetic unmasking of an epigenetically silenced microRNA in human cancer cells. *Cancer Res* **67,** 1424-1429 (2007).

56. Davis, B. N., Hilyard, A. C., Lagna, G. & Hata, A. SMAD proteins control DROSHA-mediated microRNA maturation. *Nature* **454,** 56-61 (2008).

57. Suzuki, M., Moriguchi, T., Ohneda, K. & Yamamoto, M. Differential contribution of the Gata1 gene hematopoietic enhancer to erythroid differentiation. *Mol Cell Biol* **29,** 1163-1175 (2009).

58. Yamagata, K., Fujiyama, S., Ito, S., Ueda, T., *et al.* Maturation of microRNA is hormonally regulated by a nuclear receptor. *Mol Cell* **36,** 340-347 (2009).

59. Guil, S. & Cáceres, J. F. The multifunctional RNA-binding protein hnRNP A1 is required for processing of miR-18a. *Nat Struct Mol Biol* **14,** 591-596 (2007).

60. Newman, M. A., Thomson, J. M. & Hammond, S. M. Lin-28 interaction with the Let-7 precursor loop mediates regulated microRNA processing. *RNA* **14,** 1539-1549 (2008).

61. Melo, S. A., Ropero, S., Moutinho, C., Aaltonen, L. A., *et al.* A TARBP2 mutation in human cancer impairs microRNA processing and DICER1 function. *Nat Genet* **41,** 365-370 (2009).

62. Lee, Y. S., Liu, F. & Segil, N. A morphogenetic wave of p27Kip1 transcription directs cell cycle exit during organ of Corti development. *Development* **133,** 2817-2826 (2006).

63. Obernosterer, G., Leuschner, P. J., Alenius, M. & Martinez, J. Post-transcriptional regulation of microRNA expression. *RNA* **12,** 1161-1167 (2006).

64. Ventura, A. & Jacks, T. MicroRNAs and cancer: short RNAs go a long way. *Cell* **136,** 586-591 (2009).

65. Lee, E. J., Baek, M., Gusev, Y., Brackett, D. J., *et al.* Systematic evaluation of microRNA processing patterns in tissues, cell lines, and tumors. *RNA* **14,** 35-42 (2008).

66. Calin, G. A., Dumitru, C. D., Shimizu, M., Bichi, R., *et al.* Frequent deletions and down-regulation of micro- RNA genes miR15 and miR16 at 13q14 in chronic lymphocytic leukemia. *Proc Natl Acad Sci U S A* **99,** 15524-15529 (2002).

67. Cimmino, A., Calin, G. A., Fabbri, M., Iorio, M. V., *et al.* miR-15 and miR-16 induce apoptosis by targeting BCL2. *Proc Natl Acad Sci U S A* **102,** 13944-13949 (2005).

68. Lu, M., Zhang, Q., Deng, M., Miao, J., *et al.* An analysis of human microRNA and disease associations. *PLoS One* **3,** e3420 (2008).

69. Hwang, H. C., Martins, C. P., Bronkhorst, Y., Randel, E., *et al.* Identification of oncogenes collaborating with p27Kip1 loss by insertional mutagenesis and high-throughput insertion site analysis. *Proc Natl Acad Sci U S A* **99,** 11293-11298 (2002).

70. Landais, S., Quantin, R. & Rassart, E. Radiation leukemia virus common integration at the Kis2 locus: simultaneous overexpression of a novel noncoding RNA and of the proximal Phf6 gene. *J Virol* **79,** 11443-11456 (2005).

71. Tanzer, A. & Stadler, P. F. Molecular evolution of a microRNA cluster. *J Mol Biol* **339,** 327-335 (2004).

72. Kozomara, A. & Griffiths-Jones, S. miRBase: integrating microRNA annotation and deep-sequencing data. *Nucleic Acids Res* **39,** D152-D157 (2011).

73. Ventura, A., Young, A. G., Winslow, M. M., Lintault, L., *et al.* Targeted deletion reveals essential and overlapping functions of the miR-17 through 92 family of miRNA clusters. *Cell* **132,** 875-886 (2008).

74. Foshay, K. M. & Gallicano, G. I. miR-17 family miRNAs are expressed during early mammalian development and regulate stem cell differentiation. *Dev Biol* **326,** 431-443 (2009).

75. Spierings, D. C., McGoldrick, D., Hamilton-Easton, A. M., Neale, G., *et al.* Ordered progression of stage-specific miRNA profiles in the mouse B2 B-cell lineage. *Blood* **117,** 5340-5349 (2011).

76. Neilson, J. R., Zheng, G. X., Burge, C. B. & Sharp, P. A. Dynamic regulation of miRNA expression in ordered stages of cellular development. *Genes Dev* **21,** 578-589 (2007).

77. Sharma, A., Kumar, M., Aich, J., Hariharan, M., *et al.* Posttranscriptional regulation of interleukin-10 expression by hsa-miR-106a. *Proc Natl Acad Sci U S A* **106,** 5761-5766 (2009).

78. O'Garra, A. & Vieira, P. T(H)1 cells control themselves by producing interleukin-10. *Nat Rev Immunol* **7,** 425-428 (2007).

79. O'Garra, A., Barrat, F. J., Castro, A. G., Vicari, A. & Hawrylowicz, C. Strategies for use of IL-10 or its antagonists in human disease. *Immunol Rev* **223,** 114-131 (2008).

80. Volinia, S., Calin, G. A., Liu, C. G., Ambs, S., *et al.* A microRNA expression signature of human solid tumors defines cancer gene targets. *Proc Natl Acad Sci U S A* **103,** 2257-2261 (2006).

81. Díaz, R., Silva, J., García, J. M., Lorenzo, Y., *et al.* Deregulated expression of miR-106a predicts survival in human colon cancer patients. *Genes Chromosomes Cancer* **47,** 794-802 (2008).

82. Xiao, B., Guo, J., Miao, Y., Jiang, Z., *et al.* Detection of miR-106a in gastric carcinoma and its clinical significance. *Clin Chim Acta* **400,** 97-102 (2009).

83. Guo, J., Miao, Y., Xiao, B., Huan, R., *et al.* Differential expression of microRNA species in human gastric cancer versus non-tumorous tissues. *J Gastroenterol Hepatol* **24,** 652-657 (2009).

84. Navarro, A., Marrades, R. M., Viñolas, N., Quera, A., *et al.* MicroRNAs expressed during lung cancer development are expressed in human pseudoglandular lung embryogenesis. *Oncology* **76,** 162-169 (2009).

85. Wang, Z., Liu, M., Zhu, H., Zhang, W., *et al.* Suppression of p21 by c-Myc through members of miR-17 family at the post-transcriptional level. *Int J Oncol* **37,** 1315-1321 (2010).

86. He, L., Thomson, J. M., Hemann, M. T., Hernando-Monge, E., *et al.* A microRNA polycistron as a potential human oncogene. *Nature* **435,** 828-833 (2005).

87. Xiao, C., Srinivasan, L., Calado, D. P., Patterson, H. C., *et al.* Lymphoproliferative disease and autoimmunity in mice with increased miR-17-92 expression in lymphocytes. *Nat Immunol* **9,** 405-414 (2008).

88. Olive, V., Bennett, M. J., Walker, J. C., Ma, C., *et al.* miR-19 is a key oncogenic component of mir-17-92. *Genes Dev* **23,** 2839-2849 (2009).

89. Hong, L., Lai, M., Chen, M., Xie, C., *et al.* The miR-17-92 cluster of microRNAs confers tumorigenicity by inhibiting oncogene-induced senescence. *Cancer Res* **70,** 8547-8557 (2010).

90. Ivanovska, I., Ball, A. S., Diaz, R. L., Magnus, J. F., *et al.* MicroRNAs in the miR-106b family regulate p21/CDKN1A and promote cell cycle progression. *Mol Cell Biol* **28,** 2167-2174 (2008).

91. Uren, A. G., Kool, J., Matentzoglu, K., de Ridder, J., *et al.* Large-scale mutagenesis in p19(ARF)- and p53-deficient mice identifies cancer genes and their collaborative networks. *Cell* **133,** 727-741 (2008).

92. Lum, A. M., Wang, B. B., Li, L., Channa, N., *et al.* Retroviral activation of the mir-106a microRNA cistron in T lymphoma. *Retrovirology* **4,** 5 (2007).

93. Landais, S., Landry, S., Legault, P. & Rassart, E. Oncogenic potential of the miR-106-363 cluster and its implication in human T-cell leukemia. *Cancer Res* **67,** 5699-5707 (2007).

94. Yu, Z., Wang, C., Wang, M., Li, Z., *et al.* A cyclin D1/microRNA 17/20 regulatory feedback loop in control of breast cancer cell proliferation. *J Cell Biol* **182,** 509-517 (2008).

95. Hossain, A., Kuo, M. T. & Saunders, G. F. Mir-17-5p regulates breast cancer cell proliferation by inhibiting translation of AIB1 mRNA. *Mol Cell Biol* **26,** 8191-8201 (2006).

96. Castellano, L., Giamas, G., Jacob, J., Coombes, R. C., *et al.* The estrogen receptor-alpha-induced microRNA signature regulates itself and its transcriptional response. *Proc Natl Acad Sci U S A* **106,** 15732-15737 (2009).

97. Yang, G., Zhang, R., Chen, X., Mu, Y., *et al.* MiR-106a inhibits glioma cell growth by targeting E2F1 independent of p53 status. *J Mol Med* (2011).

98. Davis-Dusenbery, B. N. & Hata, A. Mechanisms of control of microRNA biogenesis. *J Biochem* **148,** 381-392 (2010).

99. Krol, J., Loedige, I. & Filipowicz, W. The widespread regulation of microRNA biogenesis, function and decay. *Nat Rev Genet* **11,** 597-610 (2010).

100. Dijkers, P. F., Medema, R. H., Pals, C., Banerji, L., *et al.* Forkhead transcription factor FKHR-L1 modulates cytokine-dependent transcriptional regulation of p27(KIP1). *Mol Cell Biol* **20,** 9138-9148 (2000).

101. Medema, R. H., Kops, G. J., Bos, J. L. & Burgering, B. M. AFX-like Forkhead transcription factors mediate cell-cycle regulation by Ras and PKB through p27Kip1. *Nature* **404,** 782-787 (2000).

102. Yang, W., Shen, J., Wu, M., Arsura, M., *et al.* Repression of transcription of the p27(Kip1) cyclin-dependent kinase inhibitor gene by c-Myc. *Oncogene* **20,** 1688-1702 (2001).

103. Garrett-Engele, C. M., Tasch, M. A., Hwang, H. C., Fero, M. L., *et al.* A mechanism misregulating p27 in tumors discovered in a functional genomic screen. *PLoS Genet* **3,** e219 (2007).

104. O'Hagan, R. C., Ohh, M., David, G., de Alboran, I. M., *et al.* Myc-enhanced expression of Cul1 promotes ubiquitin-dependent proteolysis and cell cycle progression. *Genes Dev* **14,** 2185-2191 (2000).

105. Keller, U. B., Old, J. B., Dorsey, F. C., Nilsson, J. A., *et al.* Myc targets Cks1 to provoke the suppression of p27Kip1, proliferation and lymphomagenesis. *EMBO J* **26,** 2562-2574 (2007).

106. Cuesta, R., Martínez-Sánchez, A. & Gebauer, F. miR-181a regulates cap-dependent translation of p27(Kip1) mRNA in myeloid cells. *Mol Cell Biol* **29,** 2841-2851 (2009).

107. le Sage, C., Nagel, R., Egan, D. A., Schrier, M., *et al.* Regulation of the p27(Kip1) tumor suppressor by miR-221 and miR-222 promotes cancer cell proliferation. *EMBO J* **26,** 3699-3708 (2007).

108. Visone, R., Russo, L., Pallante, P., De Martino, I., *et al.* MicroRNAs (miR)-221 and miR-222, both overexpressed in human thyroid papillary carcinomas, regulate p27Kip1 protein levels and cell cycle. *Endocr Relat Cancer* **14,** 791-798 (2007).

109. Galardi, S., Mercatelli, N., Giorda, E., Massalini, S., *et al.* miR-221 and miR-222 expression affects the proliferation potential of human prostate carcinoma cell lines by targeting p27Kip1. *J Biol Chem* **282,** 23716-23724 (2007).

110. Vidal, A., Millard, S. S., Miller, J. P. & Koff, A. Rho activity can alter the translation of p27 mRNA and is important for RasV12-induced transformation in a manner dependent on p27 status. *J Biol Chem* **277,** 16433-16440 (2002).

111. González, T., Seoane, M., Caamaño, P., Viñuela, J., *et al.* Inhibition of Cdk4 activity enhances translation of p27Kip1 in quiescent Rb-negative cells. *J Biol Chem* **278,** 12688-12695 (2003).

112. Sheaff, R. J., Groudine, M., Gordon, M., Roberts, J. M. & Clurman, B. E. Cyclin E-CDK2 is a regulator of p27Kip1. *Genes Dev* **11,** 1464-1478 (1997).

113. Vlach, J., Hennecke, S. & Amati, B. Phosphorylation-dependent degradation of the cyclin-dependent kinase inhibitor p27. *EMBO J* **16,** 5334-5344 (1997).

114. Sutterlüty, H., Chatelain, E., Marti, A., Wirbelauer, C., *et al.* p45SKP2 promotes p27Kip1 degradation and induces S phase in quiescent cells. *Nat Cell Biol* **1,** 207-214 (1999).

115. Carrano, A. C., Eytan, E., Hershko, A. & Pagano, M. SKP2 is required for ubiquitin-mediated degradation of the CDK inhibitor p27. *Nat Cell Biol* **1,** 193-199 (1999).

116. Chu, I., Sun, J., Arnaout, A., Kahn, H., *et al.* p27 phosphorylation by Src regulates inhibition of cyclin E-Cdk2. *Cell* **128,** 281-294 (2007).

117. Grimmler, M., Wang, Y., Mund, T., Cilensek, Z., *et al.* Cdk-inhibitory activity and stability of p27Kip1 are directly regulated by oncogenic tyrosine kinases. *Cell* **128,** 269-280 (2007).

118. Kamura, T., Hara, T., Matsumoto, M., Ishida, N., *et al.* Cytoplasmic ubiquitin ligase KPC regulates proteolysis of p27(Kip1) at G1 phase. *Nat Cell Biol* **6,** 1229-1235 (2004).

119. Ishida, N., Hara, T., Kamura, T., Yoshida, M., *et al.* Phosphorylation of p27Kip1 on serine 10 is required for its binding to CRM1 and nuclear export. *J Biol Chem* **277,** 14355-14358 (2002).

120. Rodier, G., Montagnoli, A., Di Marcotullio, L., Coulombe, P., *et al.* p27 cytoplasmic localization is regulated by phosphorylation on Ser10 and is not a prerequisite for its proteolysis. *EMBO J* **20,** 6672-6682 (2001).

121. Fero, M. L., Randel, E., Gurley, K. E., Roberts, J. M. & Kemp, C. J. The murine gene p27Kip1 is haplo-insufficient for tumour suppression. *Nature* **396,** 177-180 (1998).

122. Park, M. S., Rosai, J., Nguyen, H. T., Capodieci, P., *et al.* p27 and Rb are on overlapping pathways suppressing tumorigenesis in mice. *Proc Natl Acad Sci U S A* **96,** 6382-6387 (1999).

123. Philipp-Staheli, J., Kim, K. H., Payne, S. R., Gurley, K. E., *et al.* Pathway-specific tumor suppression. Reduction of p27 accelerates gastrointestinal tumorigenesis in Apc mutant mice, but not in Smad3 mutant mice. *Cancer Cell* **1,** 355-368 (2002).

124. Di Cristofano, A., De Acetis, M., Koff, A., Cordon-Cardo, C. & Pandolfi, P. P. Pten and p27KIP1 cooperate in prostate cancer tumor suppression in the mouse. *Nat Genet* **27,** 222-224 (2001).

125. Chu, I. M., Hengst, L. & Slingerland, J. M. The Cdk inhibitor p27 in human cancer: prognostic potential and relevance to anticancer therapy. *Nat Rev Cancer* **8,** 253-267 (2008).

126. Calin, G. A., Ferracin, M., Cimmino, A., Di Leva, G., *et al.* A MicroRNA signature associated with prognosis and progression in chronic lymphocytic leukemia. *N Engl J Med* **353,** 1793-1801 (2005).

127. Narita, Y., Nagane, M., Mishima, K., Huang, H. J., *et al.* Mutant epidermal growth factor receptor signaling down-regulates p27 through activation of the phosphatidylinositol 3-kinase/Akt pathway in glioblastomas. *Cancer Res* **62,** 6764-6769 (2002).

128. Gesbert, F., Sellers, W. R., Signoretti, S., Loda, M. & Griffin, J. D. BCR/ABL regulates expression of the cyclin-dependent kinase inhibitor p27Kip1 through the phosphatidylinositol 3-Kinase/AKT pathway. *J Biol Chem* **275,** 39223-39230 (2000).

129. Weng, L. P., Brown, J. L. & Eng, C. PTEN coordinates G(1) arrest by down-regulating cyclin D1 via its protein phosphatase activity and up-regulating p27 via its lipid phosphatase activity in a breast cancer model. *Hum Mol Genet* **10,** 599-604 (2001).

130. Gao, H., Ouyang, X., Banach-Petrosky, W., Borowsky, A. D., *et al.* A critical role for p27Kip1 gene dosage in a mouse model of prostate carcinogenesis. *Proc Natl Acad Sci U S A* **101,** 17204-17209 (2004).

131. Petrocelli, T. & Slingerland, J. M. PTEN deficiency: a role in mammary carcinogenesis. *Breast Cancer Res* **3,** 356-360 (2001).

132. MOLONEY, J. B. Biological studies on a lymphoid-leukemia virus extracted from sarcoma 37. I. Origin and introductory investigations. *J Natl Cancer Inst* **24,** 933-951 (1960).

133. Blair, D. G., Oskarsson, M., Wood, T. G., McClements, W. L., *et al.* Activation of the transforming potential of a normal cell sequence: a molecular model for oncogenesis. *Science* **212,** 941-943 (1981).

134. Kool, J., Uren, A. G., Martins, C. P., Sie, D., *et al.* Insertional mutagenesis in mice deficient for p15Ink4b, p16Ink4a, p21Cip1, and p27Kip1 reveals cancer gene interactions and correlations with tumor phenotypes. *Cancer Res* **70,** 520-531 (2010).

135. Raymond, C. K., Roberts, B. S., Garrett-Engele, P., Lim, L. P. & Johnson, J. M. Simple, quantitative primer-extension PCR assay for direct monitoring of microRNAs and short-interfering RNAs. *RNA* **11,** 1737-1744 (2005).

136. Lu, J., Getz, G., Miska, E. A., Alvarez-Saavedra, E., *et al.* MicroRNA expression profiles classify human cancers. *Nature* **435,** 834-838 (2005).

137. Mellors, R. C. Quantitative cytology and cytopathology: nucleic acids and proteins in the mitotic cycle of normal and neoplastic cells. *Ann N Y Acad Sci* **63,** 1177-1201 (1956).

138. Vasmel, W. L., Matthews, E. A., Gillis, C. P., Nieland, J., *et al.* Distinct chromosomal abnormalities in murine leukemia virus-induced T- and B-cell lymphomas. *Int J Cancer* **43,** 1112-1119 (1989).

139. Wang, J., Nygaard, V., Smith-Sorensen, B., Hovig, E. & Myklebost, O. MArray: analysing single, replicated or reversed microarray experiments. *Bioinformatics* **18,** 1139-1140 (2002).

140. Guo, Z., Dose, M., Kovalovsky, D., Chang, R., *et al.* Beta-catenin stabilization stalls the transition from double-positive to single-positive stage and predisposes thymocytes to malignant transformation. *Blood* **109,** 5463-5472 (2007).

141. Thomas, P. D., Campbell, M. J., Kejariwal, A., Mi, H., *et al.* PANTHER: a library of protein families and subfamilies indexed by function. *Genome Res* **13,** 2129-2141 (2003).

142. Frey, R. S. & Mulder, K. M. TGFbeta regulation of mitogen-activated protein kinases in human breast cancer cells. *Cancer Lett* **117,** 41-50 (1997).

143. Yang, Q., Jeremiah Bell, J. & Bhandoola, A. T-cell lineage determination. *Immunol Rev* **238,** 12-22 (2010).

144. Kumar, M. S., Lu, J., Mercer, K. L., Golub, T. R. & Jacks, T. Impaired microRNA processing enhances cellular transformation and tumorigenesis. *Nat Genet* **39,** 673-677 (2007).

145. Von Bertalanffy, L., Masin, M., Masin, F. & Kaplan, L. Detection of gynecological cancer; use of fluorescence microscopy to show nucleic acids in malignant growth. *Calif Med* **87,** 248-251 (1957).

146. Westermark, U. K., Wilhelm, M., Frenzel, A. & Henriksson, M. A. The MYCN oncogene and differentiation in neuroblastoma. *Semin Cancer Biol* (2011).

147. Tibshirani, R., Hastie, T., Narasimhan, B. & Chu, G. Diagnosis of multiple cancer types by shrunken centroids of gene expression. *Proc Natl Acad Sci U S A* **99,** 6567-6572 (2002).

148. Jackson, A. L., Bartz, S. R., Schelter, J., Kobayashi, S. V., *et al.* Expression profiling reveals off-target gene regulation by RNAi. *Nat Biotechnol* **21,** 635-637 (2003).

149. Troyanskaya, O., Cantor, M., Sherlock, G., Brown, P., *et al.* Missing value estimation methods for DNA microarrays. *Bioinformatics* **17,** 520-525 (2001).

150. Breitling, R., Armengaud, P., Amtmann, A. & Herzyk, P. Rank products: a simple, yet powerful, new method to detect differentially regulated genes in replicated microarray experiments. *FEBS Lett* **573,** 83-92 (2004).

151. Kuppers, D. A., Hwang, H. C., Jackson, A. L., Linsley, P. S., *et al.* Effect of Xpcl1 activation and p27Kip1 loss on gene expression in murine lymphoma. *PLoS One* **6,** e14758 (2011).

152. Edgar, R., Domrachev, M. & Lash, A. E. Gene Expression Omnibus: NCBI gene expression and hybridization array data repository. *Nucleic Acids Res* **30,** 207-210 (2002).

153. Iritani, B. M., Forbush, K. A., Farrar, M. A. & Perlmutter, R. M. Control of B cell development by Ras-mediated activation of Raf. *EMBO J* **16,** 7019-7031 (1997).

154. Megason, S. G. & McMahon, A. P. A mitogen gradient of dorsal midline Wnts organizes growth in the CNS. *Development* **129,** 2087-2098 (2002).

155. Wu, J., Bonsra, A. N. & Du, G. in *Methods in Molecular Biology* 205-219 (Springer Verlag, United States, 2009).

156. Wrana, J. L., Attisano, L., Cárcamo, J., Zentella, A., *et al.* TGF beta signals through a heteromeric protein kinase receptor complex. *Cell* **71,** 1003-1014 (1992).

157. Cobb, B. S., Nesterova, T. B., Thompson, E., Hertweck, A., *et al.* T cell lineage choice and differentiation in the absence of the RNase III enzyme Dicer. *J Exp Med* **201,** 1367-1373 (2005).

158. Muljo, S. A., Ansel, K. M., Kanellopoulou, C., Livingston, D. M., *et al.* Aberrant T cell differentiation in the absence of Dicer. *J Exp Med* **202,** 261-269 (2005).

159. Chen, C., Ridzon, D. A., Broomer, A. J., Zhou, Z., *et al.* Real-time quantification of microRNAs by stem-loop RT-PCR. *Nucleic Acids Res* **33,** e179 (2005).

160. Nakayama, K., Ishida, N., Shirane, M., Inomata, A., *et al.* Mice lacking p27(Kip1) display increased body size, multiple organ hyperplasia, retinal dysplasia, and pituitary tumors. *Cell* **85,** 707-720 (1996).

161. Kiyokawa, H., Kineman, R. D., Manova-Todorova, K. O., Soares, V. C., *et al.* Enhanced growth of mice lacking the cyclin-dependent kinase inhibitor function of p27(Kip1). *Cell* **85,** 721-732 (1996).

162. Fero, M. L., Rivkin, M., Tasch, M., Porter, P., *et al.* A syndrome of multiorgan hyperplasia with features of gigantism, tumorigenesis, and female sterility in p27(Kip1)-deficient mice. *Cell* **85,** 733-744 (1996).

163. Feng, C., Woodside, K. J., Vance, B. A., El-Khoury, D., *et al.* A potential role for CD69 in thymocyte emigration. *Int Immunol* **14,** 535-544 (2002).

164. Schwab, S. R., Pereira, J. P., Matloubian, M., Xu, Y., *et al.* Lymphocyte sequestration through S1P lyase inhibition and disruption of S1P gradients. *Science* **309,** 1735-1739 (2005).

165. Pappu, R., Schwab, S. R., Cornelissen, I., Pereira, J. P., *et al.* Promotion of lymphocyte egress into blood and lymph by distinct sources of sphingosine-1-phosphate. *Science* **316,** 295-298 (2007).

166. Shiow, L. R., Rosen, D. B., Brdicková, N., Xu, Y., *et al.* CD69 acts downstream of interferon-alpha/beta to inhibit S1P1 and lymphocyte egress from lymphoid organs. *Nature* **440,** 540-544 (2006).

167. Nakayama, T., Kasprowicz, D. J., Yamashita, M., Schubert, L. A., *et al.* The generation of mature, single-positive thymocytes in vivo is dysregulated by CD69 blockade or overexpression. *J Immunol* **168,** 87-94 (2002).

168. Chien, W. M., Rabin, S., Macias, E., Miliani de Marval, P. L., *et al.* Genetic mosaics reveal both cell-autonomous and cell-nonautonomous function of murine p27Kip1. *Proc Natl Acad Sci U S A* **103,** 4122-4127 (2006).

169. Nakayama, T., June, C. H., Munitz, T. I., Sheard, M., *et al.* Inhibition of T cell receptor expression and function in immature CD4+CD8+ cells by CD4. *Science* **249,** 1558-1561 (1990).

170. Vacchio, M. S., Olaru, A., Livak, F. & Hodes, R. J. ATM deficiency impairs thymocyte maturation because of defective resolution of T cell receptor alpha locus coding end breaks. *Proc Natl Acad Sci U S A* **104,** 6323-6328 (2007).

171. Hoffman, E. S., Passoni, L., Crompton, T., Leu, T. M., *et al.* Productive T-cell receptor beta-chain gene rearrangement: coincident regulation of cell cycle and clonality during development in vivo. *Genes Dev* **10,** 948-962 (1996).

172. Tsukiyama, T., Ishida, N., Shirane, M., Minamishima, Y. A., *et al.* Down-regulation of p27Kip1 expression is required for development and function of T cells. *J Immunol* **166,** 304-312 (2001).

173. Molina, T. J., Kishihara, K., Siderovski, D. P., van Ewijk, W., *et al.* Profound block in thymocyte development in mice lacking p56lck. *Nature* **357,** 161-164 (1992).

174. Nourse, J., Firpo, E., Flanagan, W. M., Coats, S., *et al.* Interleukin-2-mediated elimination of the p27Kip1 cyclin-dependent kinase inhibitor prevented by rapamycin. *Nature* **372,** 570-573 (1994).

175. Zhang, X., Wharton, W., Donovan, M., Coppola, D., *et al.* Density-dependent growth inhibition of fibroblasts ectopically expressing p27(Kip1). *Mol Biol Cell* **11,** 2117-2130 (2000).

176. Stahl, M., Dijkers, P. F., Kops, G. J., Lens, S. M., *et al.* The forkhead transcription factor FoxO regulates transcription of p27Kip1 and Bim in response to IL-2. *J Immunol* **168,** 5024-5031 (2002).

177. Reif, K., Burgering, B. M. & Cantrell, D. A. Phosphatidylinositol 3-kinase links the interleukin-2 receptor to protein kinase B and p70 S6 kinase. *J Biol Chem* **272,** 14426-14433 (1997).

178. Mitchell, P. S., Parkin, R. K., Kroh, E. M., Fritz, B. R., *et al.* Circulating microRNAs as stable blood-based markers for cancer detection. *Proc Natl Acad Sci U S A* **105,** 10513-10518 (2008).

179. Arroyo, J. D., Chevillet, J. R., Kroh, E. M., Ruf, I. K., *et al.* Argonaute2 complexes carry a population of circulating microRNAs independent of vesicles in human plasma. *Proc Natl Acad Sci U S A* **108,** 5003-5008 (2011).

180. Lu, Y., Thomson, J. M., Wong, H. Y., Hammond, S. M. & Hogan, B. L. Transgenic over-expression of the microRNA miR-17-92 cluster promotes proliferation and inhibits differentiation of lung epithelial progenitor cells. *Dev Biol* **310,** 442-453 (2007).

181. Suzuki, A., Yamaguchi, M. T., Ohteki, T., Sasaki, T., *et al.* T cell-specific loss of Pten leads to defects in central and peripheral tolerance. *Immunity* **14,** 523-534 (2001).

182. Bouillet, P., Metcalf, D., Huang, D. C., Tarlinton, D. M., *et al.* Proapoptotic Bcl-2 relative Bim required for certain apoptotic responses, leukocyte homeostasis, and to preclude autoimmunity. *Science* **286,** 1735-1738 (1999).

183. Bagui, T. K., Cui, D., Roy, S., Mohapatra, S., *et al.* Inhibition of p27Kip1 gene transcription by mitogens. *Cell Cycle* **8,** 115-124 (2009).

184. Evan, G. I., Wyllie, A. H., Gilbert, C. S., Littlewood, T. D., *et al.* Induction of apoptosis in fibroblasts by c-myc protein. *Cell* **69,** 119-128 (1992).

185. Eischen, C. M., Weber, J. D., Roussel, M. F., Sherr, C. J. & Cleveland, J. L. Disruption of the ARF-Mdm2-p53 tumor suppressor pathway in Myc-induced lymphomagenesis. *Genes Dev* **13,** 2658-2669 (1999).

186. Schmitt, C. A., McCurrach, M. E., de Stanchina, E., Wallace-Brodeur, R. R. & Lowe, S. W. INK4a/ARF mutations accelerate lymphomagenesis and promote chemoresistance by disabling p53. *Genes Dev* **13,** 2670-2677 (1999).

187. Brunet, A., Bonni, A., Zigmond, M. J., Lin, M. Z., *et al.* Akt promotes cell survival by phosphorylating and inhibiting a Forkhead transcription factor. *Cell* **96,** 857-868 (1999).

188. Juntilla, M. M. & Koretzky, G. A. Critical roles of the PI3K/Akt signaling pathway in T cell development. *Immunol Lett* **116,** 104-110 (2008).

189. Essaghir, A., Dif, N., Marbehant, C. Y., Coffer, P. J. & Demoulin, J. B. The transcription of FOXO genes is stimulated by FOXO3 and repressed by growth factors. *J Biol Chem* **284,** 10334-10342 (2009).

190. Kroh, E. M., Parkin, R. K., Mitchell, P. S. & Tewari, M. Analysis of circulating microRNA biomarkers in plasma and serum using quantitative reverse transcription-PCR (qRT-PCR). *Methods* **50,** 298-301 (2010).

191. Zager, R. A., Johnson, A. C., Lund, S. & Randolph-Habecker, J. Toll-like receptor (TLR4) shedding and depletion: acute proximal tubular cell responses to hypoxic and toxic injury. *Am J Physiol Renal Physiol* **292,** F304-F312 (2007).